Evolution of mobile networks architecture and optimization of radio resource management

Joe Saad

université PARIS-SACLAY

Evolution of mobile networks architecture and optimization of radio resource management

Evolution de l'architecture du réseau mobile et optimisation de la gestion des ressources radio

Thèse de doctorat de l'université Paris-Saclay

École doctorale n° 580 : Sciences et Technologies de l'Information et de la Communication (STIC)
Spécialité de doctorat: Sciences des réseaux, de l'information et de la communication
Graduate School : Informatique et sciences du numérique
Référent : Université de Versailles-Saint-Quentin-en-Yvelines

Thèse préparée dans l'unité de recherche **DAVID (Université Paris-Saclay, UVSQ)**, sous la direction de **Kinda KHAWAM**, Maître de Conférences/HDR et la co-supervision de **Mohamad YASSIN**, Ingénieur de recherche chez Orange Innovation et **Salvatore COSTANZO**, Ingénieur de recherche chez Orange Innovation

Thèse soutenue à Versailles, le 19 mars 2024 par

Joe SAAD

Composition du jury

Membres du jury avec voix délibérative

Salah-Eddine EL AYOUBI Professeur des universités, CentraleSupélec	Président
Tijani CHAHED Professeur des universités, Télécom SudParis	Rapporteur & Examinateur
Thi-Mai-Trang NGUYEN Professeur des universités, Université Sorbonne Paris Nord	Rapporteur & Examinateur
Cédric ADJIH Chargé de recherche, INRIA	Examinateur
Artur HECKER Chargé de recherche, Huawei	Examinateur
Philippe MARTINS Professeur des universités, Télécom Paristech	Examinateur

THESE DE DOCTORAT

NNT : 2024UPASG005

université PARIS-SACLAY
ÉCOLE DOCTORALE
Sciences et technologies de l'information et de la communication (STIC)

Titre: Evolution de l'architecture du réseau mobile et optimisation de la gestion des ressources radio
Mots clés: RAN, Slicing, Allocation de ressources, Optimisation, Apprentissage automatique, Théorie des jeux

Résumé: Avec les réseaux de cinquième génération (5G), plusieurs services hétérogènes sont supportés: le service enhanced Mobile Broad-Band (eMBB) caractérisé par ses débits élevés, le service Ultra-Reliable Low-Latency Communications (URLLC) nécessitant une faible latence et le service massive Machine-Type Communications (mMTC) privilégiant une importante densité de connexions. Grâce au slicing, la coexistence de ces services sur le même réseau est possible. Le slicing divise le réseau en sous-réseaux logiques et isolés dont chaque partie est dénommée slice et attribuée à une catégorie de services. De plus, le Radio Access Network (RAN) est le lieu d'une transformation visant à désintégrer ses composants grâce à des organismes de normalisation comme l'alliance Open-RAN (O-RAN). Cette évolution apporte plusieurs avantages pour les opérateurs comme l'introduction de l'intelligence artificielle au niveau des contrôleurs. Dans ce contexte de slicing et d'évolution du RAN, l'optimisation des ressources radio est un défi majeur pour un opérateur mobile afin d'assurer la qualité de service des différents slices à partir d'algorithmes efficaces. Par conséquent, dans cette thèse, l'objectif est de proposer plusieurs algorithmes d'allocation de ressources radio en identifiant les indicateurs de performance nécessaires pour la prise de décisions. De plus, les différentes approches proposées sont comparées entre elles et à celles de l'état de l'art, y compris l'approche standard. Aussi, pour la plupart des solutions proposées, leur emplacement dans l'architecture O-RAN est discuté. Notre premier algorithme est basé sur le Dynamic Weighted Fair Queuing (DWFQ) dans un contexte multi-slice et multi-Virtual Operator (VO). Le but est de déterminer la portion de ressources attribuée à chaque VO dans chaque slice en utilisant la théorie des jeux. Dans la suite, on s'intéresse à la gestion des ressources radio au niveau d'un même opérateur. Pour cela, une deuxième approche se focalise sur l'allocation des ressources radio entre deux slices hétérogènes: eMBB et URLLC. Deux approches, centralisée basée sur le Deep-Q Networks (DQN) et distribuée basée sur un jeu non-coopératif, traitent ce problème où l'allocation des ressources se fait grâce à l'ingénierie de trafic. Dans la troisième contribution, on ajoute l'aspect numérologie (espacement entre sous-porteuses) au problème précédent avec l'étude de trois slices: eMBB, URLLC et mMTC. Pour cela, on divise la bande de l'opérateur en plusieurs Bandwidth Parts (BWPs) dont chacune est associée à une numérologie ce qui provoque l'Inter-Numerology Interference (INI). Par suite, on propose un algorithme à trois étages dont le premier étage utilise la théorie des jeux pour choisir la BWP qui servira les utilisateurs URLLC. Le deuxième étage utilise une heuristique pour déterminer la portion de ressources radio dédiée à chaque BWP. Le troisième étage utilise le DQN pour dimensionner une bande de garde entre les BWPs utilisant des numérologies différentes afin de réduire l'INI. Pour la suite, on garde toujours l'aspect multi-numérologies dans le problème mais on s'intéresse plutôt aux utilisateurs connectés simultanément à plusieurs slices. Pour ces utilisateurs, une latence additionnelle est générée à cause du BWP switching qui est nécessaire pour récupérer les ressources de chaque slice. Pour cela, notre quatrième contribution propose trois mécanismes innovants de BWP switching qui permettent de réduire la latence globale due à cet effet. Pour la dernière contribution, l'efficacité énergétique de ces utilisateurs est étudiée en proposant un algorithme qui sélectionne entre la configuration "single numerology" (une seule BWP pour tous les slices) et "multi-numerology" (BWP différente pour chaque slice) en se basant sur plusieurs facteurs comme le niveau de batterie. Cette sélection se fait à travers deux approches, centralisée basée sur un problème d'optimisation et distribuée basée sur la théorie des jeux.

université PARIS-SACLAY

ÉCOLE DOCTORALE
Sciences et technologies de l'information et de la communication (STIC)

Title: Evolution of Mobile Networks Architecture and Optimization of Radio Resource Management
Keywords: RAN, Slicing, Resource Allocation, Optimization, Machine Learning, Game Theory

Abstract: With Fifth Generation (5G) Networks, multiple heterogeneous services are supported such as the enhanced Mobile BroadBand (eMBB) service characterized by high throughput demand, the Ultra-Reliable Low-Latency Communications (URLLC) service requiring a low latency and the massive Machine-Type Communications (mMTC) service favoring a high density of connected devices. Thanks to slicing, these services can coexist on the same infrastructure. Slicing divides the network into multiple isolated logical networks named slices where each slice is attributed to a category of services. Furthermore, standardization bodies such as the Open-RAN alliance (O-RAN) focus on the evolution of the Radio Access Network (RAN) architecture including RAN components disaggregation. This evolution brings in many advantages for the operator such as the introduction of artificial intelligence at the level of the controllers. In this context of RAN evolution and slicing, the radio resource optimization is an important challenge for the mobile network operator to ensure Quality of Service (QoS) satisfaction for the different slices through efficient algorithms. Therefore, in this thesis, the objective is to propose various radio resource allocation algorithms based on the identification of the necessary Key Performance Indicators (KPIs) to take the appropriate decisions. Additionally, the proposed approaches are compared against each other and against other approaches from the state-of-the-art. Also, solutions implementation in an O-RAN compliant architecture is discussed. Our first algorithm is based on Dynamic Weighted Fair Queuing (DWFQ) in a multi-slice and multi-Virtual Operator (VO) context. The aim of this algorithm is to determine the resource portion that will be attributed to each VO in each slice using game theory. Next, we focus on the radio resource management at the level of a single operator. Therefore, the second contribution focuses on the radio resource allocation between two heterogeneous slices: eMBB and URLLC. Two approaches solve this problem where the radio resource allocation is based on traffic engineering. The first approach is a centralized one based on Deep-Q Networks (DQN) and the second is a distributed one based on a non-cooperative game. In our third contribution, we add the numerology (subcarrier spacing) aspect to the previous problem, while considering three slices: eMBB, URLLC and mMTC. For this reason, we divide the total band into multiple Bandwidth Parts (BWPs) each linked to a numerology. This causes a new type of interference called Inter-Numerology Interference (INI). Therefore, we propose a three-level algorithm where the first level uses game theory to choose the BWP that will serve the URLLC users. The second level uses heuristics to determine the portion of radio resources attributed to each BWP. The third level uses DQN to dimension the guard bands between the BWPs using different numerologies to reduce the INI effect. Subsequently, the multi-numerology aspect is retained in the problem, while considering multiple slices per user. For these users, an additional latency is induced due to BWP switching. The latter is necessary in order to retrieve the data of each slice. For this reason, our fourth contribution proposes three innovative BWP switching schemes that help to reduce the overall latency. As for our final contribution, we focus on the energy efficiency aspect of such users by proposing an algorithm that selects the most suitable BWP configuration: single numerology (a single BWP for all slices) or multi-numerology (different BWP for each slice) while taking into account multiple factors such as the battery level. This selection is done thanks to two approaches: a centralized one based on an optimization problem and a distributed one based on game theory.

To my parents Maroun and Sonia, my brothers Elie and Johnny, my sisters-in-law Laura and Corine, my niece Maria, my nephew Anthony and to every person who believed in me when I couldn't believe in myself.

"Cast all your anxiety on Him because He cares for you."

—1 Peter 5:7

"It is impossible to live without failing at something, unless you live so cautiously that you might as well not have lived at all—in which case, you fail by default."

—J.K. Rowling

Acknowledgments

This thesis has been made possible thanks to the presence of several people who have supported me along the way, to whom I would like to express my deepest gratitude.

First, I thank God who always accompanied me with His divine protection.

In addition, I would like to thank all the members of my family: my parents, my brothers, my sisters-in-law, my niece and my nephew. Special thanks to my parents, Maroun and Sonia, who respected my decision to start this thesis and always believed in me to accomplish it. Moreover, thanks to my brother Johnny, his wife Corine and their children Maria and Anthony for making my days in France more pleasant. Also, thanks to my brother Elie and his wife Laura for their support despite the distances that separate us.

Furthermore, to my supervisory team, thank you for your professionalism, kindness, guidance and invaluable advice during my thesis. More specifically, I would like to express my sincere appreciation to my thesis director and supervisor Kinda Khawam for her excellent skills, her availability and her advice (both on a professional and personal level) which were essential to the completion of this thesis and to the submission of contributions of excellent quality. I am also very grateful to my supervisors at Orange: Mohamad Yassin and Salvatore Costanzo. Thank you for ensuring the smooth running of the thesis. The quality of the contributions has improved significantly thanks to your advice and experience in the industry.

On a personal note, I would like to thank my friends and my colleagues at Orange and UVSQ who encouraged me not to give up and who created a very friendly environment during my stay in France. There are a lot of people I would like to thank but I will just mention a few: Nathalie Aad, Paul Farhat, Aya Akkawi, Ingrid Nader, Routa Moussaileb, Mariella Renno, Vanessa Nader, Youssef Hussein, Amel Tibhirt, Lucas Darlavoix, Karen Boulos, Rita Ibrahim, Meriem Mhedhbi, Ibrahim Ayoub, Juliana El-Rayess, Perla Hajjar, Maha Abou Jaoudeh, Nour Achkar, Oliver Daou, Guea Saliby, Ibrahim Lakkis, Charbel El-Abiad, Khaled Zantout and Hassan Ayash.

Last but not least, I would like to thank the members of the jury for agreeing to evaluate this thesis which is the result of the last three years of work. Thank you for your time, comments and advice.

Résumé

Plusieurs services hétérogènes sont supportés dans la cinquième génération des réseaux mobiles (5G) comme le service eenhanced Mobile BroadBand (eMBB) caractérisé par ses débits élevés, le service Ultra-Reliable Low-Latency Communications (URLLC) nécessitant une faible latence et une fiabilité élevée et le service massive Machine-Type Communications (mMTC) répondant à un besoin capacitaire en croissance exponentielle et privilégiant une faible consommation énergétique.

Grâce à son introduction en 5G, le slicing facilite la coexistence de ces services sur le même réseau physique. En effet, le slicing permet de diviser le réseau physique en sous-réseaux logiques dont chaque partie est dénommée slice. Chaque slice sera attribué à une catégorie de services. En même temps, une isolation est assurée entre les différents slices et les ressources radio seront partagées entre slices où chaque slice aura des ressources dédiées. La répartition des ressources radio entre slices reste un défi pour un opérateur mobile qui dispose d'une bande limitée à répartir entre les différents services tout en respectant la qualité de service de chacun.

Aussi, le réseau d'accès mobile ou Radio Access Network (RAN) est le lieu d'une profonde transformation visant à désintégrer ses composants et ouvrir ses interfaces grâce à des organismes de normalisation comme l'alliance Open-RAN (O-RAN) et 3rd Generation Partnership Project (3GPP) qui travaillent sur ce sujet. En effet, l'infrastructure du RAN est fermée, résistante au passage à l'échelle et difficile à programmer ce qui freine l'introduction de nouvelles applications métier. Mais grâce à cette transformation, la station de base en 5G ou g-Node B n'est plus un bloc monolithique déployé sur un matériel dédié, mais un ensemble de composants répartis dans l'architecture du RAN virtualisée: le Centralized Unit (CU), le Distributed Unit (DU) et le Radio Unit (RU) qui composent désormais la g-NodeB de la 5G. Cette désintégration apporte plusieurs avantages et défits pour les opérateurs, en particulier l'interopérabilité entre les composants de la g-NodeB, l'ouverture de leurs interfaces ainsi que l'introduction de l'intelligence artificielle pour une plus grande autonomie de ces composants. Relever ces défis est l'objectif de la 3GPP ainsi que de l'alliance O-RAN regroupant les opérateurs majeurs du secteur Télécom afin d'obtenir l'ouverture du réseau d'accès radio et le doter d'intelligence.

Dans ce contexte de slicing et d'évolution du RAN, l'optimisation des ressources radio est un défi majeur pour un opérateur mobile afin d'assurer la qualité de service des différents slices grâce à l'intelligence qui peut être ajoutée au niveau du RAN à partir d'algorithmes efficaces. Il est donc indispensable d'introduire des éléments de réseau virtualisés munis d'interfaces ouvertes et de profiter de cette évolution du RAN. De plus, la séparation envisagée du plan de contrôle et du plan de données permettra de mettre en place des mécanismes dynamiques et intelligents pour la gestion des ressources radio dans le RAN. Par conséquent, dans cette thèse, on se focalise sur ce sujet d'optimisation des ressources radio dans le contexte de slicing et évolution du RAN, avec comme objectif de proposer plusieurs algorithmes intelligents d'allocation de ressources radio en identifiant les indicateurs de performance nécessaires pour la prise de décisions et en comparant les différentes approches proposées à celles de l'état de l'art.

D'abord, notre premère proposition est un algorithme basé sur le Dynamic Weighted Fair Queuing (DWFQ) dans un contexte multi-slice et multi-Virtual Operator (VO). Le but de cet algorithme est de déter-

miner la part de ressources radio qu'on va attribuer à chaque VO dans chaque slice. Dans ce contexte, le DWFQ est utilisé pour ordonnancer les différents VOs dans chaque slice selon le poids de chaque VO dans chaque slice. Le problème est formulé par un jeu Stackelberg dont le but est de déterminer les poids des VOs ainsi que le coût monétaire à payer par le VO au fournisseur de l'infrastructure (I-P). L'implémentation de ces algorithmes dans une architecture compatible avec les spécifications O-RAN est aussi discutée.

Ensuite, on s'intéresse à la gestion des ressources radio au niveau d'un même opérateur. Pour cela, une deuxième approche se focalise en particulier sur l'allocation des ressources radio entre 2 slices et services hétérogènes (eMBB et URLLC). Deux approches, centralisée basée sur le Deep-Q Networks (DQN) et distribuée basée sur un jeu non-coopératif, traitent ce problème où l'allocation de ressources radio se fait grâce à l'ingénierie de trafic. Ceci nous permettera de sélectionner le slice qui va servir l'utilisateur avec un ajustement dynamique de ces ressources où on change la portion dédiée à chaque slice selon plusieurs facteurs comme la charge du traffic, le débit et le délai. Ces approches sont comparées entre elles et comparées avec un autre travail de l'état de l'art ainsi qu'à l'approche legacy ou statique. On discute aussi de l'emplacement de ces solutions dans l'architecture O-RAN.

Pour ce qui suit, l'aspect numérologie est intégré dans le problème. La numérologie est un nouveau concept qui désigne l'espacement entre sous-porteuses de l'Orthogonal Frequency Division Multiplexing (OFDM) qui est devenu flexible avec la 5G afin de supporter des services de faible latence comme URLLC vu que la durée de symbole et le Time Transmission Interval (TTI) diminuent avec une numérologie élevée. En effet, les différents services hétérogènes nécessitent des exigences différentes en terme de numérologies. Par exemple, le service URLLC nécessite une numérologie plus élevée que le service eMBB. Pour cela, on divise la bande de l'opérateur en plusieurs Bandwidth Parts (BWPs) qui est une partie de bande scannée par le User Equipment (UE) et associée à une numérologie. Par contre, l'existence de plusieurs BWPs avec des numérologies différentes sur la même bande va créer un nouveau type d'interférence appelé Inter-Numerology Interference (INI) à cause de la perte d'orthogonalité lorsqu'on utilise des espacements entre sous-porteuses différents. Par suite, dans ce contexte, la troisième contribution propose un algorithme à trois étages où les conditions radio des utilisateurs sont considérées et où trois slices sont étudiés: eMBB, URLLC et mMTC. Le premier étage consiste à choisir la BWP qui servira les utilisateurs URLLC entre 2 BWPs dont l'une est dédiée à URLLC et utilisant une numérologie élevée et l'autre est partagée avec eMBB avec une numérologie plus basse. Ce choix se fait par un jeu non-coopératif. Le deuxième étage utilise une heuristique afin de déterminer la portion de ressources radio dédiée à chaque BWP selon les indicateurs de performance des utilisateurs. Le troisième étage utilise le Deep Q-Networks pour dimensionner une bande de garde entre les BWPs utilisant des numérologies différentes afin de réduire l'effet INI. Finalement, on évalue la performance de cet algorithme en le comparant avec le travail précédent où une seule numérologie est utilisée et avec un autre travail de l'état de l'art où on néglige le dimensionnement de bande de garde entre BWPs. L'alignement de cette solution dans l'architecture O-RAN est aussi discuté.

Ultérieurement, on garde toujours l'aspect multi-numérologies dans le problème mais on s'intéresse plutôt aux utilisateurs connectés simultanément à plusieurs slices qui nécessitent des numérologies différentes vu que dans les travaux précédents les utilisateurs étaient connectés à un seul slice uniquement. Pour ces utilisateurs, l'allocation des ressources radio est particulière puisque l'UE ne peut pas scanner plusieurs BWPs simultanément vu qu'une seule BWP peut être active à la fois. Par suite, la solution qui existe aujourd'hui pour ces utilisateurs dans le standard est que tous les slices utilisent la même BWP et la même numérologie. Mais ceci n'est pas efficace puisque certains slices nécessitent des numérologies différentes afin d'améliorer la qualité de service de chaque slice. Une autre solution possible est de configurer pour l'UE plusieurs BWPs et faire un basculement de BWP ou BWP switching pour ces utilisateurs afin que l'UE puisse récupérer les données de chaque slice. Par contre, le BWP switching génère une latence additionnelle qui peut être nuisible pour certains services comme URLLC. Par conséquent, notre

quatrième contribution propose trois mécanismes innovants de BWP switching qui permettent de réduire la latence globale dû à cet effet. Ces trois propositions sont comparées entre elles et avec le mécanisme de BWP switching qui existe dans le standard.

Pour la cinquième et dernière contribution, on s'intéresse à l'aspect efficacité énergétique de ces utilisateurs en proposant un algorithme qui sélectionne entre la configuration "single numerology" (une seule BWP pour tous les slices) et "multi-numerology" (BWP différente pour chaque slice) en se basant sur plusieurs facteurs comme le niveau de batterie et indicateur de performance du slice. Cette sélection se fait à travers deux approches, centralisée basée sur un problème d'optimisation et distribuée basée sur la théorie des jeux. On évalue la performance de ces approches en terme d'efficacité energétique en les comparant entre elles et à l'approche standard.

Abstract

With Fifth Generation (5G) Networks, multiple heterogeneous services are supported such as the enhanced Mobile BroadBand (eMBB) service characterized by high throughput demand, the Ultra-Reliable Low-Latency Communications (URLLC) service requiring a low latency and the massive Machine-Type Communications (mMTC) service favoring a high density of connected devices.

Thanks to slicing, these services can coexist on the same infrastructure. Slicing divides the network into multiple isolated logical networks named slices where each slice is attributed to a category of services.

Furthermore, standardization bodies such as the Open-RAN alliance (O-RAN) focus on the evolution of the Radio Access Network (RAN) architecture including RAN components disaggregation. This evolution brings in many advantages for the operator such as the introduction of artificial intelligence at the level of the controllers.

In this context of RAN evolution and slicing, the radio resource optimization is an important challenge for the mobile network operator to ensure Quality of Service (QoS) satisfaction for the different slices through efficient algorithms. Therefore, in this thesis, the objective is to propose various radio resource allocation algorithms based on the identification of the necessary Key Performance Indicators (KPIs) to take the appropriate decisions. Additionally, the proposed approaches are compared against each other and against other approaches from the state-of-the-art. Also, solutions implementation in an O-RAN compliant architecture is discussed.

Our first algorithm is based on Dynamic Weighted Fair Queuing (DWFQ) in a multi-slice and multi-Virtual Operator (VO) context. The aim of this algorithm is to determine the resource portion that will be attributed to each VO in each slice using game theory.

Next, we focus on the radio resource management at the level of a single operator. Therefore, the second contribution focuses on the radio resource allocation between two heterogeneous slices: eMBB and URLLC. Two approaches solve this problem where the radio resource allocation is based on traffic engineering. The first approach is a centralized one based on Deep-Q Networks (DQN) and the second is a distributed one based on a non-cooperative game.

In our third contribution, we add the numerology (subcarrier spacing) aspect to the previous problem, while considering three slices: eMBB, URLLC and mMTC. For this reason, we divide the total band into multiple Bandwidth Parts (BWPs) each linked to a numerology. This causes a new type of interference called Inter-Numerology Interference (INI). Therefore, we propose a three-level algorithm where the first level uses game theory to choose the BWP that will serve the URLLC users. The second level uses heuristics to determine the portion of radio resources attributed to each BWP. The third level uses DQN to dimension the guard bands between the BWPs using different numerologies to reduce the INI effect.

Subsequently, the multi-numerology aspect is retained in the problem, while considering multiple slices per user. For these users, an additional latency is induced due to BWP switching. The latter is necessary in order to retrieve the data of each slice. For this reason, our fourth contribution proposes three innovative BWP switching schemes that help to reduce the overall latency.

As for our final contribution, we focus on the energy efficiency aspect of such users by proposing an

algorithm that selects the most suitable BWP configuration: single numerology (a single BWP for all slices) or multi-numerology (different BWP for each slice) while taking into account multiple factors such as the battery level. This selection is done thanks to two approaches: a centralized one based on an optimization problem and a distributed one based on game theory.

Acronyms

3GPP	Third Generation Partnership Project
5G	Fifth Generation
AI	Artificial Intelligence
AMF	Access and Mobility management Function
API	Application Programming Interface
BDQ	Branching Dueling Q-networks
BS	Base Station
BWP	Bandwidth Part
CAPEX	Capital Expenditures
CCDF	Complementary Cumulative Distribution Function
CDF	Cumulative Distribution Function
CMDP	Constrained Markov Decision Process
CQI	Channel Quality Indicator
DCI	Downlink Control Information
DL	Downlink
DQN	Deep Q-Networks
DRL	Deep Reinforcement Learning
DRX	Discontinuous Reception
DWFQ	Dynamic Weighted Fair Queuing
eMBB	enhanced Mobile BroadBand
FIP	Finite Improvement Path
FR	Frequency Range
GB	Guard Band
gNB	next generation NodeB
GPS	General Processor Sharing
ICI	Inter-Carrier Interference
ILP	Integer Linear Programming
INI	Inter-Numerology Interference
IoT	Internet of Things
ISI	Inter-Symbol Interference
I-P	Infrastructure Provider

KKT	Karush-Kuhn-Tucker
KPI	Key Performance Indicator
LTE	Long Term Evolution
MAC	Medium Access Control
MARL	Multi-Agent Reinforcement Learning
ML	Machine Learning
mMTC	massive Machine-Type Communications
NE	Nash Equilibrium
NFV	Network Function Virtualization
near-RT RIC	near-Real Time RAN Intelligent Controller
Non-RT RIC	Non-Real Time RAN Intelligent Controller
NR	New Radio
OFDM	Orthogonal Frequency Division Multiplexing
OPEX	Operational Expenditures
O-DU	O-RAN Distributed Unit
O-RAN	Open-RAN Alliance
PDCCH	Physical Downlink Control Channel
PF	Proportional Fairness
PLMN ID	Public Land Mobile Network Identity
PNE	Pure Nash Equilibrium
PoA	Price of Anarchy
PRB	Physical Resource Block
QoS	Quality of Service
RAN	Radio Access Network
RL	Reinforcement Learning
RLC	Radio Link Control
RRC	Radio Resource Control
SCS	SubCarrier Spacing
SDN	Software-Defined Networks
SE	Stackelberg Equilibrium
SLA	Service Level Agreement
SINR	Signal-to-Interference-plus-Noise Ratio
SOTA	State-Of-The-Art
sTTI	short TTI
S-NSSAI	Single-Network Slice Selection Assistance Information
TDD	Time-Division Duplex
TTI	Transmission Time Interval
UE	User Equipment

UL	Uplink
URLLC	Ultra-Reliable and Low-Latency Communications
V2X	Vehicle-to-Everything
VO	Virtual Operator
WFQ	Weighted Fair Queuing

Contents

List of Tables

List of Figures

Chapter 1

Introduction

Network slicing and the evolution of the Radio Access Network (RAN) with the Open-RAN Alliance (O-RAN) architecture are enablers for reducing the mobile network operator's Capital Expenditures (CAPEX) and Operational Expenditures (OPEX). By making the RAN more flexible, open, efficient and autonomous, it can face the new challenges in terms of capacity and requirements for heterogeneous services in Fifth Generation mobile networks (5G) such as the Ultra-Reliable and Low-Latency Communications (URLLC) and massive Machine-Type Communications (mMTC) services in addition to the enhanced Mobile Broadband (eMBB) service. Among these challenges, radio resource optimization is an important one. In fact, the operator disposes of a limited amount of band that should be distributed astutely among the different services to ensure Quality of Service (QoS) satisfaction and high users' Key Performance Indicators (KPIs). This chapter presents the new challenges of a 5G mobile network operator along with the motivations behind the new mentioned features. Afterwards, the network slicing concept is addressed where we focus on RAN slicing in particular. Further, the evolution of mobile networks and the RAN are discussed where the O-RAN architecture is presented. Additionally, the radio resource allocation problem in this context is also discussed. Finally, the thesis objectives, the summary of contributions and the thesis organization are also detailed in this chapter.

1.1 5G Concepts and Services

Additional services with different QoS constraints are supported in Fifth Generation (5G) New Radio (NR) compared to its predecessor Long-Term Evolution (LTE) where only services requiring high throughput are supported. This creates a new challenge for the mobile network operator to support all these services by respecting the Service Level Agreement (SLA) of each class of service and ensuring QoS satisfaction. This SLA can take the form of minimum throughput, maximum tolerated latency, etc. Therefore, the main motive of 5G is to address these new heterogeneous demands and classes of service in terms of Key Performance Indicator (KPI) satisfaction, implementation, flexibility, security, scalability and isolation.

1.1.1 The Classes of Services in 5G

There are three main classes supported in 5G [5]:

- The enhanced Mobile Broadband (eMBB) service characterized by high data rates (up to 20 Gb/s in the downlink and up to 10 Gb/s in the uplink). This particular service requires a high bandwidth and is used for applications such as online streaming and gaming. Therefore, it necessitates a large payload but can tolerate a higher latency compared to other classes. Also, it is supported in LTE. Nonetheless,

5G NR aims to increase the data rate for this particular class with the increasing demand of mobile traffic.

- The Ultra-Reliable and Low-Latency Communications (URLLC) service distinguished by high reliability ($1 - 10^5$) and low latency with a tolerated target latency of 1 ms as stated by the Third Generation Partnership Projet (3GPP) [6][7][8]. It mainly concerns applications such as connected cars and connected medicine. The URLLC packets are composed of small payload, therefore this service does not require a high throughput.
- The massive Machine-Type Communications (mMTC) service requiring a high connection density of nodes (up to 1 Million connections/km^2) and a low energy consumption to improve devices' battery life and autonomy [9]. Similar to URLLC, mMTC packets are of small payload with a few bytes [10]. It is mainly used for Internet of Things (IoT) applications and can tolerate a higher latency than URLLC and a lower throughput than eMBB.

Table 1.1 summarizes the characteristics of each service.

Table 1.1: 5G Services

Service	Requirements	Applications
eMBB	High throughput High payload	Streaming, Gaming, etc.
URLLC	Low Latency High Reliability Low Payload	Connected cars, Connected medicine, etc.
mMTC	Low energy consumption High connection density Low Payload	IoT

1.1.2 Flexible Numerology and Radio Frame Structure

In order to support these various services, the flexible numerology concept was introduced where the numerology refers to the Orthogonal Frequency Division Multiplexing (OFDM) subcarrier spacing. When the latter is increased, the OFDM symbol duration is reduced which helps reducing latency for services such as URLLC [11]. In fact, in 5G NR and similar to LTE, a radio frame is fixed to 10 ms. This radio frame contains 10 subframes each of 1 ms. However, unlike LTE, the Subcarrier Spacing (SCS) is flexible and no longer fixed to 15 kHz [12]. A numerology μ designates a specific SCS. In fact, each subcarrier transports 1 OFDM symbol. Hence, we can observe the reduction of OFDM symbol duration with increasing numerologies.

A Physical Resource Block (PRB), which is the smallest unit of radio resources allocated to a user, is composed of 12 subcarriers in the frequency domain and a variable number of OFDM symbols in the time domain. A Transmission Time Interval (TTI) or slot is defined as 14 OFDM symbols in the time domain. Therefore, since the PRB and TTI depend on the OFDM symbol duration, their duration is reduced with a higher numerology. Consequently, a subframe contains a variable number of slots depending on μ.

Furthermore, to support low-latency devices such as URLLC, 5G NR proposes the use of mini-slots or short TTIs (sTTI) [13]. A sTTI is smaller than a TTI and it can occupy 2, 4 or 7 OFDM symbols in the time domain. It is mainly used to allocate resources to another device (URLLC) on an on-going slot to immediately serve the concerned URLLC user. Figure 1.1 represents the frame, subframe, TTI, sTTI, and PRB concepts in 5G NR.

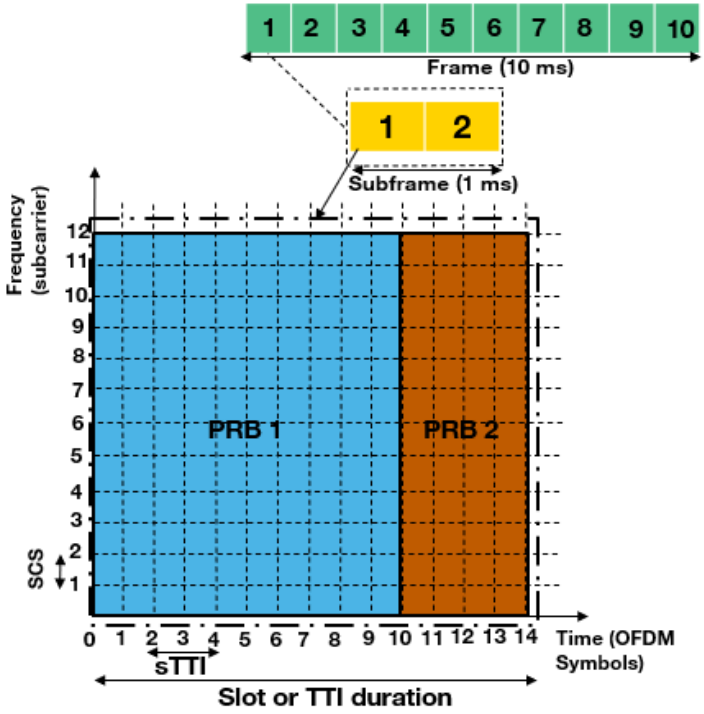

Figure 1.1: Frame, subframe, slot and PRB representations in 5G NR

However, there are multiple factors for the choice of numerology.

In fact, modifying the numerology does not only impact the TTI and PRB durations but can also affect the Doppler effect. The latter particularly impairs communications subject to high mobility. It destroys the orthogonality of OFDM subcarriers causing Inter-Carrier Interference (ICI) [14]. Nonetheless, a higher numerology mitigates the Doppler effect.

Simultaneously, Inter-Symbol Interference (ISI) is a resulting effect of the use of a higher numerology. In fact, ISI appears when the symbol duration is lower than the highest delay spread of the multi-path effect. Hence, with a higher μ, the symbol duration is reduced to a certain value that could be lower than the highest tolerated delay spread which induces ISI. Consequently, in 5G NR where two Frequency Ranges (FR) are adopted (FR1: sub-6 GHz and FR2: mmWave [12]), higher numerologies can be used with mmWaves that are associated with smaller cells where the risk of ISI is minimal, whereas lower numerologies are used in the sub-6 GHz.

Additionally, the choice of numerology depends on the concerned service. Smaller TTIs (higher numerologies) are used for services requiring stringent delays such as URLLC to reduce latency while larger TTIs (smaller numerologies) are preferred for services requiring high throughput such as eMBB since they offer higher spectral efficiency and larger transport block size to support higher payloads [15]. As for mMTC, it does not require a specific numerology and maintains the SCS of LTE ($\mu = 0$) as specified in the work in [16].

There are five supported numerologies in 5G NR where $\mu = 4$ can be used to broadcast signals at mmWave. Table 1.2 summarizes these numerologies along with their concepts for every numerology μ.

When multiple heterogeneous services are proposed by the mobile network operator, multiple numerologies on the same band may be used. For this reason, the concept of Bandwidth Part (BWP) is proposed in 5G NR [17].

Table 1.2: 5G Numerologies

μ	0	1	2	3	4
SCS (kHz)	15	30	60	120	240
OFDM Symbol Duration (μs)	71.35	35.68	17.84	8.92	4.46
TTI Duration (ms)	1	0.5	0.25	0.125	0.0625
Slots in one subframe	1	2	4	8	16
Subframes in one frame	10	10	10	10	10
Frequency Range	FR1	FR1	FR1-2	FR2	FR2
Doppler Effect	High	High	Low	Low	Low
Multipath Effect	Low	Low	High	High	High
Suitable service	eMBB/mMTC	eMBB	URLLC	URLLC	URLLC

1.1.3 BWP and INI

A BWP is a set of contiguous PRBs (a chunk of the band) scanned by the User Equipment (UE) and linked to a certain numerology as displayed in Fig. 1.2 [18]. The configured BWP can be narrower than the carrier bandwidth where the UE monitors this BWP to retrieve and send its signals. Since the UE is not monitoring the entire bandwidth, high energy efficiency is ensured.

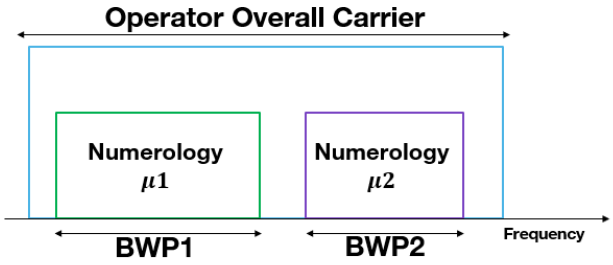

Figure 1.2: BWP Multi-Numerology Use Case

UEs can have up to four configured BWPs on the Downlink (DL) and four on the Uplink (UL) but only one BWP is active at a time. A BWP switch can be performed for UEs running different types of services using different numerologies and a default BWP is automatically configured for UEs that do not have a specific BWP configuration. The aim of this concept is to decouple the UE bandwidth from the carrier bandwidth for power saving purposes and multi-numerology use for multi-service support [19].

However, the use of multiple numerologies on the same band causes Inter-Numerology Interference (INI) due to the loss of orthogonality between subcarriers when different SCS are used. In fact, with OFDM, the subcarriers are orthogonal to each other. However, this orthogonality is only maintained if the subcarriers use the same SCS. Therefore, INI is the result of interference between subcarriers using disparate SCS as shown in Fig. 1.3 from the work in [1] that represents the interfering subcarriers using different numerologies with arbitrary units (a.u.).

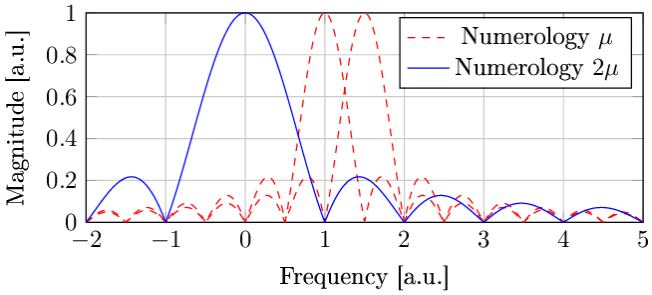

Figure 1.3: Interfering numerologies based on [1] with a.u. as arbitrary units

In fact, INI has been widely studied in the literature. There are many factors that impact the INI according to the works in [20, 21, 1, 22] which are summarized below:

- The SCS [20, 21, 1, 22]: the higher the numerology is, the less it is exposed to INI while smaller numerologies are more exposed to INI. Additionally, the higher the SCS offset, the higher the INI.
- The number of active subcarriers [20, 21, 22] knowing that the higher this number, the higher the INI.
- The power offset between different numerologies [20, 21] causing a higher INI.
- Windowing [20, 21, 1, 22] that helps reducing the INI.
- The use of a Guard Band (GB) [20, 21, 1, 22] that reduces the INI at the expense of reducing spectral efficiency.

Therefore, the use of a GB is highly recommended between BWPs using different numerologies.

While these concepts allow the support of the 5G three classes to a certain extent, network slicing remains a paramount enabler.

1.2 Network Slicing

Network slicing is an end-to-end solution, where the physical infrastructure is divided into multiple isolated logical networks called slices that can be customized to provide specialized and differentiated services. Note that network slicing could be further improved by employing Network Function Virtualization (NFV) (where the components are virtualized) and Software-Defined Networks (SDN) (where a separation between control and user planes occurs) [23]. Hence, slicing allows the coexistence of heterogeneous services on the same network by creating a slice for each service and ensuring isolation between them. Moreover, according to the current standards [24], a UE can be connected to up to 8 slices simultaneously. Additionally, the slice is identified by its Single- Network Slice Selection Assistance Information (S-NSSAI) and is built on top of the physical network which includes the Radio Access Network (RAN), transport and core networks [25] as can be seen in Fig.1.4.

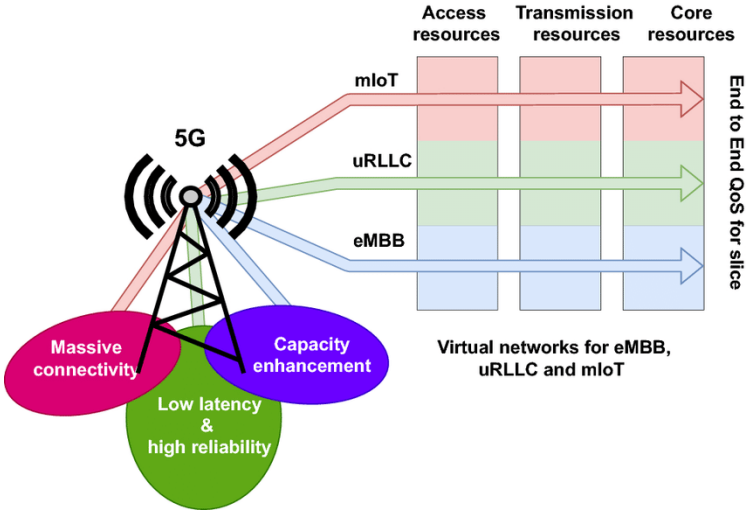

Figure 1.4: Network Slicing for the three 5G Classes [2]

In this thesis, we focus on radio resource management solutions for improving the performances of RAN slicing.

1.2.1 RAN Slicing

In the context of the end-to-end slicing process, the RAN takes an important role especially regarding the mechanisms for allocating radio resources. Radio resources need to be attributed in an efficient manner by allocating to each slice the appropriate amount of resources. Each slice or type of service will be attributed dedicated radio resources as can be seen in Fig. 1.5. Authors in [26] discuss RAN slicing along with its benefits and implementation challenges.

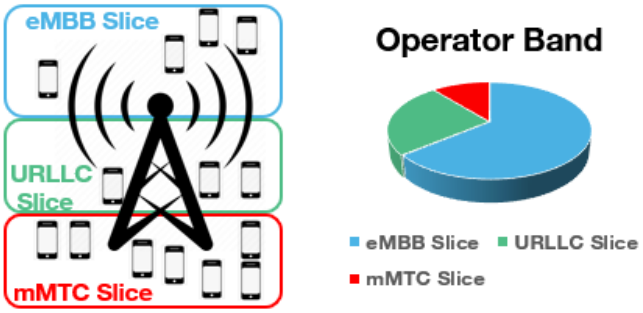

Figure 1.5: RAN Slicing for the three 5G Classes

Nonetheless, the evolution of the RAN architecture is an enabler for network slicing solutions. This is discussed in the next section.

1.3 Evolution of mobile networks

In 5G, the evolution of the core network is witnessed where the separation of the control and user plane functions using SDN has been implemented [27]. In addition, the virtualization of each component is possible. Thus, each entity is responsible of a specific function using NFV as can be seen in Fig. 1.6.

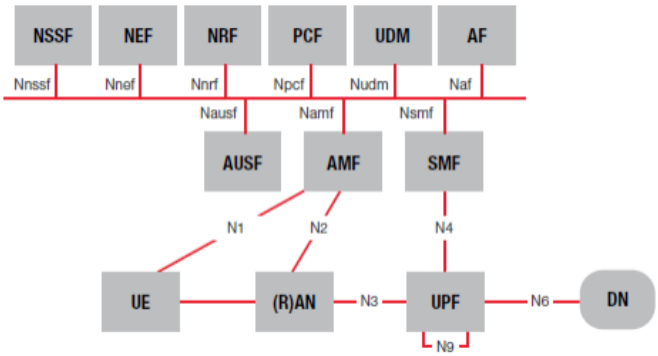

Figure 1.6: 5G Core Network [3]

However, this separation has not been fully done in the RAN. Moreover, to enhance the use of multiple slices, the same evolution on the RAN is required.

1.3.1 Evolution of the RAN

Standardization bodies such as 3GPP and the Open-RAN Alliance (O-RAN) [28] are focusing on RAN architecture evolution by disaggregating RAN components to have more efficient and smarter networks [4][28][29]. There are many advantages brought by this evolution including:

- Reduced Latency due to the disaggregation of components and optimization of the software stack
- Reduced Capital Expenditures (CAPEX) and Operational Expenditures (OPEX) by using open interfaces while exploiting NFV where any material can be used to ensure a specific function
- More efficient and intelligent RAN due to the intelligence introduced at the level of the RAN intelligent controllers
- Improved Radio Resource Management due to the implementation of efficient resource management algorithms
- Improved IT Resource Management due to elasticity

In fact, with the RAN evolution, the next generation NodeB (gNB) is no longer a monolithic entity where intelligence and functions are difficult to be added and updated. It will be decomposed to multiple entities where each entity is responsible of a specific function and protocol layer. This decomposition of the gNB is proposed as part of the O-RAN architecture.

1.3.2 O-RAN Architecture

The RAN architecture proposed by O-RAN is represented in Fig. 1.7.

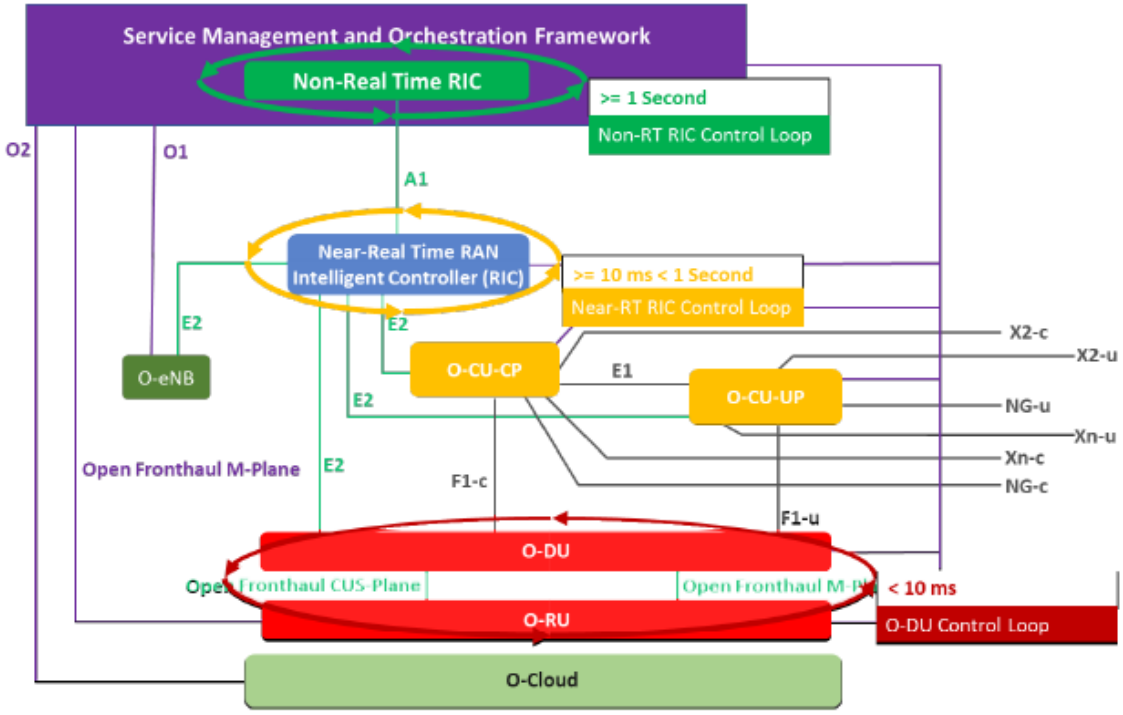

Figure 1.7: O-RAN Architecture [4]

There are several entities in that architecture where each is responsible of a specific function in the RAN. The most important ones that involve the radio resource allocation process are the following:

- The Non-Real Time RAN Intelligent Controller (Non-RT RIC): This entity is responsible of policies and control loops within a time scale larger than 1 s. Artificial Intelligence (AI), Machine Learning (ML), optimization, or game theory algorithms can be implemented at this level for policy optimization. An application running at this level is called rApp.

- The near-Real Time RAN Intelligent Controller (near-RT RIC): This entity is responsible of policies and control loops within an interval of 10 ms to 1 s. The model that was trained offline in the Non-RT RIC can be executed at the level of the near-RT RIC based on the network KPIs and other inputs. An application running at this level is called xApp.

- The O-RAN Distributed Unit (O-DU): It is the entity responsible of the higher physical layer, Medium Access Control (MAC) and Radio Link Control (RLC) layers. MAC layer is where the scheduler operates in order to perform radio resource allocation every TTI. Scheduling algorithms with a control loop smaller than 10 ms can be implemented at this level.

This RAN evolution will help solving radio resource optimization by the implementation of intelligent resource allocation algorithms.

1.4 Radio Resource Optimization

In this slicing and RAN evolution context, radio resource optimization remains a paramount challenge for a mobile network operator. In fact, the latter owns a limited amount of band which is its scarce resource.

Therefore, the partitioning and allotment of this band among the different slices and users should be performed efficiently and astutely. This particular problem is at stake since it will affect users' performance and services' KPIs. Additionally, a static slicing scheme (where the amount of resources attributed to each slice is fixed) is not an efficient solution due to the sporadic nature of traffic. Therefore, a dynamic slicing algorithm taking into account the users' KPIs, traffic and radio conditions is required especially when multiple parameters come into play such as the numerology, INI and incurred monetary cost. Also, the type of service should be considered as resources may be attributed differently depending on the service.

1.4.1 Radio Resource Allocation for eMBB and URLLC

From a radio resource management perspective, eMBB requires high throughput for its high payload. Therefore, a larger bandwidth should be attributed for this service. The higher the number of PRBs attributed to the user, the higher its QoS satisfaction. This is not the case for the URLLC service which requires a low latency and has a small payload. Therefore, the availability of PRBs is only required for this service instead of the high number of offered PRBs to ensure prompt service. In fact, 3GPP proposes two scheduling options for the coexistence of these 2 services to satisfy their KPIs [30]:

- Orthogonal scheduling where the resources for eMBB and URLLC are separated and an amount of bandwidth is dedicated to the URLLC service as displayed in Fig. 1.8. This option is possible thanks to slicing and radio resource partitioning where each service has dedicated radio resources. The use of multiple numerologies for each service is possible with this option since each service may have a different bandwidth part and a higher numerology can be used for URLLC bandwidth. With this option, two reservation mechanisms are considered: *semi static* where the Base Station (BS) intermittently broadcasts the frame structure including the numerology and *dynamic* where the frame structure is updated regularly. The drawback of this approach is that it can lead to a waste of radio resources in the absence of an efficient radio resource allocation when there are no active URLLC users. Hence, dynamic slicing should be considered.
- Preemptive scheduling where the URLLC packets are scheduled on top of ongoing eMBB transmissions to ensure prompt service and low latency using sTTI as can be seen in Fig. 1.9. Hence, some eMBB users' transmission will be interrupted for short TTIs to schedule URLLC packets. Two mechanisms are considered for this approach: *puncturing* where eMBB transmissions are allocated zero power when URLLC traffic is overlapped and *superposition* where the BS chooses non-zero transmission powers for eMBB and URLLC users. Since the URLLC scheduling occurs on top of eMBB transmission, a single numerology should be used for both services as they are sharing the same PRBs and therefore the same BWP. The drawback of this option is the degradation of eMBB performance with URLLC prioritization.

Figure 1.8: Orthogonal Scheduling for eMBB and URLLC coexistence

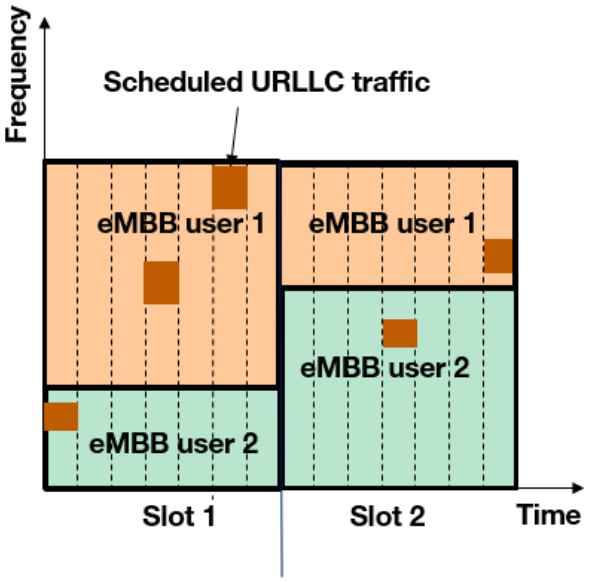

Figure 1.9: Preemptive Scheduling for eMBB and URLLC coexistence

Hence, both these options should be considered when managing radio resources.

1.4.2 Radio Resource Allocation for mMTC

As for the mMTC service, it is not demanding from a radio resource management perspective and it only requires a high connection density and number of connected devices [31]. In fact, the mMTC service tolerates a lower throughput than eMBB and a higher latency than URLLC as specified in Table 4 from the work in [16]. Furthermore, the main requirements for mMTC are low energy consumption and high connection density which can be better tackled from an energy efficiency perspective which is not the main focus of this thesis. Therefore, taking into account this class is not complicated.

1.4.3 Users connected to multiple slices

Other aspects that should be considered when allocating radio resources include users connected to multiple slices as they should be treated differently from users connected to a single slice due to additional complexity. Practically, one user can be associated to eight different slices. Hence, a one-to-M mapping between one user and different slices is possible where $M_{max} = 8$ [24]. In fact, users connected to multiple services may be configured with multiple BWPs as each service may use a different numerology. Nonetheless, since only one BWP can be active at a time and scanned by the UE, a frequent BWP switching should be performed for these UEs to retrieve the data for each service or slice if these services use different numerologies. Therefore, two BWP configuration options are envisaged for these users:

- Single numerology and BWP where all services use the same numerology and BWP. This option avoids complex BWP switching and additional delays and is currently adopted as the baseline approach for these users in the standard. Nevertheless, it is not optimal to use the same numerology for all services as heterogeneous services may requires different numerologies to optimize performance for each service. For example, URLLC requires a higher numerology. Also, since a single BWP is scanned by the UE, this option may reduce energy consumption when a narrow BWP is selected for all services.

Table 1.3: DCI-Based BWP Switching Delay

SCS (kHz)	Slot Duration (ms)	Switch Delay in time slots UE type 1	Switch Delay in time slots UE type 2
15	1	1	3
30	0.5	2	5
60	0.25	3	9
120	0.125	6	18

- Multi-numerology where each service may use a different numerology to optimize its QoS performance but at the cost of additional delays due to BWP switching. In addition, this option may increase energy consumption due to scanning different and wider BWPs.

When adopting the multi-numerology option, multiple ways can be used to perform a BWP switch including:

- The BWP inactivity timer where a BWP switch to the default BWP is performed after a certain time of inactivity by the UE.
- The Downlink Control Information (DCI)-Based BWP Switch which is the fastest method to perform a BWP switch where the DCI indicates a change of BWP [18].

The DCI is a set of information transmitted by the BS to the terminal through the Physical Downlink Control Channel (PDCCH) including information about users' scheduled data in the frequency and time domain, BWP indicator, and modulation and coding scheme [32]. It has multiple formats including DL, UL, reduced overhead and can be used to indicate a change of BWP after a modification of the BWP indicator which is included in the DCI destined for the UE. When this happens, a BWP switch is performed with a predefined switching delay given by Table 1.3 [18][33]. An additional note is that when the BWP switching requires a change of numerology (SCS), the switching delay is determined based on the smaller numerology or SCS from the table. Additionally, for the inactivity timer BWP switching, the switching delay to the default BWP after the expiry of BWP inactivity timer is the same as the DCI-based BWP switching delay [18]. Furthermore, the current baseline process for multi-slice users adopting the multi-numerology option is to perform a DCI-Based BWP Switch each time the UE is retrieving its data from different services as can be seen in Fig. 1.10. Hence, the UE retrieves its eMBB data on BWP 1 after decoding its first DCI. Afterwards, it decodes the

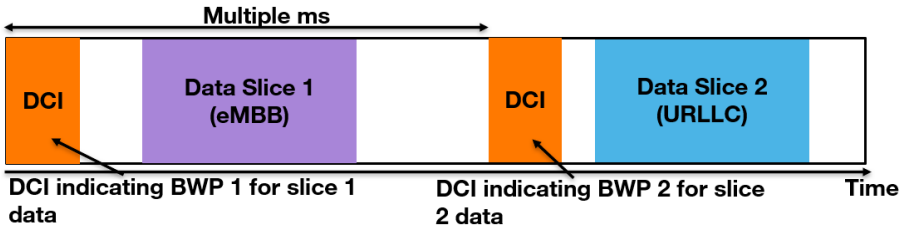

Figure 1.10: Current BWP Switching Process for Users Connected to Multiple Slices

second DCI specifying a BWP Switch and retrieves its URLLC data on BWP 2. Therefore, the UE must wait for the next DCI to perform the BWP switch, which could occur after multiple time slots (multiple ms) [34], incurring an additional delay that could violate the maximum tolerated latency of 1 ms for URLLC services [6]. Hence, the radio resource allocation problem is challenging for these users depending on whether to prioritize QoS performance or reduce additional delays and energy consumption.

1.4.4 Modeling Tools for the Radio Resource Allocation Problem

In the literature, a variety of tools are used to model the radio resource allocation problem ranging from simple heuristics and game theory to complex optimization problems and Artificial Intelligence (AI) and Machine Learning (ML) techniques. Thus, we introduce key concepts of the tools mostly used in the scope of this thesis to model the various problems. These tools rely on optimization problems, Deep-Q Networks (DQN) and game theory presented hereafter.

Optimization Problems

An optimization problem is a problem where we define a certain objective function that should be maximized or minimized by choosing adequate decision variables. The defined problem can be subject to certain equality and inequality constraints. The decision variables can be either continuous or discrete and the devised problem can be either linear or non-linear depending on the objective function and constraints.

For non-linear convex problems (where the objective function and the constraints are convex), we can use the Karush-Kuhn-Tucker (KKT) conditions to find the optimal decision variables. These KKT conditions are first-order derivative tests where first-order derivatives as well as equality and inequality constraints are taken into account.

Another form of optimization problems is Integer Linear Programming (ILP) where the variables take integer values and the objective function and constraints are linear. For these ILP problems, we can use the CPLEX solver to solve them. The CPLEX solver can be downloaded and integrated in programming platforms such as Matlab and Python.

DQN Background

Deep Q-Networks is a ML method where a certain agent takes an action which moves the state of the environment from one to another while generating a certain reward to assess the benefit of the action. Each state has a value function which is the expected return or estimate of future rewards that can be received from that state. Hence, it evaluates and measures the benefit of ending up in the latter state. Consequently, it is also important to evaluate the effectiveness of a state-action pair which is also called Q-value and is none other than the value function of the state-action pair. The relationship between the state value function and action-state value function is expressed in the following equation (1.1):

$$V(s) = \max_{a} Q(s, a) \tag{1.1}$$

In this equation, $V(s)$ is the value function of state s and $Q(s, a)$ is the value function of the state s and action a pair.

The learning process of the agent is based on a trial-and-error process where the agent interacts and explores the environment to take the most adequate decision and follow the best policy. The optimal decisions can be taken thanks to these Q-values which are learned by the agent using this formula:

$$Q_{new}(s, a) = Q_{old}(s, a) + \alpha_t[R + \gamma \max_{a_*} Q(s', a_*) - Q_{old}(s, a)] \tag{1.2}$$

where α_t is the learning rate and γ is the discount factor. Based on Equation (1.2), the Q-value of an action-state pair (s, a) is obtained via bootstrapping by adding the Q-value of the previous iteration to the temporal difference multiplied by the learning rate. The temporal difference is none other than the immediate reward R from moving from state s to state s' to which we add the estimate of the value

function of state s' multiplied by a discount factor and then subtract the Q-value of the previous iteration. Additionally, neural networks are used with DQN to find the approximate values of Q-values. In that case, the states are the inputs for the neural networks and the outputs are the corresponding Q-values per action that will be determined via training. To enhance the training data set and avoid any correlation of the data, DQN uses experience replay which relies on storing and sampling the data randomly to have appropriate Q-values. Once these Q-values are learned, the optimal strategy and policy can be followed after finding a balance between exploration of the unknown and exploitation of known results which is done using an ϵ-greedy strategy where the agent chooses a random action with probability ϵ and the best learned action with probability $1 - \epsilon$. By fine-tuning ϵ, the algorithm converges to the optimal strategy based on the Q-values.

Thus, the following elements should be defined in a DQN context:

- The agent taking the decisions.
- The environment and its states.
- The possible actions taken by the agent.
- The reward function used to assess the benefits of the actions.

Non-Cooperative Games

Non-Cooperative Games are a branch of game theory mainly used to model a competition between rational players where each player seeks to select a strategy that optimizes its cost or utility function in a selfish and autonomous manner. In a non-cooperative game, it is important to define:

- The set of players.
- The set of strategies or actions of each player.
- The set of objective functions (utility or cost functions) that the players attempt to optimize.

In these games, we seek the Nash Equilibrium (NE) which is an equilibrium state where each of the players attains its optimum in response to other players' strategies and where no player profits from deviating from such an equilibrium unilaterally. Some games may possess mixed NEs instead of a Pure NE (PNE). With Mixed NEs, the players randomize and mix between different actions depending on a probability distribution. This is different from Pure NEs where players select a single action. Therefore, the existence of the PNE and the way to attain it depend on the devised game. In fact, finite games (games that should end after a finite number of moves) are guaranteed to possess at least one mixed NE. Nonetheless, in most of our contributions, we were able to prove the existence of a PNE for these games thanks to the Finite Improvement Path (FIP) property [35]. In fact, these types of games feature the existence of a potential function which commonly represents the quality of the different strategy profiles for all players [36]. Hence, the change of a user strategy leads to a change in its cost function equal to the change in the potential function, leading to convergence to a PNE.

When a game $\mathcal{G}$ is an unweighted non-cooperative game where players only have 2 strategies, it has the FIP property according to [37]. In an unweighted game $\mathcal{G}$, users share a common set of actions and the cost function of a player after its strategy selection is specific to that user only and is non-decreasing in the number of players selecting the same strategy. Moreover, games with FIP are guaranteed to converge to PNE through Best Response dynamics [38].

A possible implementation of the Best Response algorithm is as follows:

Each player in turn, will choose the strategy minimizing its cost function in response to other players' strategies till convergence is reached where the chosen strategies of each player are the same from the previous round.

Thus, once we prove that the targeted game has the FIP property, we can resort to the best response dynamics to attain the PNE.

Stackelberg Game

A Stackelberg Game is a two-stage non-cooperative game which also belongs to a game theory branch. In the first stage, a certain player or a leader moves first by selecting a certain strategy that optimizes its utility or cost function. Afterwards, in the second stage, other players or followers move after this leader by selecting their adequate strategies following the leader's action in a non-cooperative manner. In this type of game, we seek the Stackelberg Equilibrium (SE) which is a NE between the leader and the followers. To reach this state, certain game conditions should be met to prove its existence and uniqueness. Additionally, we can use the backward induction method to find the SE where we first find the optimal solution of the second stage and use it to find the optimal solution of the first one at the level of the leader.

Finally, all of these tools are the most important ones that are used in our thesis work to model the radio resource allocation problem in the context of slicing and RAN evolution. This problem is an important topic for a mobile network operator. For this reason, it is the main focus of this thesis whose objectives are detailed in the next section.

1.5 Thesis Objectives

As mentioned, this thesis focuses on the radio resource optimization in the context of slicing and RAN evolution which will help a mobile network operator to improve users' KPIs and services' QoS. This facilitates the support of multiple slices. Thus, the main objectives of our work are the following:

- Propose innovative radio resource allocation mechanisms while benefiting from open interfaces of the O-RAN architecture and slicing
- Identify the necessary KPIs needed for the radio resource allocation problem
- Model the radio resource allocation problem while considering all the mobile network's constraints
- Simulate the proposed solutions and compare them to other solutions from the state-of-the-art

To attain these objectives, many algorithms and mechanisms are proposed in this context through our thesis contributions which are presented in the next section.

1.6 Thesis Contributions

There are many aspects to consider for the radio resource allocation problem in a multi-slice setting including the multi-Virtual Operator (VO) aspect, the services heterogeneity and KPIs, the multiple numerologies and users' multi-slice connectivity. For this reason, we propose new algorithms taking into account these aspects. We start by a general approach and then we zoom into the specifics by adding recursively a layer of complexity to the problem. Hence, our first contribution tackles the radio resource allocation problem for a multi-VO context where we aim to determine the band allotted to each VO from the Infrastructure Provider (I-P)'s radio resources depending on the incurred monetary cost. Next, our second and third

contributions tackle this problem at the level of a single VO for users connected to a single slice where we distribute dynamically the radio resources of the VO between heterogeneous slices. The second contribution proposes a slicing radio resource management algorithm for the eMBB and URLLC slices but without taking into account the numerology, the mMTC slice and users' radio conditions and arrival process whereas the third contribution considers these missing aspects. Finally, we conclude our work with the fourth and fifth contributions where the radio resource allocation problem takes into account users connected to multiple slices. Particularly, the fourth contribution considers this problem from a latency perspective where we aim to reduce it by proposing new BWP switching schemes and the fifth contribution tackles it from an energy efficiency perspective where we dynamically choose for each user the BWP configuration (multi-numerology or single numerology) based on energy efficiency and QoS parameters.

A Multi-Slice Multi-Operator Dynamic Weighted Fair Queuing RAN Scheduling in a Game Theoretic Framework

In our first contribution, we tackle the problem from a general and simple perspective where multiple VOs compete over radio resources provided by an I-P. Each VO is identified by its Public Land Mobile Network Identity (PLMN ID) and the total band owned by the I-P is divided statically between multiple slices. In each slice, the VOs share the radio resources where each is attributed a specific portion and number of PRBs based on its PLMN-ID and S-NSSAI. A lot of works from the State-Of-The-Art (SOTA) focus on the dynamic resource allocation between slices. However, less focus is put on the resource allocation at the slice level, particularly when multiple VOs are sharing the resources within a slice [39][40][41][42]. Therefore, the objective of this work is to optimize resource allocation among competing VOs in a slice using two approaches:

- A centralized approach based on a Stackelberg game steered by the I-P that seeks to maximize the monetary revenue provided by VOs whereas the latter try to strike a balance between maximizing the obtained slice throughput and reducing the cost incurred by the I-P.
- A distributed approach based on a non-cooperative game where VOs compete over radio resources in a way that reduces the incurred cost to be paid to the I-P while maximizing their slice throughput.

The scheduling of VOs in a slice is based on the Dynamic Weighted Fair Queuing (DWFQ) algorithm which was previously used for scheduling multiple services with different throughput requirements in a single network [43]. In fact, Weighted Fair Queuing (WFQ) [44] is a General Processor Sharing (GPS)-like scheduling algorithm known to guarantee a fraction of the total capacity deemed "weight". It is envisaged to provide a set of Application Programming Interfaces (APIs) to regulate the WFQ weights dynamically in accordance to the VOs fluctuating needs per slice. Therefore, the objective of this work is to propose an algorithm that determines the optimal weights and monetary cost to be paid by the VOs using both approaches while aligning this solution with the O-RAN architecture.

Crowding Game and Deep Q-Networks for Dynamic RAN Slicing in 5G Networks

After proposing an algorithm that determines the amount of portion allotted to each VO by the I-P, we focus on a single VO where the radio resource allocation between its slices is dynamically tackled specifically for two heterogeneous services eMBB and URLLC since the slices were not differentiated in the previous contribution. In this contribution, a single numerology is considered and a dynamic RAN resource allocation algorithm is proposed based on traffic engineering. It efficiently attributes resources to each slice

depending on the slice's SLA by affecting users to slices that may differ from their service types if their performance target is met. Hence, a user can be attributed PRBs dedicated to another service. Furthermore, the resource allocation between slices is adjusted based on the slice load and users' performances admitted in the slice. This algorithm is applied via two approaches: a distributed approach based on a non-cooperative crowding game and a centralized approach based on Deep-Q Networks (DQN) where the slice allocation to users of any service type is performed by an intelligent entity depending on the QoS constraints. Both schemes are compared against one another and against another work from the SOTA and the implementation of both schemes in the O-RAN architecture is discussed.

A Three-Level Slicing Algorithm in a Multi-Slice Multi-Numerology Context

In the third contribution, the numerology aspect, the mMTC slice, preemptive and orthogonal scheduling, the radio conditions of users as well as their traffic conditions are added to the previous problem for a single operator. Therefore, a three-level slicing algorithm that allocates resources to each of the three 5G classes (eMBB, URLLC and mMTC) is proposed in this context where:

- The first level selects the numerology-specific BWP that will serve URLLC users between two BWPs: one that is shared with eMBB users using a lower numerology and where preemptive scheduling occurs and the second is dedicated to URLLC users using a higher numerology. This level uses game theory.
- The second level allots the band for each BWP to determine the number of resources attributed to each slice using heuristics.
- The third level uses DQN to dimension a guard band between BWPs using different numerologies to avoid INI and radio resource wastage.

This algorithm is compared to the previous work and to another work from the SOTA. Its implementation in the O-RAN architecture is also discussed.

Novel BWP Schemes for Multi-Numerology and Multi-Slice Radio Access Networks

In the fourth contribution, attention is brought to users connected to multiple slices which are rarely considered in the SOTA. For these users, the multi-numerology BWP configuration improves slice's QoS performance since each slice will use its appropriate numerology but at the cost of inflicting additional delays due to BWP switching. For this reason, we propose three novel BWP switching schemes that help reduce overall latency:

- The first solution relies on the DCI format modification to include multiple BWPs to be scanned by the UE.
- The second solution adjusts the DCI frequency by increasing it for users connected to multiple slices.
- The third solution adjusts the BWP inactivity timer and default BWP to prioritize a premium service over another.

These three solutions are compared against each other and against the current BWP switching (baseline) process.

Energy efficient BWP Configuration for Multi-Slice Users

For the fifth and final contribution, the same type of users as the previous work are studied but from an energy efficient perspective. Therefore, we propose two algorithms: a distributed one based on a congestion game and a centralized one based on an optimization problem where we select for each multi-slice user the appropriate BWP configuration between the multi-numerology and single numerology configuration depending on the users' battery level and other energy efficiency parameters. Both algorithms are compared against each other and against the standardized BWP configuration for these users.

1.7 Thesis Organization

The remaining of this thesis is organized as follows: the radio ressource allocation problem in the context of RAN evolution and slicing is surveyed in chapter 2. In this chapter, a wide review on the existing approaches in the SOTA is detailed, after which we summarize the existing works. Chapter 3 presents the radio resource allocation problem in a multi-slice and multi-VO context. Performance evaluation of the proposed algorithms is discussed along with the implementation of these solutions in the O-RAN architecture. Then, the next chapters focus on radio resource allocation for users connected to a single slice. In chapter 4, we focus on a single VO and propose dynamic slicing algorithms using two approaches that efficiently attribute the radio resources for two slices eMBB and URLLC without consideration of the numerology. The efficiency of these algorithms compared to another work from the SOTA and their implementation in the O-RAN architecture are discussed. Chapter 5 describes a three-level slicing algorithm solution that allocates the radio resources for three slices: eMBB, URLLC and mMTC in a multi-numerology setting while taking into account users' radio conditions, INI and traffic arrival which were not considered in previous contributions. Therefore, the complexity of the problem is increased with the numerology and users' aspects. This algorithm is evaluated in both low and high traffic modes and compared to other works from the SOTA including our previous work. Additionally, its compliance with the O-RAN architecture is discussed.

In chapter 6, we shift our attention from users connected to a single slice to the radio resource allocation problem for users connected to multiple slices where we propose three different solutions to improve the BWP switching process for these users by reducing overall latency and improving the slices' QoS specifically for the multi-numerology scenario. The proposed solutions are compared against each other and against the baseline BWP switching process.

In chapter 7, the same multi-slice users are studied from an energy efficiency perspective where the radio resource allocation is based on a dynamic selection between the single and multi-numerology BWP configuration options using a centralized and distributed approach. These approaches are compared against each other and against the baseline approach.

Chapter 8 concludes the thesis and enlists the short, medium and long term perspectives for future work.

Chapter 2

Radio Resource Allocation in the Context of Slicing and RAN Evolution in the Literature

Given that radio resource allocation is an important topic to improve users' performance, dynamic slicing where resources attributed to each slice are dynamically adjusted has been widely studied in the literature in various contexts: multi-numerology, heterogeneous services, downlink, uplink, etc. These works also use many tools from game theory and ML methods to simple heuristics. This chapter focuses on the SOTA existing solutions in the same context of our work while providing an overview of the dissimilarities of these works compared to ours. First, a survey on radio resource allocation in a multi-VO context is presented. Next, the works tackling this problem in the context of heterogeneous services are discussed. Then, works taking into account the numerology aspect are detailed. Afterwards, the radio resource allocation problem for users connected to multiple slices in the SOTA is explored. Finally, we conclude with a highlight on the differences of these works from ours.

2.1 Radio Resource Allocation for Multi-VO

A number of works in the literature propose a solution for the allocation of a bandwidth to each VO by the I-P. For example, the proposed solution in [45] takes into account the interaction between the I-P and the VOs according to a Stackelberg Game. With this solution, the I-P seeks to maximize its monetary profit while the VOs try to maximize their bandwidth allocation. Another work [46] in the same vain uses a multi-leader multi-follower Stackelberg game where the leaders are the wireless backhaul providers and the followers are the wireless access providers. Additionally, optimization techniques were used in [47] to allocate the radio resources among different operators while taking into account the channel conditions constraints.

In the scope of this thesis, we adopt the same approach to represent the radio resource allocation problem for multiple VOs while adding the slicing context which was missing from the mentioned works except the work in [47]. Nonetheless, in our work, channel conditions are not considered to determine the resources for each VO since this problem is tackled from a higher level whereas radio conditions are considered at a lower level when solving the resource attribution for each service at the level of a single VO. Therefore, we first determine the band allotted to each VO by the I-P to decide later on how to distribute this VO allotted band between its different services and slices. Particularly for the band attribution to each VO, a Stackelberg game where a sole leader is the I-P and the VOs are the followers and a non-cooperative crowding game are used to model the problem in a multi-slice setting. In addition, unlike these works, the

DWFQ scheduling algorithm is used to dynamically partake the slice capacity according to weights tasked by the different VOs. In fact, DWFQ has been previously used for scheduling of different types of services with different QoS constraints ([44],[43]), whereas in the scope of our work, it is used for the allocation of slice resources among different VOs depending on the monetary cost which is rarely taken into account.

2.2 Radio Resource Allocation in a Single VO Multi-Slice Context

Radio resource attribution to different slices or RAN dynamic slicing [26] has been widely tackled in the SOTA using many techniques. For example, the work in [48] focused on the dynamic RAN slicing for elastic types of services. Authors in [49] propose a dynamic RAN slicing solution for radio resource allocation between slices based on networks' KPIs and traffic classification. Game theory was used to address the dynamic RAN slicing problem for inelastic services in some works such as the work in [50]. Many other works used ML and Reinforcement Learning (RL) techniques for resource allocation between slices such as the works in [51], [52], [53]. In [51] and [53], Multi-Agent Reinforcement Learning (MARL) was used to dynamically allocate the slice resources based on the SLA satisfaction per capacity utilization. Particularly for [51], the solution has been aligned with 3GPP and O-RAN specifications. In other works such as [52], Neural Networks were used to dynamically allocate the resources based on KPIs and to calibrate the QoS parameters as agreed upon in the SLA. Other tools were witnessed in some works including [54] where authors solved the RAN slicing resource allocation and admission control optimization problem using Lyapunov Optimization while the work in [55] tackled this problem using fuzzy logic. Different from our work, the previously cited works were based only on bandwidth allocation adjustment for each slice whereas in our work, traffic engineering is used where the slice serving the user is selected in addition to a dynamic readjustment of slice resources.

Some works ([56], [57]) tackled this problem in a multi-cell context using game theoretic solutions for resource allocation in a multi-cell context whereas other works such as [58] considered a single BS and addressed the resource allocation problem considering two services URLLC and eMBB. In fact, many works tackle this problem for two slices eMBB and URLLC as these two services are the most demanding from a radio resource allocation perspective and where both orthogonal and preemptive scheduling are investigated. Some tackle it via preemptive scheduling such as [58] where it is settled by solving an optimization problem modelling the assignment of a mini-slot to URLLC users inside a PRB allocated to eMBB users. Similarly, the work in [59] tackles this preemptive scheduling approach by applying Deep Reinforcement Learning (DRL) to improve eMBB performance while taking into account the URLLC constraints. Also, authors in [60] propose an optimal approach for preemptive scheduling using a multi-objective Integer Linear Programming (ILP) problem formulation. Others tackle it via orthogonal scheduling such as the work in [61] where the resources of each service were separated thanks to slicing and a two-timescale algorithm based on Lyapunov Optimization was introduced to efficiently allocate the bandwidth for each slice on a long-timescale and to control the power consumption and user satisfaction on a short-timescale. Another example of orthogonal scheduling is the work in [62] which proposes a proactive resource reservation mechanism for URLLC users in a multi-cell context taking into account multiple factors including eMBB performance. Furthermore, the work in [63] proposed a dynamic RAN virtual resource allocation scheme for sub-channel allocation and power control based on a Constrained Markov Decision Process (CMDP) to allocate these resources between three slices. However, these works focus only on one option (orthogonal scheduling or preemptive scheduling) while we factor in our work both options.

Other interesting approaches to tackle this problem are a RAN slice selection algorithm which are

used in [64] and [65]. In [64], a RAN slice selection algorithm is proposed based on throughput, delay and blocking rate satisfaction degrees. The problem was settled by solving a Knapsack problem. Nonetheless, the authors did not consider a resource allocation scheme based on the slice monetary cost and service type. Additionally, an adjustment of the resource allocation between slices was not taken into account as the bandwidth for each slice was fixed. This is not the case for the work in [65] which tackles the dynamic RAN slicing problem based on both a slice selection process and a resource allocation adjustment between slices using a non-cooperative crowding game and its alignment with the O-RAN architecture. In the scope of this thesis, similar to the work in [65], we use both traffic engineering based on a slice selection process similar to the work in [64] and a dynamic readjustment of slice resources. We also extended the work in [65] by proposing a redefined game theoretic algorithm and a centralized DQN algorithm while adding the numerology aspect as well as users' radio conditions.

Additionally, few works have mapped their solution with an existing O-RAN architecture ([66],[51]). In fact, the work in [66] discussed the main challenges that should be standardized in O-RAN, while evaluating the performance of a dynamic resource allocation algorithm that selects the best-suited scheduling algorithm from a predefined set of scheduling algorithms using DRL while authors in [51] use ML to propose an O-RAN compliant solution for the inter-slice radio resource allocation problem. Also, the work in [67] proposes a RL-based framework that adapts the radio resource scheduling. This solution is also deployed as an xApp in the near-RT RIC. Another work in [68] mitigates the conflicts between multiple xApps to enhance the performance of power allocation and radio resource management thanks to a team learning approach which improves cooperation between these xApps. Nonetheless, these works only consider the throughput and bit rate as KPIs and they are based only on re-dimensioning the slices by increasing the allocated bandwidth instead of better using the available bandwidth through savvy traffic engineering. In addition, these works did not address the multi-numerology problem between different services which is considered in the scope of the thesis.

In fact, in the scope of our work, we first tackle the radio resource allocation problem between slices at the level of a single VO by considering only eMBB and URLLC. The problem is solved by proposing an algorithm using traffic engineering and a dynamic readjustment of slice resources based on users' KPIs. The proposed algorithm is tackled via two approaches: a distributed one based on a congestion game and a centralized one based on DQN. Afterwards, we propose another solution where we add to this problem the mMTC slice, the numerology aspect, users' radio conditions and users' arrival process. In addition, both options preemptive and orthogonal scheduling are taken into account in this work. This is done by considering a BWP that is shared between eMBB and URLLC slices using the same numerology with preemptive scheduling and another BWP dedicated solely for the URLLC slice using a higher numerology (orthogonal scheduling). In addition, instead of studying and optimizing the scheduling of URLLC packets on top of eMBB transmissions, we rather focus on the selection of the numerology-specific BWP that should be scanned by each URLLC user in a way that improves eMBB performance which might be impacted by the preemptive scheduling.

2.3 Radio Resource Allocation in a Multi-Slice Multi-Numerology Context

Since we consider the numerology aspect in our work, works tackling this concept in the literature should be reviewed. In fact, several works in the SOTA delve in the numerology selection problem. For example, in [15], authors use ML to select the most suitable TTI for eMBB and URLLC services. Authors in [14] propose a numerology selection algorithm based on the varying channel conditions including the radio conditions,

doppler spread and delay spread for Vehicle-to-Everything (V2X) services. Nonetheless, these works use a dynamic approach for the numerology selection problem where the numerology used throughout the entire bandwidth is modified based on multiple KPIs and channel criteria. This is different from the approach used in our work where multiple numerologies are used on the same band and a dynamic numerology selection process is performed for URLLC users.

Since the use of multiple numerologies on the same band causes INI, some works focus on this problem. For example, authors in [69] propose a Guard Band (GB) implementation to reduce INI without spectral efficiency loss. Moreover, the work in [70] reduces the need for adaptive GBs by proposing an astute interference-aware scheduling algorithm. This is similar to a part of the problem tackled in our work with the proposal of a three-level algorithm. Nonetheless, in our work, we select a GB from a predefined list from the 3GPP standards [12] using a DQN reward function that depends on the BWP band attributions, network parameters, and users' KPIs. Finally, the work in [71] derives an analytical model for the Inter-Numerology Interference. In our work, we use these findings to formulate the problem and set the hypothesis taking into account the INI as well as using the formulated analytical expressions to measure the INI and propose ways to reduce it through smart radio resource allocation.

In fact, in our work, we focus on the radio resource allocation between different slices in a multi-numerology setting while mitigating the INI and selecting the appropriate numerology-specific BWP for URLLC users. A number of similar works from the literature tackle the radio resource allocation problem for eMBB and URLLC in a multi-slice and multi-numerology context. For example, the work in [72] studies the performance of two scenarios, with and without slicing, while selecting the optimal numerology and packet scheduler. However, the INI and dynamic resource allocation between slices were not addressed. In another work, [73], the authors propose a radio resource allocation algorithm for eMBB and URLLC based on Branching Dueling Q-networks (BDQ) in a multi-slice multi-numerology context. In this work, the algorithm consists of allocating a part of the spectrum, designated by BWP, to a user belonging to a certain type of service (eMBB or URLLC) while mitigating the INI. However, the proposed model in [73] slightly differs from the one defined by 3GPP where a BWP is shared between users and was introduced to support multiple services and energy efficiency whereas in [73], a BWP is a radio resource allocation unit (a part of the spectrum) allotted exclusively to each user. Furthermore, unlike our work, the mMTC service, the preemptive scheduling problem and the dimensioning of a guard band between BWPs using different numerologies to mitigate the INI are not addressed.

Therefore, what distinguishes the approaches used in our work from other works is the consideration of both preemptive and orthogonal scheduling, the adjustment of the radio resources of each slice using users' KPIs, and implementing a guard band between BWPs using different numerologies to mitigate the INI. All of these aspects are considered in the same algorithm instead of focusing on a sole problem. Hence, this is done by the proposal of a three-level slicing algorithm for users connected to a single slice where:

- The first level of the algorithm focuses on an efficient BWP selection for the URLLC users based on two possible options (the one shared with the eMBB slice and the other exclusively dedicated to the URLLC slice) in order to mitigate the eMBB performance degradation from preemptive scheduling while taking into account the URLLC latency and energy efficiency constraints. This is realized using a Game theoretical approach.

- The second level of the algorithm proposes a heuristic approach that adjusts the radio resources of each BWP and slice based on users' KPIs including URLLC latency which is rarely considered in the SOTA. Hence, this level helps mitigating radio resource wastage in presence of traffic variation especially for orthogonal scheduling.

- The third level of the algorithm focuses on reducing the INI effect induced by the use of multiple

numerologies. This is done by carefully dimensioning a guard band between BWPs using different numerologies to improve users' performance hindered by the INI. The guard band is carefully dimensioned using DQN.

2.4 Radio Resource Allocation for Multi-Slice Users

The previously mentioned works focus on users connected to a single slice. In fact, users connected to multiple slices are rarely considered. Therefore, very few works consider the radio resource allocation problem for users connected to multiple slices. This is the case of the work in [31] where DRL is used to schedule radio resources to users that can be connected to multiple slices, each dedicated to a certain service in a multi-numerology context, where the algorithm also selects an appropriate numerology. Additionally, the work in [74] extends the work in [31] using Mixed-Integer Linear Programming. Nevertheless, the BWP Switching and energy efficiency aspects are not considered in these works which is the focus of our work. BWP switching is a very important point to consider for users connected to multiple slices with different numerologies requirements as it affects these users' performance with additional latency. In fact, BWP switching is studied in the SOTA such as the work in [75] where the impact of BWP switching on network performance is evaluated. Also, authors in [76] propose a method to handle BWP Inactivity Timer to reduce latency and increase throughput especially when there is a large measurement gap performed by the UE. Nevertheless, these works do not consider the slicing context or users with multi-slice connectivity.

In this thesis, multi-slice users are considered from two perspectives:

- That of latency, where we aim to reduce it by enhancing the BWP switching mechanism which is ignored for these users in the SOTA. This is done by proposing three innovative BWP switching schemes that help reduce overall latency.
- That of energy efficiency (which is rarely considered for these users), where we propose a scheme that flexibly selects either a single numerology BWP configuration or multi-numerology BWP configuration for each multi-slice UE depending on the UE characteristics since resorting to a single choice is detrimental to UEs performances in terms of QoS satisfaction and energy efficiency.

2.5 Conclusion

To conclude, Tables 2.1, 2.2, 2.3 and 2.4 summarize the difference between the scope of our work with existing works in the SOTA in the different radio resource optimization problems for slicing.

In fact, in this thesis, we first tackle the radio resource allocation problem in a multi-slice multi-VO setting where we use the DWFQ algorithm to schedule the resources among VOs. After determining the share of resources for each VO, we focus on a single VO and on users connected to a single slice where we aim to solve the resource allocation problem in a multi-slice context. We propose a first O-RAN compliant solution where only eMBB and URLLC are considered and the numerology aspect is ignored. With this solution, the algorithm is based on both traffic engineering and a dynamic re-adjustment of slice resources contrarily to existing works where only one option is considered. Afterwards, the numerology, mMTC slice and users' radio conditions are considered in a second single VO multi-slice solution. This solution relies on a three-level slicing algorithm in a multi-slice and multi-numerology context where the first level selects the appriopriate numerology-specific BWP for URLLC users using a crowding game, the second level adjusts the band for each slice based on users' KPIs using heuristics and the third level dimensions a GB between BWPs using different numerologies with DQN to reduce INI. This is different from other

existing works where some aspects of the problem are missing (INI consideration, adjustment of slice resources, numerology selection...) and only one topic is focused on. Additionally, this solution considers both orthogonal and preemptive scheduling for eMBB and URLLC coexistence whereas existing works only focus on a single scheduling solution for optimization. Finally, in the last part of the thesis, we focus on users connected to multiple slices. In the SOTA and for these users, the problem is focused only on radio resource allocation to optimize QoS satisfaction without taking into account additional latency due to BWP switching which decreases QoS satisfaction and energy efficiency aspect. For this reason, we propose a first solution for these users where we aim to reduce the latency due to BWP switching by enhancing this process. The second solution relies on the selection of an energy-efficient BWP configuration (multi-numerology or single numerology) in order to reduce energy consumption and optimize QoS satisfaction at the same time. All proposed solutions are compared to other solutions from the SOTA and/or the legacy standardized scheme whenever possible.

The next chapter formulates the first contribution which is the radio resource allocation problem in a Multi-Slice Multi-VO context.

Problem Context	Existing Works	Our Work
Multi-Slice and Multi-VO	• Multi-leader/Single-leader Multi-follower Stackelberg game to solve the problem • Slicing rarely considered • Optimization techniques to allocate resources using radio conditions among VOs • No alignment with O-RAN architecture	• Use of DWFQ scheduling algorithm • Two approaches: distributed and centralized • Distributed approach based on a crowding game • Centralized based on a Stackelberg game with a sole leader (I-P) • Only monetary cost and throughput taken into account at this level • O-RAN compliant solution

Table 2.1: Differences between our approaches and existing works related to Multi-Slice Multi-VO Radio Resource Optimization Problem

Problem Context	Existing Works	Our Work
Single VO and Multi-Slice	• Dynamic adjustment of slice resources using different KPIs and multiple tools including game theory and DRL • Slice selection for a UE depending on QoS satisfaction • Focus only on eMBB and URLLC while considering either preemptive or orthogonal scheduling • O-RAN alignment solution rarely considered	• Two solutions proposed • First solution based on traffic engineering (Slice selection) and a dynamic readjustment of slice resources for eMBB and URLLC • Two approaches for first solution: distributed based on a crowding game and centralized based on DQN • First solution is compared with another SOTA work and legacy scheme • Second solution is a three-level algorithm that considers eMBB, URLLC and mMTC slices, both preemptive and orthogonal scheduling for eMBB and URLLC and numerology aspect • Second solution compared to first solution and another SOTA work • O-RAN compliant solution

Table 2.2: Differences between our approaches and existing works related to Multi-Slice Single VO Radio Resource Optimization Problem

Problem Context	Existing Works	Our Work
Multi-Slice and Multi-Numerology	• Numerology selection algorithms depending on multiple factors • INI-aware scheduling • Scheduling based on BWP (numerology and amount of PRBs) attribution to each user without INI consideration	• Proposal of a three-level solution for three slices: eMBB, URLLC and mMTC and using three different numerologies • First level selects the numerology-specific BWP for URLLC users using a crowding game • Second level adjusts slices' resources based on users' KPIs and using heuristics • Third level mitigates INI by setting a GB between BWPs using different numerologies using DQN • O-RAN compliant solution

Table 2.3: Differences between our approaches and existing works related to Multi-Slice Multi-Numerology Radio Resource Optimization Problem

Problem Context	Existing Works	Our Work
Users connected to multiple slices	• Solution using DRL to attribute resources for users connected to multiple slices with different numerologies • BWP switching is not taken into account • Energy efficiency is not taken into account	• Two solutions • First solution relies on reducing latency for multi-slice users by enhancing BWP switching process • First solution compared to standard BWP switching process • Second solution selects the BWP configuration (single numerology or multi-numerology) to enhance energy efficiency for multi-slice users • Two approaches for second solution: centralized using an optimization problem and distributed using a congestion game • Second solution compared with legacy scheme

Table 2.4: Differences between our approaches and existing works related to Multi-Slice Users Radio Resource Optimization Problem

Chapter 3

A Multi-Slice Multi-Operator Dynamic Weighted Fair Queuing RAN Scheduling in a Game Theoretic Framework

In our first contribution, the radio resource allocation problem is tackled in a multi-slice multi-VO context. Therefore, this chapter focuses on scheduling the slices' radio resources among VOs. Two approaches are considered: a distributed one based on a non-cooperative game where VOs compete to obtain their resources by minimizing their incurred monetary cost and increasing their throughput and a centralized one based on a Stackelberg Game where the I-P seeks to maximize its monetary profit and the VOs seek to strike a balance between incurred monetary cost and attributed band. This is different from existing works where the DWFQ was not used in such a context and was previously used to allocate resources among flows from different classes of service. Particularly, for the distributed approach, two models are used: a linear model and a proportional fairness model where both models are compared against each other. Moreover, for the centralized approach, a global approach is also portrayed to compare it with the Stackelberg Game approach. Additionally, we aim to find the optimal weights and monetary cost set by the I-P. Both centralized and distributed approaches are detailed and evaluated for performance analysis. Finally, the implementation of these algorithms in the O-RAN architecture is also discussed.

3.1 Introduction

The radio resource allocation problem is a major challenge for the mobile network operator especially in the context of slicing and RAN evolution. Therefore, it is important to address this problem in a multi-VO context since multiple VOs may share an I-P's radio resources. For this reason, we propose a DWFQ scheduling algorithm that allocates the share of resources to each VO which is different from SOTA works where DWFQ was used to schedule flows from different classes of service. In this chapter, only the partitioning of the I-P band between the VOs is considered depending on the incurred monetary cost. Therefore, the attached users and the scheduling at the level of each VO remain outside the scope of this work. This problem can be tackled through a distributed and centralized approach. In the distributed approach, the problem is represented as a crowding game where the VOs compete over the share of resources. With this approach, two models are considered: a linear model and a Proportional Fairness (PF) model. These models are evaluated and compared against each other. As for the centralized approach, a global approach is discussed first where the I-P aims to maximize the utility function of each VO. Afterwards, this approach is represented as a Stackelberg Game where the I-P seeks to maximize its monetary profit in the

first stage and the VOs strive to strike a balance between the monetary cost to be paid and the share of resources obtained in the second stage. This contribution makes a way for the I-P to control the attributed DWFQ weights to each VO. The rest of this chapter is organized as follows:

Section 3.2 introduces the system model of the addressed problem. Afterwards, Sections 3.3 and 3.4 detail the distributed approach of the proposed solution and its performance evaluation while Sections 3.5 and 3.6 discuss the centralized approach and its performance evaluation. The alignment of the solution with the O-RAN architecture is examined in Section 3.7. Finally, Section 3.8 concludes the chapter.

3.2 System Model

The system model of the radio resource allocation problem in a multi-slice and multi-VO context is represented in Fig. 3.1.

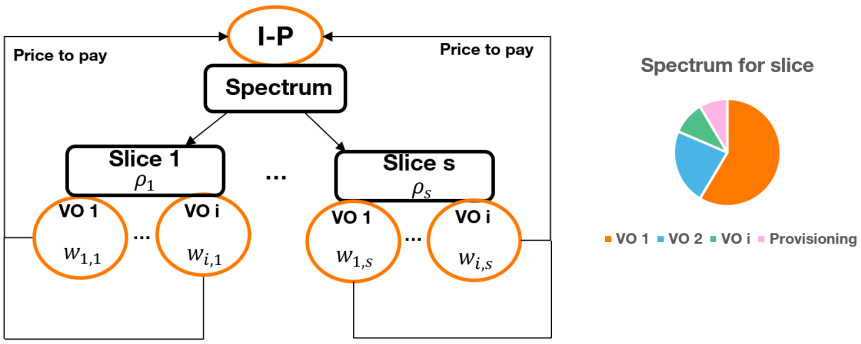

Figure 3.1: System Model for Multi-Slice Multi-VO context

As can be seen, we consider an I-P owning a certain spectrum and a set of Virtual Operators $\mathcal{I}$ with VO $i \in \mathcal{I}$ and a set of Slices $\mathcal{S}$ with slice $s \in \mathcal{S}$. The I-P spectrum is divided between the multiple existing slices. Therefore, each slice s has a capacity (in PRBs) ρ_s and the VOs coexist on each slice where each VO i is given a share of resources, namely a weight as an input for the WFQ scheduler. We denote by w_{is} the weight of VO i in slice s such as $0 < w_{is} < 1 \, \forall i \in \mathcal{I}$ and $\sum_i w_{is} \leq 1$. Hence, the whole slice capacity may not be completely utilized, in that case, the surplus amount might be used for provisioning (arrival of a new operator, traffic fluctuation of admitted operators ...). Therefore, the capacity of VO i in slice s is given by [44]:

$$C_{is}^{VO} = \frac{w_{is}\rho_s}{w_{is} + \sum_{j \neq i} w_{js}} \tag{3.1}$$

where κ_{is} is the monetary cost that VO i has to pay in slice s to the I-P for using the infrastructure.

Accordingly, we consider that the utility function of VO i in slice s has the following form:

$$U_{is} = \frac{w_{is}}{w_{is} + \sum_{j \neq i} w_{js}} - \alpha_s w_{is} \kappa_{is} \rho_s \tag{3.2}$$

with α_s a normalizing factor. In this equation, the first term corresponds to the band and throughput of VO i given by (3.1) and the second term corresponds to the cost inflicted by the I-P for asking for a share w_{is} of the slice s capacity. The VO will try to increase its throughput while paying attention to the incurred cost. The higher the weight, the higher the share of resources, and hence the higher the cost to be paid. Note that each VO i needs to get a minimal share of resources denoted by w_{is}^{min} to satisfy its SLA requirements in terms of throughput, latency, and capacity demands. Since all operators have a minimum share of

resources given by the SLA, they are able to maximize their weights without deteriorating other operators' conditions.

3.3 Distributed Approach

In this approach, each VO selfishly and autonomously strives to increase its utility function. Therefore, the problem is portrayed as a competition among greedy VOs for shared capacity with a non-cooperative game $\mathcal{G}$. The game framework is presented as follows:

- The set of players is the set of VOs $\mathcal{I}$.
- The set $\mathcal{W} = \{w_{is}$ with $0 < w_{is} < 1 \; \forall i \in \mathcal{I}$, $w_{is} \geq w_{is}^{min}$ and $\sum_{i \in \mathcal{I}} w_{is} < 1\}$ is the set of strategies since each player will strive to obtain the highest weight for a higher share of resources.
- A set of utility functions U_{is} that quantify the players' profitability over the possible outcomes of the game. Each VO i maximizes its utility function by choosing the appropriate strategy w_{is} for each slice s.

As for the utility function, we consider two models: the first is a *Linear model* where the utility of any VO i is the sum of its utilities per slice while the second model is a *Proportional Fairness (PF) model* that imposes proportional fairness among slices. We will target the Nash Equilibrium (NE) which is an equilibrium state that was already presented in Chapter 1 in subsection 1.4.4.

3.3.1 Linear Model

In this model, we consider the following utility function:

$$U_i = \sum_{s \in \mathcal{S}} \frac{w_{is}}{w_{is} + \sum_{j \neq i} w_{js}} - \sum_{s \in \mathcal{S}} \alpha_s w_{is} \kappa_{is} \rho_s \tag{3.3}$$

Proposition 1. *The utility function is strictly concave.*

Proof. The first derivative of the utility function is:

$$\frac{\partial U_{is}}{\partial w_{is}} = \frac{\sum_{j \neq i} w_{js}}{(w_{is} + \sum_{j \neq i} w_{js})^2} - \alpha_s \kappa_{is} \rho_s \tag{3.4}$$

The second derivative of the utility function is:

$$\frac{\partial^2 U_{is}}{\partial w_{is}^2} = \frac{-2 \sum_{j \neq i} w_{js}}{(w_{is} + \sum_{j \neq i} w_{js})^3} \tag{3.5}$$

We can see from (3.5) that the second derivative is strictly negative which means that the utility function is strictly concave. □

Proposition 2. *The NE exists and can be attained.*

Proof. Since the utility function is strictly concave according to Proposition 1 and continuous in w_{is} and since the set of strategies $\mathcal{W}$ is convex and compact, NE exists and is unique as proven by [77]. Further, as the utility functions are strictly concave, the unique NE can be attained by Best Response Dynamics. □

The best response dynamics consist in each VO maximizing in turn its own utility function in response to other VO strategies. It amounts for each VO to solving the following optimization problem:

$$\begin{aligned} \max_{w_{is}} \quad & U_{is} \\ \text{subject to:} \quad & 0 < w_{is} < 1 \\ & \sum_{i \in \mathcal{I}} w_{is} < 1 \\ & w_{is} \geq w_{is}^{min} \end{aligned} \tag{3.6}$$

Since the optimization problem (3.6) is convex, the Karush-Kuhn-Tucker (KKT) conditions enable determining the optimum for each VO i (i.e. the NE at convergence). Therefore, the NE is the solution of the following KKT conditions:

$$\frac{\partial U_{is}}{\partial w_{is}} - \gamma = \frac{\sum_{j \neq i} w_{js}}{(w_{is} + \sum_{j \neq i} w_{js})^2} - \alpha_s \kappa_{is} \rho_s - \gamma = 0 \tag{3.7}$$

$$\gamma \cdot (1 - \sum_{j \neq i} w_{js} - w_{is}) = 0 \tag{3.8}$$

$$w_{is} \geq w_{is}^{min} \tag{3.9}$$

If $\gamma = 0$, from (3.7), we can find w_{is}:

$$w_{is} = \sqrt{\frac{\sum_{j \neq i} w_{js}}{\alpha_s \kappa_{is} \rho_s}} - \sum_{j \neq i} w_{js} \tag{3.10}$$

If $\gamma \neq 0$, from (3.8) and (3.9), we can find w_{is}:

$$w_{is} = max(1 - \sum_{j \neq i} w_{js}; w_{is}^{min}) \tag{3.11}$$

At each round, each VO will calculate the weight based on (3.10) and (3.11) until convergence is reached when all VOs choose the same strategies as in the previous round. This behavior is described in the following algorithm (Algorithm 1).

Input : Monetary cost κ_{is}, Slice Capacity ρ_s, Minimal values of w_{is}
Output: Optimal Weight w_{is}
1 Initialize $w_{is} = w_{is}^{min}$;
2 **repeat**
3 | Each VO calculates its weight that obeys $w_{is}^* = \text{argmax}_{w_{is} \in \mathcal{W}} U_{is}$ given the other VOs strategies;
4 **until** *Attaining Nash Equilibrium*;

Algorithm 1: Weight Calculation based on Best Response Dynamics

3.3.2 PF Model Among Slices

In this model, we enforce Proportional Fairness among the slices as follows:

$$U_i^{PF} = \alpha \sum_{s \in \mathcal{S}} \ln \frac{w_{is}\rho_s}{w_{is} + \sum_{j \neq i} w_{js}} - \sum_{s \in \mathcal{S}} \beta_s w_{is} \kappa_{is} \rho_s \tag{3.12}$$

With α and β_s normalizing factors.

Proposition 3. *The utility function is strictly concave.*

Proof. The first derivative of the utility function is:

$$\frac{\partial U_{is}^{PF}}{\partial w_{is}} = \frac{\alpha \sum_{j \neq i} w_{js}}{w_{is}(w_{is} + \sum_{j \neq i} w_{js})} - \beta_s \kappa_{is} \rho_s \tag{3.13}$$

The second derivative of the utility function is:

$$\frac{\partial^2 U_{is}^{PF}}{\partial w_{is}^2} = \frac{-\alpha \sum_{j \neq i} w_{js}(2w_{is} + \sum_{j \neq i} w_{js})}{w_{is}^2 (w_{is} + \sum_{j \neq i} w_{js})^2} \tag{3.14}$$

We can see from Equation (3.14) that the second derivative is strictly negative which means that the utility function is strictly concave. □

Similarly to the previous model, the unique NE can be attained by Best Response Dynamics where each VO solves the optimization problem by maximizing in turn its utility function to obtain its weight and repeat the round until convergence as explained in Algorithm 1. Since the optimization problem at each round is convex, the KKT conditions determine the optimum at each best response (hence the Nash Equilibrium at convergence) and is given by the following:

$$\frac{\partial U_{is}^{PF}}{\partial w_{is}} - \gamma = \frac{\alpha \sum_{j \neq i} w_{js}}{w_{is}(w_{is} + \sum_{j \neq i} w_{js})} - \beta_s \kappa_{is} \rho_s - \gamma = 0 \tag{3.15}$$

$$\gamma \cdot (1 - \sum_{j \neq i} w_{js} - w_{is}) = 0 \tag{3.16}$$

$$w_{is} \geq w_{is}^{min} \tag{3.17}$$

If $\gamma = 0$, from (3.15), we can find w_{is} which is the solution of the second-degree equation:

$$w_{is}^2 + w_{is} \sum_{j \neq i} w_{js} - \frac{\alpha \sum_{j \neq i} w_{js}}{\beta_s \kappa_{is} \rho_s} = 0 \tag{3.18}$$

Equation (3.18) leads us to finding w_{is}:

$$w_{is} = \frac{\sum_{j \neq i} w_{js}}{2} (-1 + \sqrt{1 + \frac{4\alpha}{\beta_s \kappa_{is} \rho_s \sum_{j \neq i} w_{js}}}) \tag{3.19}$$

If $\gamma \neq 0$, from (3.16) and (3.17), we can find w_{is}:

$$w_{is} = max(1 - \sum_{j \neq i} w_{js}, w_{is}^{min}) \tag{3.20}$$

3.4 Performance Evaluation of the Distributed Approach

We implemented Algorithm 1 with both models using CVX Mosek in Matlab to calculate the weights at NE. We assume that the I-P holds a spectrum of 50 MHz with a SCS of 15 KHz. Thus, the maximum number of PRBs offered by the I-P is 270 [78]. Simulation parameters are provided in Table 3.1.

Table 3.1: Simulation Parameters for Multi-Slice Multi-VO Problem

Parameter	Description	Value
$\lvert\mathcal{I}\rvert$	Number of operators	4
$\lvert\mathcal{S}\rvert$	Number of slices	3
ρ_s	Capacity per slice (in PRBs)	$80, 90, 60$
w_{is}^{min}	The minimum weight attributed	$0.1\ \forall i\ \forall s$
α_s (Linear model)	Normalizing factor	$\approx 10^{-4}$
α (PF model)	Normalizing factor	≈ 0.5
β_s (PF model)	Normalizing factor	$\approx 10^{-2}$

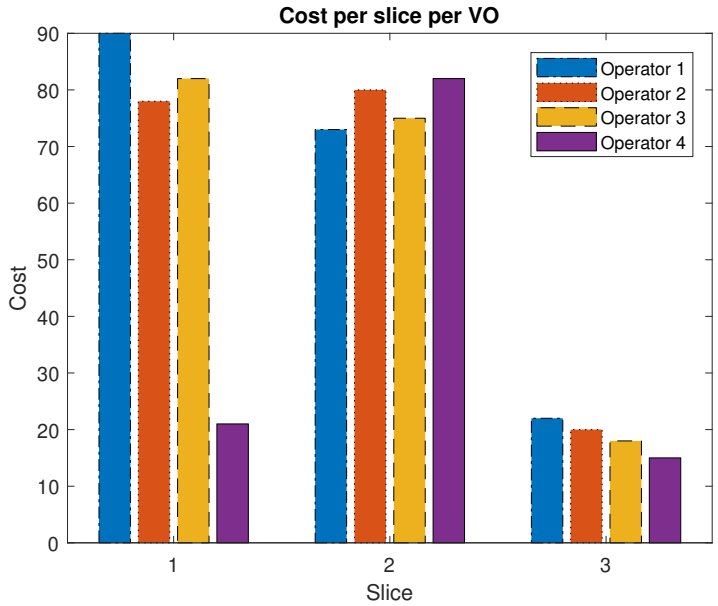

Figure 3.2: Cost input values for each VO in each Slice

Regarding the monetary cost that the VO has to pay for the I-P, we attributed different values for each VO in each slice to better assess its impact. We consider that the cost unit is the local currency of the I-P and the maximum price used to charge the VO is 100. Figure 3.2 shows the values of cost attributed for each operator in each slice. We calculated the weights using both models and obtained the results depicted in Fig. 3.3 and Fig. 3.4.

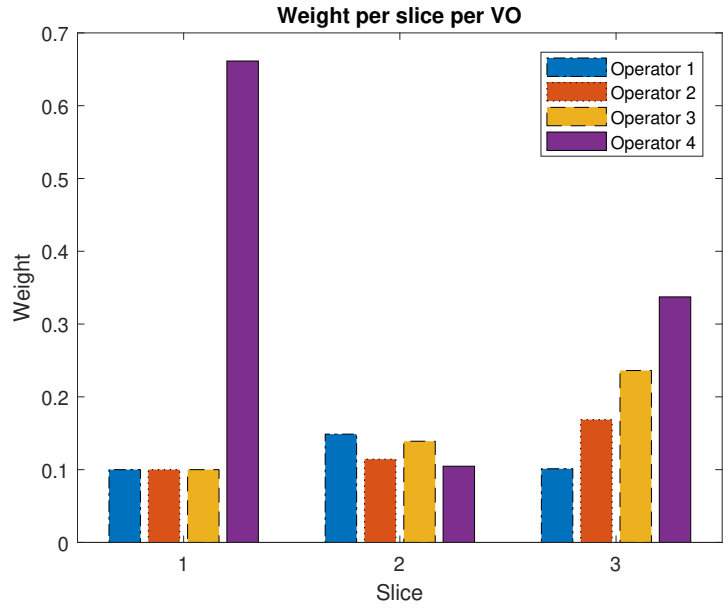

Figure 3.3: Weights at Nash Equilibrium using the Linear model

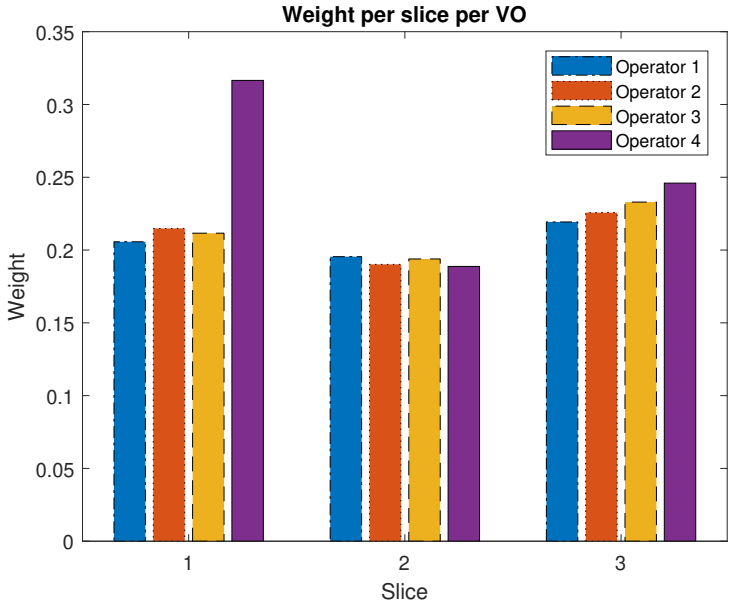

Figure 3.4: Weights at Nash Equilibrium using the PF model

From the obtained results, we can see that the weight attributed is inversely proportional to the cost in both models which is logical according to Equations (3.10) and (3.19). Also, when there is a big gap between the cost values as can be seen in slice 1, that gap transfers to the weight values of the linear model where the VO having the lowest cost is being attributed the highest weight while the other VOs with a higher cost are being attributed the minimal weight. With the PF model, the weights are closer in values and the gap is reduced compared to the linear model while the minimal weight value is not reached in the PF model. This can be explained by the fact that the PF model tries to ensure fairness among VOs by attributing closer values while maintaining an inversely proportional relation with the cost. However, it is more useful

for the infrastructure operator to control the gap among the attributed weights values by fine-tuning the monetary cost. Therefore, we will adopt the linear model and further add a differentiating factor β_{is} to control the cost among the VOs. Accordingly, the utility function of the linear model (3.3) becomes:

$$U_{is} = \frac{w_{is}}{w_{is} + \sum_{j \neq i} w_{js}} - \alpha \beta_{is} w_{is} \kappa_{is} \rho_s \tag{3.21}$$

And equation (3.10) becomes:

$$w_{is} = \sqrt{\frac{\sum_{j \neq i} w_{js}}{\alpha \beta_{is} \kappa_{is} \rho_s}} - \sum_{j \neq i} w_{js} \tag{3.22}$$

3.5 Centralized Approach

3.5.1 Global Approach

In this approach, the I-P will maximize in a centralized fashion the sum of the utility functions of all the serviced VOs in each slice. The used utility function is the one using the linear model from the distributed approach. Accordingly, we will maximize the following function:

$$U^s_{tot}(w_{i1}, ..., w_{i|\mathcal{S}|}) = \sum_i U_{is} = 1 - \alpha_s \kappa_{is} \rho_s \sum_i w_{is} \tag{3.23}$$

It corresponds to solving the following optimization problem:

$$\begin{aligned} \max_{w_{is}} \quad & U^s_{tot} \\ \text{subject to:} \quad & 0 < w_{is} < 1 \\ & \sum_{i \in \mathcal{I}} w_{is} < 1 \\ & w_{is} \geq w^{min}_{is} \end{aligned} \tag{3.24}$$

The optimization problem is convex as the objective function as well as all constraints are linear. Maximizing the objective function, with w_{is} as the decision variables boils down to minimizing w_{is} which means setting the weights to their minimal values $w_{is} = w^{min}_{is}$. This can be explained by the fact that with the global approach, the optimal solution would be that each VO uses its minimum of share of resources to avoid disturbing the other VOs.

The same analysis cannot be applied to the PF model as the global utility is not a concave function.

For these reasons, we tackle the centralized approach from a different perspective with a Stackelberg Game.

3.5.2 Stackelberg Game Approach

Another way to model the centralized approach is to formulate the interaction between the cost set by the provider on allotted capacity and the capacity share needed by the VOs as a two-stage Stackelberg Game. In the first stage, the infrastructure operator announces the monetary cost of resources, followed by the second stage where each VO determines its needed share of resources as a weight of the WFQ algorithm to strike a balance between a satisfactory throughput and an affordable cost paid to the I-P. Therefore, the infrastructure provider is the leader while the VOs are the followers. Note that the second stage is a non-cooperative game played for a given instance of monetary cost outputted by the I-P.

Stage 1: The Leader Stage

At the leader stage, the I-P aim is to maximize its total revenue and hence we consider for the I-P the following utility function:

$$U_{I-P} = \sum_{s} \rho_s \sum_{i} \kappa_{is} w_{is} \tag{3.25}$$

This leads to the following optimization problem for the leader:

$$\begin{aligned} \max_{\kappa_{is}} \quad & U_{I-P} \\ \text{subject to:} \quad & 0 < \kappa_{is} \leq \kappa_{max} \end{aligned} \tag{3.26}$$

Therefore, the I-P will maximize its utility function with the cost as the optimization variable while avoiding exceeding a maximal cost κ_{max}.

Stage 2: The Followers Stage

At the followers' stage, we consider the utility function with the differentiated linear model defined in (3.21). Each of the VOs try to maximize its utility function with the constraints defined in (3.6). The solution for this optimization problem is already defined in equation (3.22) when $\gamma = 0$ and in equation (3.11) when $\gamma \neq 0$.

Stackelberg Equilibrium

In a Stackelberg Game, we try to find the Stackelberg Equilibrium (SE) where no player has profit in deviating unilaterally as explained in subsection 1.4.4 of Chapter 1.

Accordingly, a SE is an equilibrium point (w^*_{is}, κ^*_{is}) defined as follows:

$$U_{I-P}(w^*_{is}, \kappa^*_{is}) \geq U_{I-P}(w^*_{is}, \kappa_{is}), \forall \kappa_{is} \tag{3.27}$$

$$U_{is}(w^*_{is}, \kappa^*_{is}) \geq U_{is}(w_{is}, \kappa^*_{is}), \forall w_{is} \tag{3.28}$$

We derive the SE of the devised Stackelberg game by using the backward induction method. For that aim, we first derive the optimal weight shares (w^*_{is}) of VO $i \in \mathcal{I}$ and $\forall s \in \mathcal{S}$ in Stage 1, obtained from equations (3.22) and (3.11) and inject them in equation (3.25) to obtain the optimal solution of Stage 1 (i.e. κ^*_{is}).

Optimal Solution for Stage 1

As previously stated, we inject (3.22) if $\gamma = 0$ and (3.11) if $\gamma \neq 0$ in equation (3.25). Accordingly, we will obtain the following utility function for the I-P when $\gamma = 0$:

$$\begin{aligned} U_{I-P} &= \sum_{s} \rho_s \sum_{i} \kappa_{is} \left(\sqrt{\frac{\sum_{j \neq i} w_{js}}{\alpha \beta_{is} \kappa_{is} \rho_s}} - \sum_{j \neq i} w_{js} \right) \\ &= \sum_{s} \sum_{i} \sqrt{\frac{\kappa_{is} \rho_s \sum_{j \neq i} w_{js}}{\alpha \beta_{is}}} - \kappa_{is} \rho_s \sum_{j \neq i} w_{js} \end{aligned} \tag{3.29}$$

Proposition 4. *The utility function is strictly concave.*

Proof. The first derivative of the utility function of the I-P is:

$$\frac{\partial U_{I-P}}{\partial \kappa_{is}} = \frac{1}{2}\sqrt{\frac{\rho_s \sum_{j\neq i} w_{js}}{\kappa_{is}\alpha\beta_{is}}} - \rho_s \sum_{j\neq i} w_{js} \tag{3.30}$$

The second derivative of the utility function is:

$$\frac{\partial^2 U_{I-P}}{\partial \kappa_{is}^2} = \frac{-1}{4}\sqrt{\frac{\rho_s \sum_{j\neq i} w_{js}}{\kappa_{is}^3\alpha\beta_{is}}} \tag{3.31}$$

We can see from Equation (3.31) that the second derivative is strictly negative which means that the utility function is strictly concave. □

In that case, as (3.26) is a convex optimization problem, the KKT conditions enable determining a global optimum which is the Stackelberg Equilibrium. The KKT conditions are:

$$\frac{\partial U_{I-P}}{\partial \kappa_{is}} - \theta = \frac{1}{2}\sqrt{\frac{\rho_s \sum_{j\neq i} w_{js}}{\kappa_{is}\alpha\beta_{is}}} - \rho_s \sum_{j\neq i} w_{js} - \theta = 0 \tag{3.32}$$

$$\theta(\kappa_{is} - \kappa_{max}) = 0 \tag{3.33}$$

If $\theta = 0$, from (3.32), we can find κ_{is}:

$$\kappa_{is} = \frac{1}{4\alpha\beta_{is}\sum_{j\neq i} w_{js}\rho_s} \tag{3.34}$$

If $\theta \neq 0$, from (3.33), we can find κ_{is}:

$$\kappa_{is} = \kappa_{max} \tag{3.35}$$

When $\gamma \neq 0$, we obtain the following utility function for the I-P when injecting (3.11) in equation (3.25):

$$\begin{aligned} U_{I-P} &= \sum_s \rho_s \sum_i \kappa_{is}(1 - \sum_{j\neq i} w_{js}) \\ &= \sum_s \sum_i \rho_s\kappa_{is} - \sum_s \sum_i \rho_s\kappa_{is} \sum_{j\neq i} w_{js} \end{aligned} \tag{3.36}$$

As (3.36) is a linear function in κ_{is}, therefore the optimal solution would be to use the maximum cost which leads back to (3.35).

SE Algorithm

The algorithm used to obtain the Stackelberg Equilibrium is represented in Algorithm 2.

Input : Slice capacity ρ_s, beta factor β_{is}, random values of w_{is} and κ_{is}
Output: Optimal monetary cost κ_{is} and weights w_{is}
1 Initialize w_{is};
2 **repeat**
3 The I-P calculates κ_{is} based on (3.26), (3.29), (3.36);
4 Each VO calculates its weight based on maximizing the utility function (3.21);
5 **until** *Attaining weights and costs stabilization*;

Algorithm 2: Stackelberg Equilibrium Algorithm for Multi-VO Weight and Cost Calculations

First, we initialize the weights to random values obeying the constraints in set $\mathcal{W}$. Then, we repeat the costs and weights values computation based on the optimization problems of the leader and followers stages until convergence when costs and weights no longer vary.

Proposition 5. *The iterative update of Algorithm 2 converges to a unique fixed point which is the unique SE.*

To that end, we prove that the updating function $P(w)$ based on (3.22) obeys specific criteria [46]:

$$w_{is}^{(t+1)} = P_{is}^{h}(w_{-is}^{(t)}) = \sqrt{\frac{w_{-is}^{(t)}}{\alpha\beta_{is}\kappa_{is}\rho_s}} - w_{-is}^{(t)} \quad \forall i \in \mathcal{I} \quad \forall s \in \mathcal{S} \tag{3.37}$$

where $w_{-is}^{(t)}$ are the weights at iteration t of other VOs in slice s ($w_{-is}^{(t)} = \sum_{j \neq i} w_{js}^{(t)}$).

These criteria are as follows:

- Positivity: $P(w) > 0$
- Monotonicity: if $w \geq w'$ then $P(w) \geq P(w')$
- Scalability: $\forall \mu > 1, \mu P(w) \geq P(\mu w)$
- Two-sided Scalability: $\forall \mu > 1, \frac{1}{\mu} w \leq w' \leq \mu w$ results in $\frac{1}{\mu} P(w) < P(w') < \mu P(w)$

We show in Appendix A.1 that $P(w)$ verifies all these conditions.

3.6 Performance Evaluation for Centralized Approach

We implemented Algorithm 2 using CVX Mosek in Matlab to calculate the weights and costs at SE. We list the numerical values for our simulations in Table 3.2. Figures 3.5 and 3.6 show the values of the beta factor that we used as an input for Algorithm 2 in presence of 2 and 4 operators, respectively.

Table 3.2: Numerical values for simulations for Centralized Approach Multi-Slice Multi-VO

Parameter	Description	Value
$\|\mathcal{I}\|$	Number of operators	2 or 4
$\|\mathcal{S}\|$	Number of slices	3
ρ_s	Capacity per slice (in PRBs)	$60, 70, 80$
w_{is}^{min}	The minimum weight attributed	$0.1\ \forall i\ \forall s$
α	Normalizing factor	$\approx 10^{-4}$
κ_{max}	Maximum Cost	100

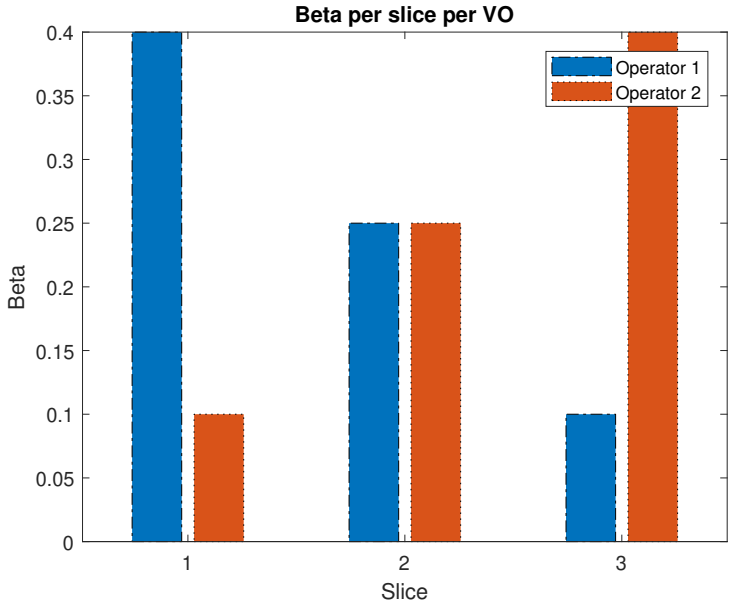

Figure 3.5: Beta factors for each operator in each slice for 2 operators

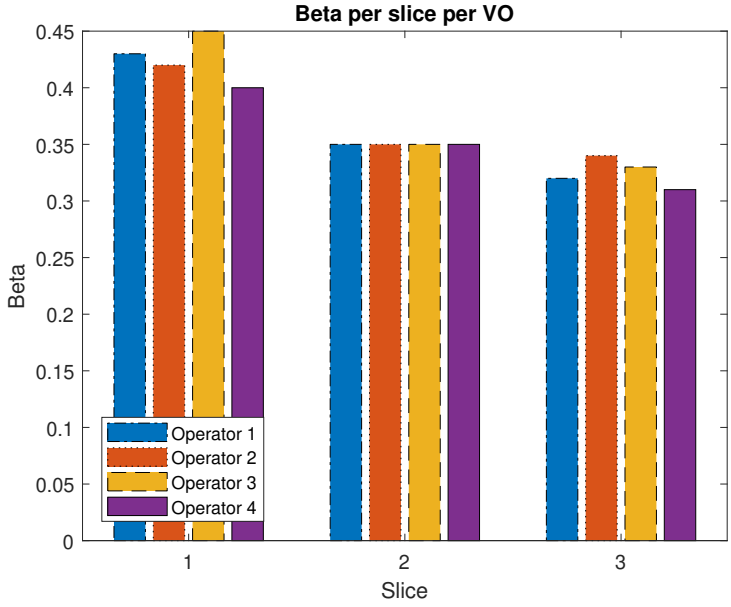

Figure 3.6: Beta factors for each operator in each slice for 4 operators

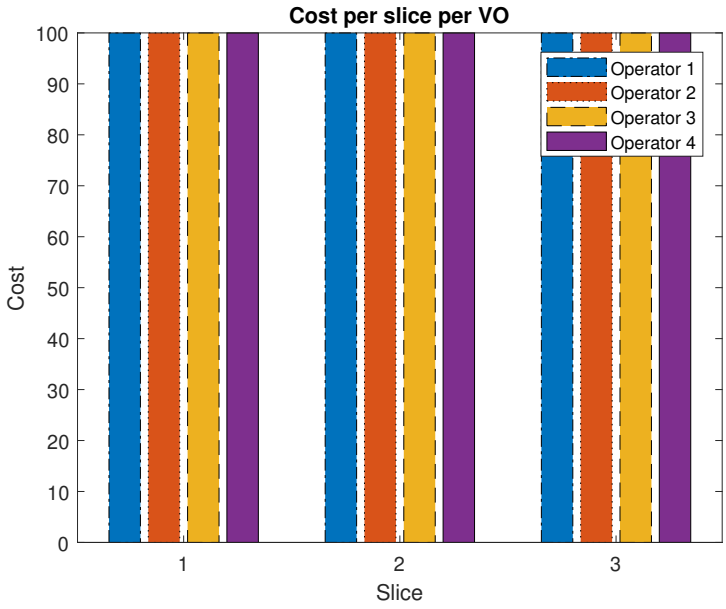

Figure 3.7: Cost values at SE for 4 operators

We find that at convergence, the optimal solution for the cost is to use the maximum cost κ_{max} for any number of operators. This can be seen in Fig. 3.7.

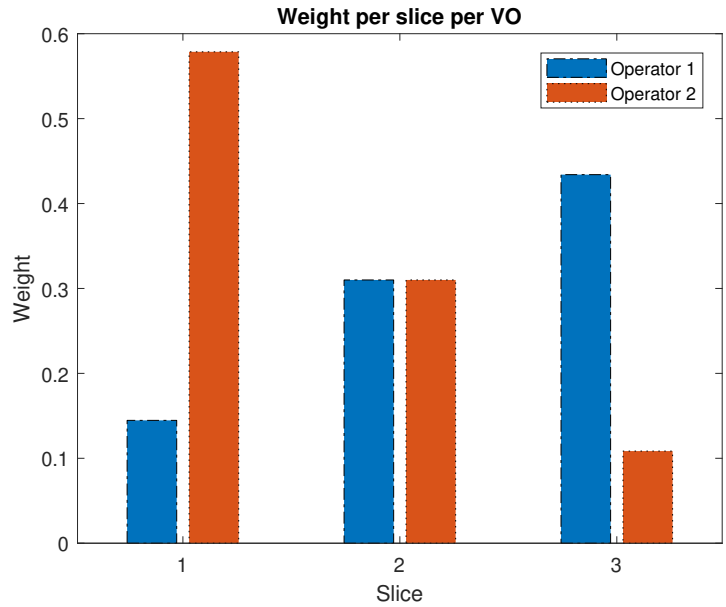

Figure 3.8: Weight values at SE for 2 operators

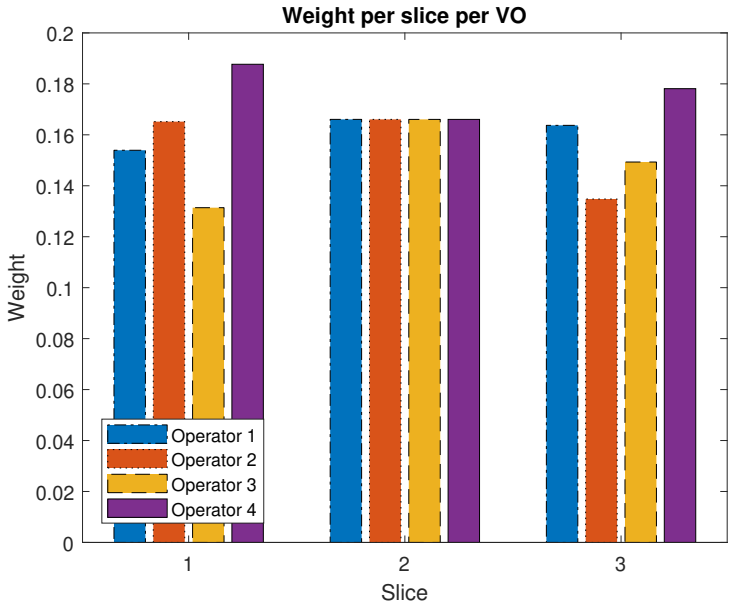

Figure 3.9: Weight values at SE for 4 operators

As for the weights, they converge to values that are inversely proportional to the beta factors as seen in Fig. 3.8 and Fig. 3.9. Since the cost becomes equal for all operators in all slices, the only differentiating factor between operators is the beta factor. The weights and beta have an inversely proportional relation as can be seen from equation (3.22). It can also be noted that the weight at convergence is also inversely proportional to the capacity of the slice (also evident by equation (3.22)).
We can also point out that in the case of 2 operators, there is a direct inverse proportionality relation between the beta factors and weights, proven mathematically as follows:

Proposition 6. *The weight is directly inversely proportional to the beta factor in case of two operators.*

Proof. The weight of the first operator in any slice s has the following expression from equation (3.22):

$$w_{1s} = \sqrt{\frac{w_{2s}}{\alpha\beta_{1s}\kappa_{1s}\rho_s}} - w_{2s} \tag{3.38}$$

Similarly, the weight of the second operator in the same slice has the following expression from equation (3.22):

$$w_{2s} = \sqrt{\frac{w_{1s}}{\alpha\beta_{2s}\kappa_{2s}\rho_s}} - w_{1s} \tag{3.39}$$

From (3.38), we find that:

$$w_{1s} + w_{2s} = \sqrt{\frac{w_{2s}}{\alpha\beta_{1s}\kappa_{1s}\rho_s}} \tag{3.40}$$

From (3.39), we deduce:

$$w_{1s} + w_{2s} = \sqrt{\frac{w_{1s}}{\alpha\beta_{2s}\kappa_{2s}\rho_s}} \tag{3.41}$$

From (3.40) and (3.41), we can find that:

$$\sqrt{\frac{w_{2s}}{\alpha\beta_{1s}\kappa_{1s}\rho_s}} = \sqrt{\frac{w_{1s}}{\alpha\beta_{2s}\kappa_{2s}\rho_s}} \tag{3.42}$$

From (3.42), since the cost for both operators at SE is equal to κ_{max}, it leads to:

$$\frac{w_{2s}}{w_{1s}} = \frac{\beta_{1s}}{\beta_{2s}} \tag{3.43}$$

□

Therefore, the beta factor can be a parameter that can be used by the I-P to control the weights attributed to the VOs while maintaining maximal revenues.

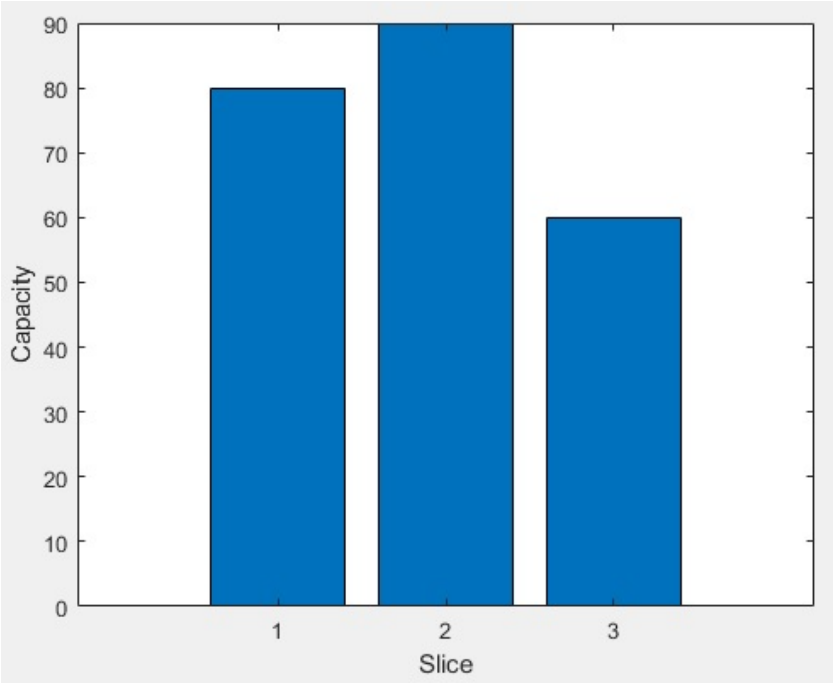

Figure 3.10: Slice Capacity input for 4 operators

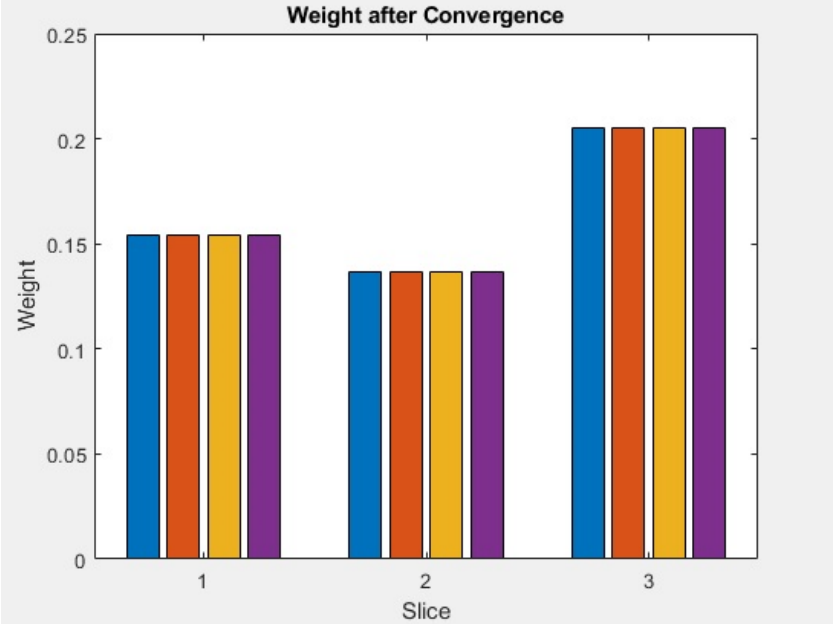

Figure 3.11: Weight values at SE for 4 operators without Beta Factor

In fact, without the use of a beta factor, weights at convergence are the same for every operator and are inversely proportional to the slice capacity as proven by Equation (3.22) since the cost for all operators at SE is equal to κ_{max} and the slice capacity is the only differentiating factor when the beta factor is missing. This is clear in Figs. 3.10 and 3.11 that represent the slice capacity as an input for 4 operators and the weights at SE for 4 operators without a beta factor respectively.

3.7 Implementation in O-RAN

In this section, we discuss how we envision the implementation of the proposed algorithms in the O-RAN architecture [4].

Both Algorithms 1 and 2 take approximately several minutes (more than 1 s) to reach Nash and Stackelberg Equilibria. With a confidence level of 95% and for 4 operators, it takes on average up to 9 iterations per slice to attain the NE ($\approx$ 20 s per slice) and up to 12 iterations per slice to attain the SE ($\approx$ 30 s per slice). Therefore, these algorithms will be implemented at the Non-RT RIC level to calculate the adequate monetary cost and weights for the slice scheduling. The latter weights will be given to the O-DU over O1 interface to allocate the resources in the RAN according to the DWFQ scheduler. To summarize, the Non-RT RIC will determine, according to Algorithms 1 and 2, the weights of the DWFQ Scheduler that operates at the O-DU.

3.8 Concluding Remarks

In this chapter, a dynamic WFQ scheduler was proposed to allocate resources in a multi-slice and multi-VO context orchestrated by the infrastructure provider. The weights of the WFQ scheduler for each VO in each slice were determined via two main approaches, a distributed one based on a non-cooperative game and a centralized one based on a Stackelberg game:

- For the concave non-cooperative game, we proved the existence of the unique NE attained by best-response dynamics for a given resource cost.
- In the Stackelberg game approach, the I-P is the leader whose strategy is the resource monetary cost while the VOs are the followers whose strategy is the resource share of WFQ scheduler.
- Extensive simulations highlighted the significance of the devised algorithms that enable the I-P to control the attributed weight and apply service differentiation among VOs thanks to fine-tuning the preset incurred monetary cost in the distributed approach and a VO differentiating factor in the centralized approach.
- The implementation of the proposed approaches in the O-RAN architecture was also discussed.

After proposing an algorithm to attribute radio resources between multiple VOs, we focus on a single VO to determine its radio resource allocation between its multiple slices and services in an efficient manner. This particular problem is analyzed in the following chapter.

Chapter 4

Crowding Game and Deep Q-Networks for Dynamic RAN Slicing in 5G Networks

The previous chapter focused on the radio resource allocation problem in a multi-slice multi-VO setting to determine the share of each virtual operator. Next, we focus on the partitioning of the VO attributed band between its slices. Therefore, this chapter tackles the problem in a single virtual operator and multi-slice context particularly for two slices: eMBB and URLLC. In this problem, a single numerology and a fixed number of users connected to a single slice with average radio conditions are considered. Two approaches are proposed: a centralized one based on Deep-Q Networks and a distributed one based on a crowding game. Both approaches rely on a dynamic adjustment of slice resources and on traffic engineering where the slice serving the user is selected based on the user's KPI (throughput or delay) that depends on the selected slice. Both approaches are compared against each other and against a state-of-the-art work considering solely the slice selection aspect without a dynamic adjustment of radio resources. Also, our dynamic approach is compared to the legacy scheme where users' association to their respective slice remains unchanged. Results prove high efficiency of our proposed approaches. Their implementation in the O-RAN architecture is also discussed.

4.1 Introduction

Following the determination of the band attributed to each VO, it is up to each VO to decide how to attribute the radio resources for each serviced slice. Therefore, we propose a dynamic slicing algorithm that allocates the radio resources to each slice depending on users' KPI: throughput and delay. The proposed solution may be centralized or distributed and combines traffic engineering and a dynamic adjustment of slice resources contrarily to other SOTA works focusing on one option especially the latter. This work proposes a new coexistence method for eMBB and URLLC services that is different from existing methods such as orthogonal and preemtive scheduling thanks to traffic engineering. Also, average radio conditions and a fixed number of users are considered. The mMTC slice, users' radio conditions and arrival process and the numerology aspect are left for consideration in the next chapter which is an extension of the work tackled in this chapter. The distributed approach of the proposed solution is represented as a crowding game where each user selects its slice selfishly and autonomously to satisfy its KPI. This is different from the centralized approach that uses DQN where an agent chooses the slice for each user using a global reward function. Both approaches are compared against each other and against a SOTA work [64] that focuses only on a slice selection scheme and overlooks dynamic adjustment of resources between slices. In addition, we compare results to the legacy scheme where the association between users and slices remains invariant. The rest of this chapter is organized as follows:

Section 4.2 establishes the system model of the problem. The distributed and centralized approaches tackling this problem along with their performance evaluation are discussed in Sections 4.3, 4.4, 4.5 and 4.6. Section 4.7 goes through the compliance of the proposed solutions with the O-RAN architecture while Section 4.8 compares both distributed and centralized approaches. Finally, concluding remarks are enlisted in Section 4.9.

4.2 System Model

As can be seen in Fig. 4.1 that represents the system model, we consider a single gNB and a set of N_{users} users connected to a single slice. Consequently, a user cannot be served by more than one slice since it only has one type of communication service. Additionally, only two services are studied: URLLC and eMBB. We consider an operator having N_{RBtot} PRBs that are shared among two slices, namely an URLLC slice and an eMBB slice. Hence, the total number of resources is divided into two subsets with N_{RBE} the number of PRBs for the eMBB slice and N_{RBU} for the URLLC slice.

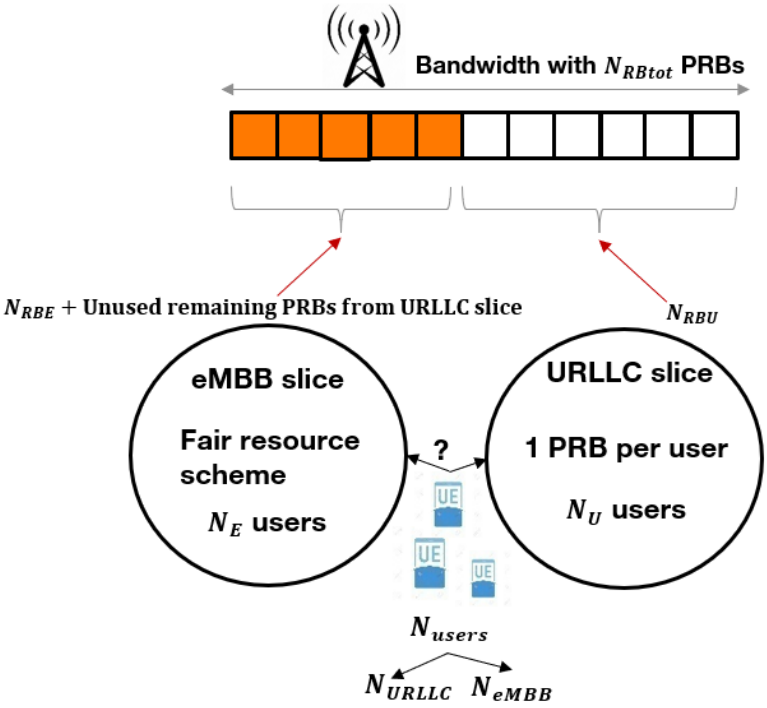

Figure 4.1: System Model for Dynamic Slicing Algorithm for eMBB and URLLC

In our approach, the resource allocation is performed dynamically which is different from the legacy scheme where users are associated with their "natural" slice (e.g. an eMBB (resp. URLLC) type user is serviced by the eMBB (resp. URLLC) slice). In our proposal, the user belonging to a given service type may be attributed resources endowed to other service types depending on its cost function, for increased flexibility and effectiveness. In other words, an URLLC type user has the flexibility to choose the eMBB slice and vice versa if the user gets a lower cost from an alternate slice. This can happen for instance in case the user's natural slice is too crowded, or when the alternate slice offers good performances at a lower monetary cost. Note that the proposed solution is not necessarily compliant with current 3GPP standards in terms of user-slice association procedure. In 3GPP standards, the latter is managed by the base station and the user is associated with a slice identified by its unaltered S-NSSAI [25] as done by the legacy scheme.

Nevertheless the goal of this work is to investigate a novel concept based on traffic engineering that can inspire future standardization, where the UE gets involved in slice selection process; therefore, pushing network intelligence down to the end devices while proving its efficiency.

As for the URLLC general requirements as stated by the 3GPP, the latency should not exceed 1 ms for a reliability of $1 - 10^5$ [6][7][8]. Hence, as an URLLC service requires a maximum tolerated delay, we adopt the assumption that the availability of one PRB per user with a duration of 1 ms is sufficient to fulfill these requirements and any additional PRBs allocated may not be beneficial to the URLLC type user contrary to an eMBB user requiring a minimum guaranteed throughput at the cost of increased delay. In other words, one PRB per user in the URLLC slice ensures minimal delay for all users. Therefore, in the URLLC slice, a resource allocation scheme is applied to ensure minimal delay that does not exceed the maximum tolerated delay, whereas for the eMBB slice, a resource allocation scheme is applied to ensure maximal throughput that surpasses the minimum guaranteed throughput.

We will use the following notations displayed in Table 4.1 for ease of comprehension:

Table 4.1: Symbol Description for Dynamic Slicing Problem

Symbol	Description
N_{URLLC}	Number of URLLC type users
N_{eMBB}	Number of eMBB type users
N_{users}	Total number of users within the system and equal to $N_{URLLC} + N_{eMBB}$
N_U	Number of users that selected the URLLC slice (attributed resources based on the minimal delay scheme algorithm)
N_E	Number of users that selected the eMBB slice (attributed resources based on the maximal throughput scheme algorithm)
N_{RBU}	Number of PRBs initially allocated for the URLLC slice
N_{RBE}	Number of PRBs initially allocated for the eMBB slice
N_{RBtot}	Total number of PRBs and equal to $N_{RBE} + N_{RBU}$

Initially, we apply the legacy scheme from the state-of-art: $N_U = N_{URLLC}$ and $N_E = N_{eMBB}$. During the dynamic resource allocation process, a user can be served by a slice that does not necessarily correspond to its S-NSSAI type if that strategy optimizes its cost/reward function. As previously mentioned, in each slice, a resource allocation scheme compliant with its service type is applied. For the URLLC slice, a minimal delay scheme is sought for and thus, each user linked to this scheme is granted only 1 PRB which ensures sufficient throughput. In fact, the KPI in this slice is immediate service and low latency, hence, bestowing additional PRBs to a user does not impact positively the user's KPI. This is applied when $N_U \leq N_{RBU}$. Otherwise, the resource allocation is based on a fair resource sharing scheme. For the eMBB slice, the fair resource scheme is always applied for all users: in turn, every user gets all available PRBs. Furthermore, the unused PRBs linked with the URLLC slice are allocated to the eMBB slice (when $N_U \leq N_{RBU}$) to ensure an efficient resource allocation between the slices. This is due to the fact that additional PRBs are beneficial for the performance of eMBB users (requiring high throughput) which is not the case for URLLC users that require a prompt service but low throughput. Thus, an eMBB user will select its natural eMBB slice when the latter provides a high throughput.

For the sake of simplicity in this work, average radio conditions are considered and only the bandwidth partitioning between slices is considered rather than the PRB scheduling at the slice level. We denote by C_{ap}^k the average rate achieved by one PRB with the considered average radio conditions. A user k having its resources attributed by the eMBB slice (where maximal throughput is sought for) will have its throughput

Thr_k calculated as follows:

$$Thr_k^{eMBB} = \begin{cases} C_{ap}^k \cdot \frac{(N_{RBE}+(N_{RBU}-N_{users}+N_E))}{N_E} & \text{if } N_U < N_{RBU} \\ C_{ap}^k \cdot \left(N_{RBE}/N_E\right) & \text{Otherwise} \end{cases}$$

In fact, when $N_U < N_{RBU}$, users in the eMBB slice profit from unused PRBs from the URLLC slice. Otherwise, PRBs dedicated for the eMBB slice are equally shared among users that selected the latter.

A user k having its resources attributed by the URLLC slice (where minimal delay is sought for) will have throughput Thr_k, calculated as follows:

$$Thr_k^{URLLC} = \begin{cases} C_{ap}^k & \text{if } N_U \leq N_{RBU} \\ C_{ap}^k \cdot \left(N_{RBU}/N_U\right) & \text{Otherwise} \end{cases}$$

Additionally, the performance of the eMBB user is characterized by the realized throughput while the performance of the URLLC user is characterized by the endured delay.

The delay of a user k associated with eMBB slice is calculated as $Del_k^{eMBB} = 1/Thr_k^{eMBB}$ inspired by the work in [79], whereas the endured delay by user k in the URLLC slice is calculated as follows:

$$Del_k^{URLLC} = \begin{cases} 0 & \text{if } N_U \leq N_{RBU} \\ \left(\frac{N_U}{N_{RBU} \cdot C_{ap}^k}\right) & \text{Otherwise} \end{cases}$$

In fact, when $N_U \leq N_{RBU}$, a user is guaranteed one PRB which leads to minimal cost for a URLLC user. Otherwise, PRBs are equally shared among users in the URLLC slice and the cost equals the ensuing delay.

4.3 Distributed Dynamic RAN Slicing for eMBB and URLLC

In the distributed approach, the dynamic RAN Slicing scheme is portrayed as a non-cooperative game where players compete over a shared resource. Thus, it is defined as a multi-player game $\mathcal{G}$ where the players are the users competing over the allocated PRBs (the resource) in any slice. The framework of the game is presented as follows:

- The set $\mathcal{K}$ is the set of players (mobile users)
- The set $\mathcal{S} = \{e, u\}$ is the set of strategies where e and u designate the slice selection action for the eMBB and URLLC slices respectively. Let y_k denote the strategy of user k and whose components are the binary variables $y_{k,s}$ equal to 1 when user k chooses the slice s. Hence, $\mathbf{y} = (y_k)_{k \in \mathcal{K}} \in \mathcal{S}$ is a pure strategy profile, and $\mathcal{S} = S_1 \times S_2 ... \times S_K$ is the space of all profiles
- The set of cost functions $\{C_1, C_2, ..., C_K\}$ quantify the players' profitability over the possible outcomes of the game and are given by Equation (4.1).

4.3.1 Game objectives and cost functions

The objective of each user is to minimize its cost function by selecting the appropriate strategy which corresponds to the appropriate slice. The cost function is defined based on the user type. Consequently, an eMBB user has a cost function which takes into account the throughput whereas the cost function of the URLLC user accounts for the experienced delay. We consider the following cost function for a user k selecting a given slice:

$$C_k^{slice} = \begin{cases} \left(D_k/Thr_k^{slice}\right) + c_{slice} & \text{if user } k \text{ is of type eMBB} \\ \left(Del_k^{slice}/T_k\right) + c_{slice} & \text{if user } k \text{ is of type URLLC} \end{cases} \quad (4.1)$$

where:

- D_k denotes the comfort rate of an eMBB type user as defined in the SLA.
- T_k coins the acceptable delay of an URLLC type user as defined in the SLA.
- c_{slice} is the monetary cost of selecting the slice (eMBB or URLLC).

4.3.2 Choice of parameters

The cost function parameters (D_k, T_k, c_{eMBB}, c_{URLLC}) should be well defined which is discussed in this subsection.

The more PRBs are allocated to the eMBB slice, the greater is the user satisfaction. Therefore, it can be considered that $D_k \geq n \cdot C_{ap}^k$ where $n > 1$. Consequently, the eMBB user will select the service offering more PRBs. As for the acceptable delay, since the URLLC user is satisfied with one PRB, this leads to $T_k = 1/C_{ap}^k$ which makes the URLLC user more likely to choose the slice guaranteeing one PRB in each scheduling epoch. $0 \leq c_{eMBB} \leq c_{URLLC}$ is a condition that should be applied to push eMBB users towards slice e as long as their throughput is acceptable in order to protect slice u from overload. However, when slice e is too overloaded, an eMBB user might accept to pay "more" in slice u in order to get at least C_{ap}^k. As for URLLC users, slice u is largely preferred when $N_U \leq N_{RBU}$ as they are granted 1 PRB leading to zero delay (which is strictly lower than the delay realized in slice e), as long as c_{URLLC} is not prohibitive.

The convergence to the Pure Nash Equilibrium (PNE) is examined in the next subsection 4.3.3 where the PNE is defined and convergence to it is proven.

4.3.3 The Pure Nash Equilibrium

The Pure NE is the state sought to be attained in a non-cooperative game which was already defined in Chapter 1 in subsection 1.4.4. In this state, each player would have chosen an optimal strategy in response to other players' strategies. Our game $\mathcal{G}$ is a finite game which is guaranteed to possess a mixed NE but not Pure NEs. The former leads to a continuous change of strategy according to a probability distribution which can be cumbersome. Nonetheless, $\mathcal{G}$ has the Finite Improvement Path (FIP) property which proves the existence of PNE [35]. The proof of this property is given by the following:

Proposition 7. *$\mathcal{G}$ has the FIP property.*

Proof. $\mathcal{G}$ is an unweighted non-cooperative game since it is a game where users share a common set of actions and the cost function of a user after selecting a particular action is specific to that user only and is non-decreasing in the number of users choosing that same action. These types of games (Unweighted games) have the FIP property when players only have 2 strategies (e and u) according to [37]. □

Finally, $\mathcal{G}$ is guaranteed to converge to the PNE through the Best Response dynamics [38].

Hence, at each round of the Best Response, a user k goes through all available strategies and chooses the strategy (*i.e*, $s \in \mathcal{S}$) that provides it the lowest cost.

The behavior of the Best Response is described in Algorithm 3.

Input : Slice cost
Output: Slice selection based on lowest cost
1 Slice u is selected for URLLC users;
2 Slice e is selected for eMBB users;
3 **repeat**
4 | Calculation of cost slice C_k^{eMBB} and C_k^{URLLC} by each user;
5 | Slice with lowest cost is selected by the user;
6 **until** *Same slice as previous round is selected by the user*;

Algorithm 3: Dynamic Slicing Best Response Dynamics Algorithm

In the next section, the convergence time of the algorithm and its comparison with the legacy scheme and SOTA algorithm in [64] are discussed.

4.4 Performance Evaluation of the Distributed Game based Algorithm

For the simulation results, we used Matlab to assess a variety of KPIs given the number of URLLC users N_{URLLC} for our proposed solution, a SOTA algorithm in [64] taking into account only the slice selection aspect without a dynamic readjustment of resources, as well as the legacy scheme. The different KPI metrics used to evaluate the performance are the following:

- The service reliability of the URLLC slice which is defined as follows:

$$\begin{cases} 100 & \text{if } N_{URLLC} \leq N_{RBU} \\ \frac{N_{RBU}}{N_{URLLC}} \times 100 & \text{Otherwise} \end{cases}$$

  Therefore, the service reliability is equal to 100% if all URLLC users are guaranteed to have at least 1 PRB. Otherwise, it will be equal to the percentage of time where a user meets its required delay when a fair resource time sharing is applied.

- The throughput of all eMBB users

- The resource utilization efficiency of the URLLC Slice

As for the parameters, Table 4.2 displays the used simulation parameters.

Table 4.2: Dynamic slicing distributed approach simulation parameters

Parameter	Description	Value
C_{ap}^k	Throughput per PRB	1 Mb/s
N_{RBtot}	Total number of PRBs	50 PRB
N_{users}	Total number of users	40 users
D_k	The comfort rate of an eMBB user	$2 \cdot C_{ap}^k$
T_k	The comfort delay of an URLLC user	$1/C_{ap}^k$
c_{eMBB}	The cost of selecting the eMBB slice	1
c_{URLLC}	The cost of selecting the URLLC slice	1.677

We consider that $N_{RBU} = 20$ PRB are initially allocated for the URLLC slice and $N_{RBE} = 30$ PRB for the eMBB slice. As opposed to our algorithm, for the Legacy Scheme and SOTA algorithm in [64], N_{RBU} and N_{RBE} are fixed and do not change. The reason for this assignment is that we consider that more PRBs are needed for the eMBB slice to ensure a good throughput while less PRBs are required for the URLLC slice since 1 PRB is sufficient to satisfy the QoS of one user.

Figure 4.2 shows the variation of the throughput of all eMBB users when N_{URLLC} changes for our proposed algorithm, the SOTA slice selection algorithm [64] and legacy scheme.

The total throughput realized by our proposed approach is higher than in the Legacy scheme when $N_{URLLC} \leq 20$. The opposite happens when $N_{URLLC} > 20$. This is because the resources for the URLLC slice are allocated to the eMBB slice when there are few URLLC users. However, the fact that the Legacy scheme outperforms the dynamic scheme when $N_{URLLC} > 20$ is due to the allocation of the eMBB slice resources to the URLLC slice to satisfy their QoS requirements and reduce their cost functions. Additionally, our dynamic RAN slicing algorithm gives precedence to the URLLC slice performances over the eMBB slice. Compared to the SOTA slice selection algorithm [64], our algorithm always realizes better eMBB throughput results for any number of URLLC users with a maximum gain of 20%. This is due to the adjustment of the resource allocation between slices in our algorithm which is not taken into account in the SOTA algorithm that only provides the best slice selection for each user based on realized throughput and delay.

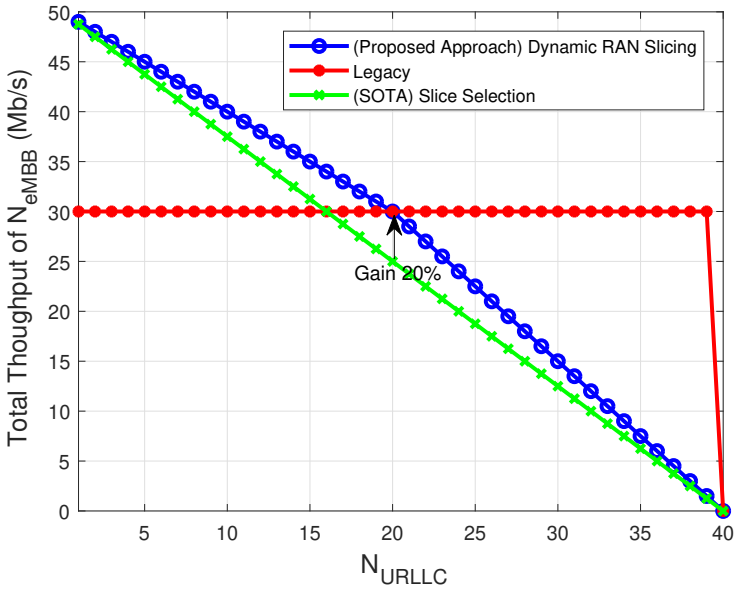

Figure 4.2: Total Throughput of eMBB type Users (Mb/s)

Figure 4.3 displays the variation of the Resource Utilization efficiency of the URLLC Slice as a function of N_{URLLC}. As can be seen, the utilization efficiency is 100% for all values of N_{URLLC} in our proposed dynamic scheme and SOTA algorithm [64] as opposed to the legacy scheme where there is an under-utilization of resources when $N_{URLLC} \leq 20$ and an over-utilization of resources when $N_{URLLC} > 20$. This is due to the adaptability of our dynamic slice selection algorithms to the varying demands of users and its endeavour to grant the URLLC users one PRB, which is necessary to satisfy their QoS requirements. The legacy scheme fails to do this. Consequently, the efficiency of both dynamic algorithms over the legacy scheme is proven when resources are over-provisioned for $N_{URLLC} \leq 20$ and under-provisioned for $N_{URLLC} > 20$.

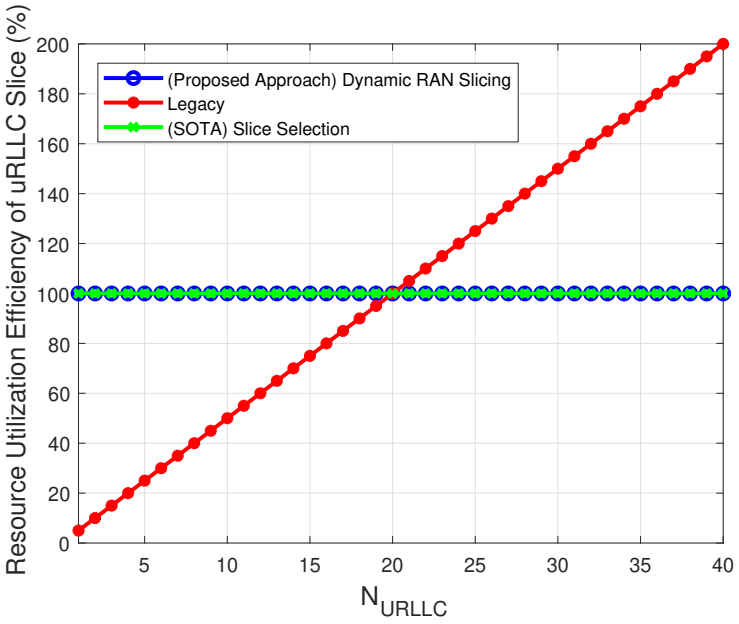

Figure 4.3: Resource Utilization Efficiency of URLLC Slice (%)

In Fig. 4.4, the URLLC Service Reliability is represented as a function of N_{URLLC} where our algorithm is compared against the legacy scheme and SOTA slice selection algorithm [64]. Recall that $N_{eMBB} = N_{users} - N_{URLLC}$. The advantage of both our proposed and SOTA algorithms is clear over the legacy scheme since both our proposition and the SOTA algorithm provide the same result, which is 100% of reliability for any number of URLLC users whereas this is only the case for the legacy scheme when $N_{URLLC} \leq 20$. This proves the adaptability of these algorithms when faced with a service load variation and the ability of the solution to provide constant reliability regardless of the URLLC load conditions even with a high resource utilization rate (as can be seen in Fig. 4.3). Conversely, the legacy scheme which always provides 20 PRBs for the URLLC slice shows a performance degradation for the URLLC slice when $N_{URLLC} > 20$ since it will not be able to guarantee 1 PRB in that case for all URLLC users. Additionally, when the number of URLLC users reaches its maximum (40), the service reliability plummets down to 50%. This can be explained by the fact that these 40 URLLC users are sharing 20 PRBs and each user gets its required service only half of the time. Therefore, our algorithm is adapted in a way to satisfy the increasing demand of the URLLC slice which is not the case for the Legacy scheme where the URLLC slice performance deteriorates in case of overload.

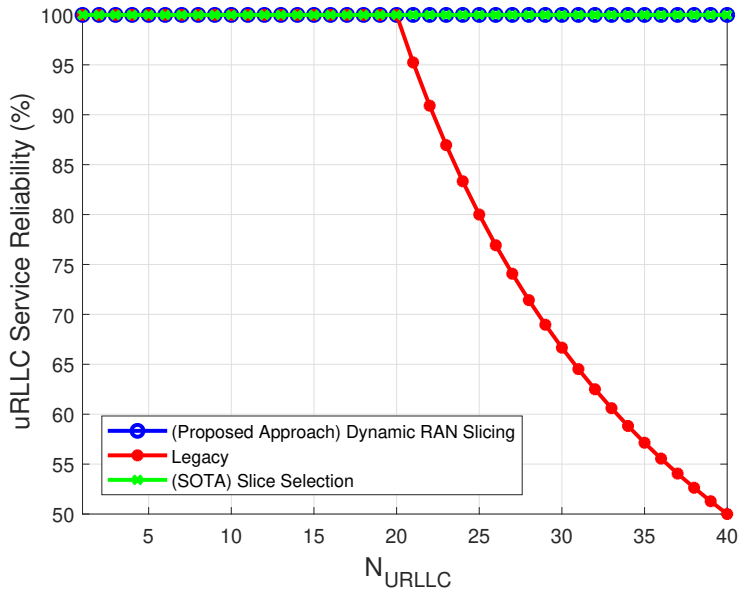

Figure 4.4: URLLC Service Reliability (%)

Finally, our algorithm provides better throughput results for eMBB users than the SOTA algorithm while ensuring simultaneously a high URLLC service reliability and high resource utilization efficiency, which are two advantages shared with the SOTA algorithm over the legacy scheme.

4.5 Centralized Dynamic RAN Slicing

The slicing algorithm which was tackled in the previous section with a distributed non-cooperative crowding game is tackled in this section using a DQN algorithm. DQN was already introduced and detailed in Chapter 1 in subsection 1.4.4. Consequently, it is important to define the state, actions and rewards of the problem which will be discussed in the next subsections.

4.5.1 The agent, environment and states

In our algorithm, the environment is none other than the number of URLLC and eMBB users along with their slice selection distribution between the URLLC slice and eMBB slice. The states can be identified as the association between the users and their choice of slice that will serve them (u or e). Therefore, each time a slice selection is changed for a user, the state of the environment is changed. It is also worth noting that the agent is none other than the Base Station controllers that collect the appropriate metrics from the mobile users and take the appropriate actions by adjusting the slice selection for each user. Consequently, it is important to pinpoint the actions that change the state of the environment and the reward functions used during each change of state.

4.5.2 The actions

Initially, we consider that each user is linked to their "natural" slice as is done in the state-of-art. Therefore, the URLLC users are associated to the URLLC slice while the eMBB users are associated to the eMBB slice. Subsequent to these initial conditions, two possible actions can be taken for each user: either switch the

user to another slice (from u to e or vice-versa) or keep the user in its current slice. Therefore, the action taken by the agent is either to keep or change the slice selection for each user. Each action taken by the agent will move the environment from a state to another while generating a reward that is used by the agent to assess the benefit of this action. The choice of this set of actions (keep or change slice per user) is to reduce the number of possible actions which in turn reduces the complexity of the algorithm. In a classic approach, the number of possible actions is $2^{N_{users}}$ since two slices are considered. Therefore, the complexity is reduced from $2^{N_{users}}$ to $2 \times N_{users}$ when narrowing down the overall actions to a per user action.

4.5.3 The reward function

As stated before, the crowding game is a decentralized approach where any user selfishly and autonomously selects a strategy that improves its own cost function. The DQN algorithm is a centralized approach as the reward function is global and takes into account all users KPIs to decide the optimal apportionment of users over the slices.

After taking an action for a given user to keep or modify its slice selection, the reward of this action takes into account the KPIs specific to each user. If the user is of type eMBB, its KPI is the ratio of the user throughput over its comfort throughput ($\frac{Thr_k}{D_k}$). The higher this ratio, the more beneficial it is to the system. This leads to counting it as a positive reward. If the user is of type URLLC, its KPI is the ratio of the user delay over its comfort delay ($\frac{Del_k}{T_k}$). The higher this ratio, the less beneficial it is to the system. This leads to counting it as a negative reward (in other words, a penalty). Moreover, an additional reward is considered to motivate users to favor the slice matching their service type.

Therefore, if the action is to keep the slice selection, the reward is expressed as follows where R_{add} is the bonus reward:

$$R_{keep} = \sum_{k \in eMBB} \frac{Thr_k}{D_k} - \sum_{k \in URLLC} \frac{Del_k}{T_k} + R_{add} \tag{4.2}$$

If the action is to change the slice for the user, the bonus reward is not taken into account and the reward is expressed as follows:

$$R_{change} = \sum_{k \in eMBB} \frac{Thr_k}{D_k} - \sum_{k \in URLLC} \frac{Del_k}{T_k} \tag{4.3}$$

Note that Thr_k and Del_k are the same as previously defined in the system model in section 4.2.

4.5.4 The DQN Algorithm Workflow

The DQN algorithm is described in Algorithm 4.

As seen in the algorithm, first we create the DQN agent with the definition of its number of inputs and outputs to retrieve the Q-values based on neural networks. Afterwards, for any given number of URLLC and eMBB users simulating the distribution of the users among the slices, we initialize the latter and associate them with their natural slice which is e for the eMBB slice and u for the URLLC slice. In the next step, we repeat the process where either a random action is taken with probability ϵ or an action with the highest Q-value is executed with probability $1 - \epsilon$. The action is either to keep or modify the slice selection for each user. In that process, we calculate the throughput and delay for users to retrieve the reward following the taken action which will be stored along with the newly reached state to find the optimal Q-values based on gradient descent. Once convergence is reached, the optimal policy is retrieved and the appropriate decisions are taken. The whole process is represented in Fig. 4.5 where the Non-Real Time RIC and near-Real Time RIC are the Base Station controllers.

Input : Q-values
Output: Slice selection action based on optimal Q-values
DQN inputs (states, discount factor...) and outputs (actions) are defined;
repeat
    Slice e is selected for eMBB users;
    Slice u is selected for URLLC users;
    repeat
        Take a random action with probability ϵ or highest Q-value action with probability $1 - \epsilon$ to keep or change the slice selection for each user;
        Calculate throughput and delay for users;
        Calculate the reward generated following the action taken;
        Calculate the Q-values;
        Update these values by gradient descent;
    until *Optimal Q-values and policy are found*;
until *All users distributions among service types have been simulated*;

Algorithm 4: Dynamic Slicing for eMBB and URLLC DQN Algorithm

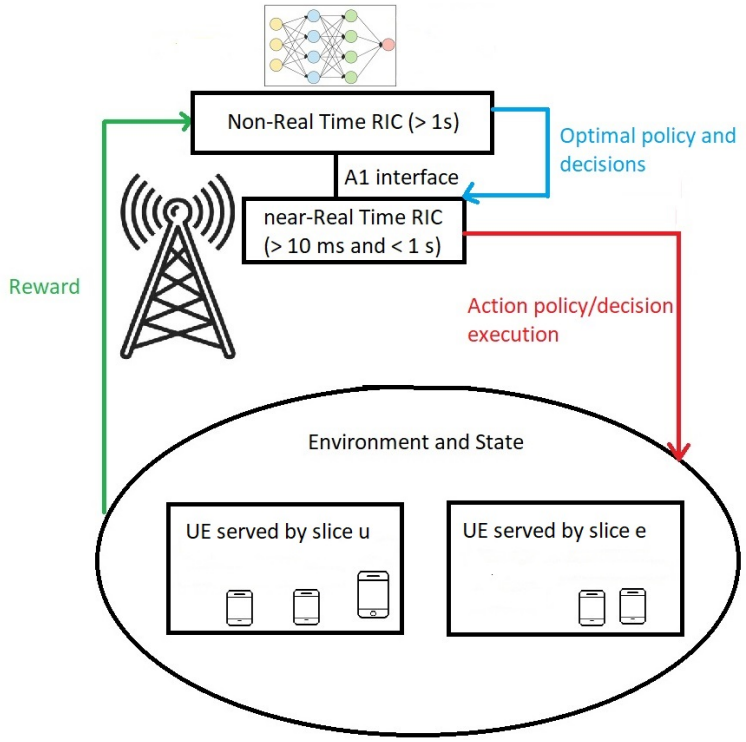

Figure 4.5: Dynamic Slicing for eMBB and URLLC DQN Process

4.6 Performance Evaluation of the Centralized DQN based Algorithm

For the algorithm implementation, we used Python with the Pytorch library. We also used the parameters in Table 4.3 for Algorithm 4.3. The same parameters for the distributed crowding game are used for the

Table 4.3: DQN Dynamic Slicing Algorithm parameters

Parameter	Description	Value
C_{ap}^{k}	Throughput per PRB	1 Mb/s
N_{RBtot}	Total number of PRBs	50 PRB
N_{users}	Total number of users	40 users
D_k	Comfort rate of an eMBB user	$2 \cdot C_{ap}^{k}$
T_k	Comfort delay of an URLLC user	$1/C_{ap}^{k}$
R_{add}^{eMBB}	Reward for keeping eMBB slice	1.3
R_{add}^{URLLC}	Reward for keeping URLLC slice	1

centralized DQN algorithm. As for R_{add}^{eMBB} and R_{add}^{URLLC} which denote the bonus reward, they are fine-tuned to obtain logical rewards and reach fast convergence for the agent training. Note that the condition $R_{add}^{eMBB} > R_{add}^{URLLC}$ ensures that changing the assigned slice for URLLC users can be more rewarding since a change of slice is required for these users when the attributed resources are not sufficient.

Initially, similar to the crowding game, we consider 20 PRBs to be allocated for the URLLC slice and 30 PRBs for the eMBB slice with the minimal delay scheme applied to all URLLC users and maximal throughput scheme applied to all eMBB users. Hence, $N_{RBU} = 20$ and $N_{RBE} = 30$. As for the KPIs used to evaluate the efficiency of the algorithm, we used the same KPIs as the crowding game algorithm: the service reliability, the total throughput, the resource utilization efficiency. Additionally, the required number of iterations to reach convergence is assessed.

With the DQN approach, a learning phase of the Q-values is required to attain convergence and take the appropriate decisions. This phase depends on multiple parameters including the discount factor, learning rate, the ϵ-greedy strategy affecting the balance between the exploration and exploitation of the environment, and the number of episodes required to train the agent.

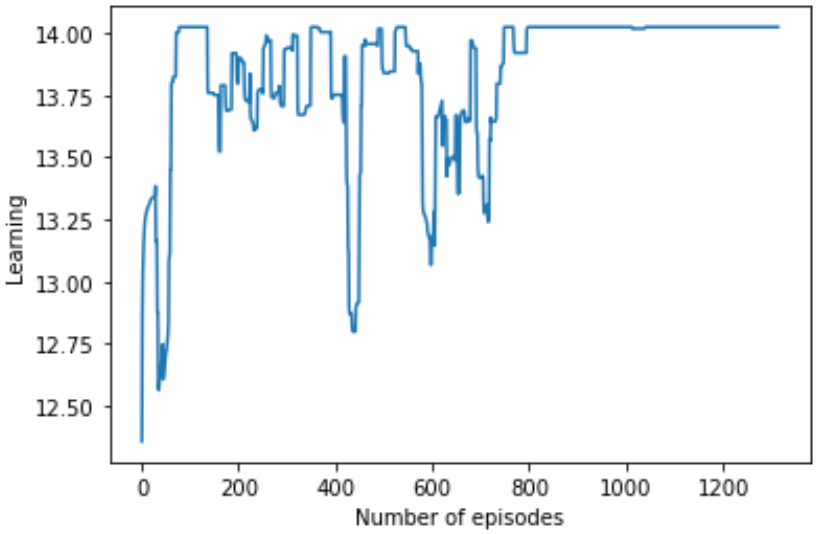

Figure 4.6: Learning phase with random DQN parameters

Figure 4.6 represents the learning phase of the Q-values as a function of the number of episodes with random parameters (learning rate, ϵ-greedy strategy ...) for a certain distribution of users between eMBB and URLLC services. We can see that a high number of episodes is required to reach convergence since

the agent requires to explore the environment. Nevertheless, we repeated the simulations multiple times with different combinations of parameters leading to the finding of an astute choice of these parameters requiring less number of episodes and less learning time. The algorithm was also adapted to stop the training once the state of the environment stabilizes after a certain number of episodes (due to convergence) which helps reducing the offline training time.

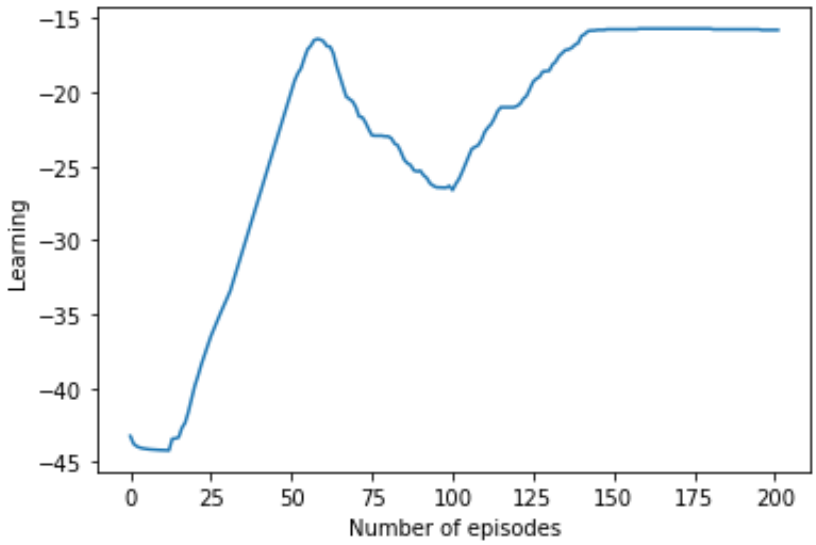

Figure 4.7: Learning phase with optimized DQN parameters

Therefore, Fig. 4.7 represents the learning phase of the Q-values as a function of the number of episodes with the optimized parameters. We can see that the number of episodes required to reach convergence is greatly reduced. Thanks to this fine-tuning of parameters and algorithm adaptation, the performance results improved significantly as we can see in Figs. 4.8 and 4.9.

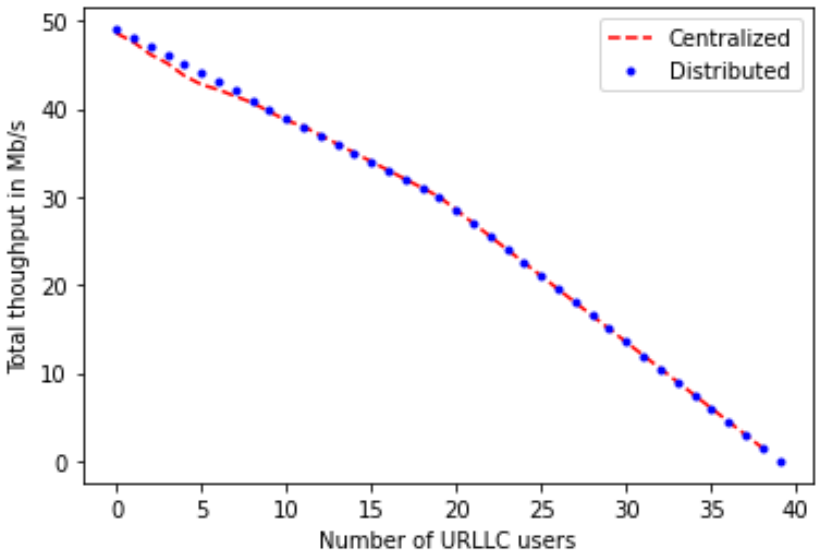

Figure 4.8: Total Throughput for eMBB users with Centralized and Distributed algorithms with random DQN parameters

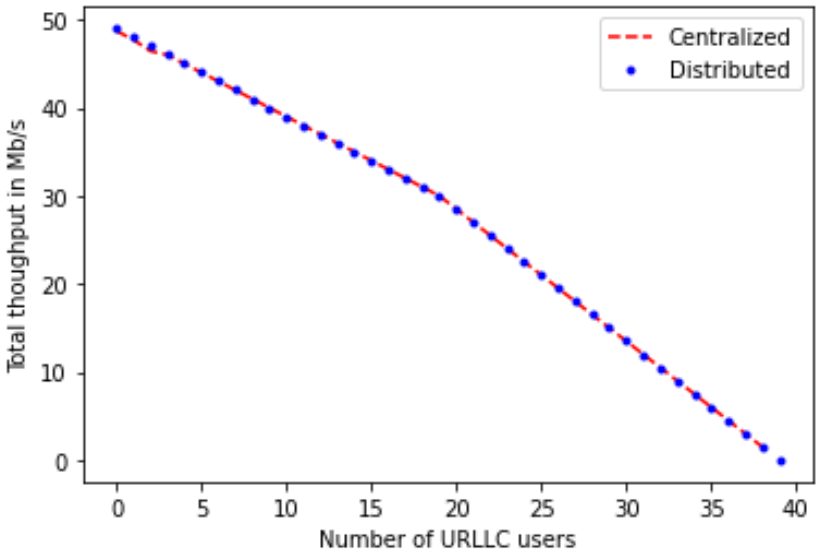

Figure 4.9: Total Throughput for eMBB users with Centralized and Distributed algorithms with fine-tuned DQN parameters

In both figures, we visualize the total throughput for eMBB users as a function of the number of URLLC users using both the centralized and distributed algorithms after convergence. Nevertheless, Fig. 4.8 displays the performance with random DQN parameters while fine-tuned parameters are considered in Fig. 4.9. In both figures, the eMBB total throughput has almost the same performance for both the centralized and distributed approach. However, with the fine-tuned parameters (Fig. 4.9), the curves almost match for the distributed and centralized approaches and realize the same performances indicating equivalent results. This is due to the fact that with fine-tuned parameters, both centralized and distributed algorithms converge to the same strategy (slice selection for user) leading to the same performance results. Hence, both algorithms outperform the legacy scheme when the number of URLLC users is below 20 which is not the case when it is above 20 owing to the algorithms adaptability to fulfill the URLLC QoS requirements by shifting the resources from the eMBB slice to the URLLC slice to attenuate any performance deterioration. For this reason as well, both our distributed and centralized algorithms outperform the SOTA slice selection [64] with a maximum gain of 20 %.

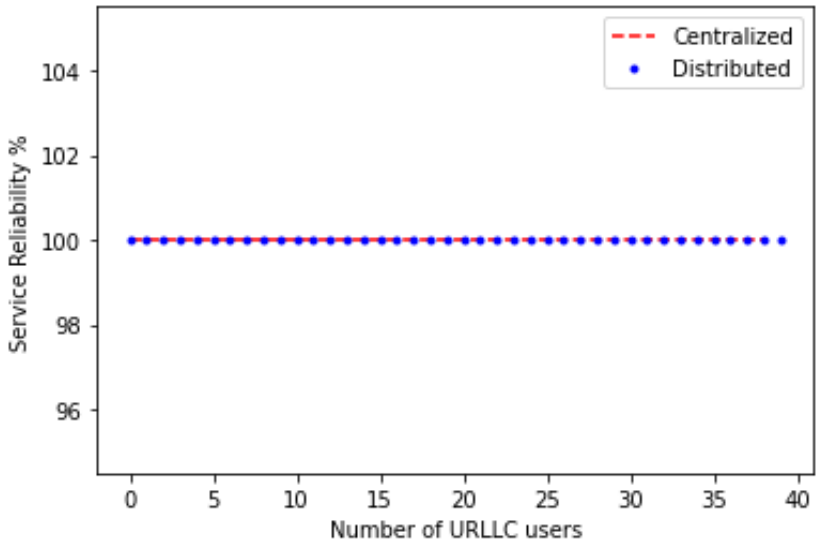

Figure 4.10: Service Reliability for URLLC users using DQN (centralized) and crowding game (distributed) approaches

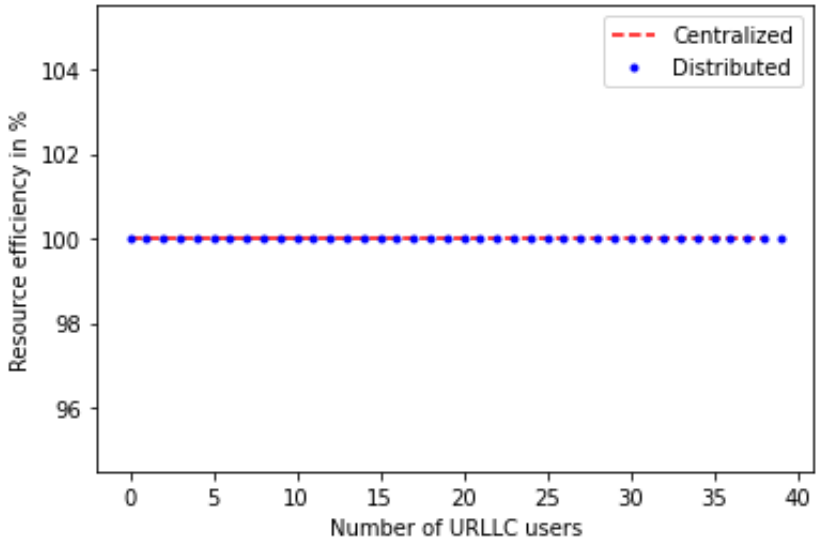

Figure 4.11: Resource utilization efficiency with centralized and distributed algorithms

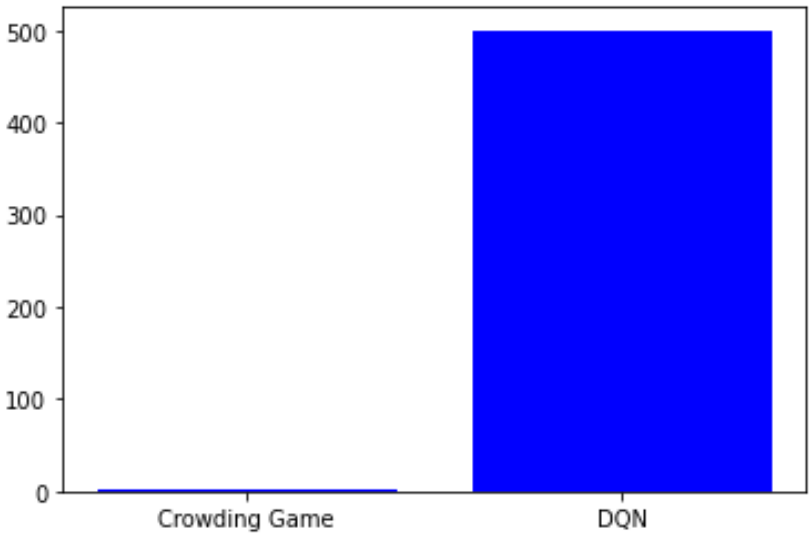

Figure 4.12: Maximum number of iterations to reach convergence for DQN and Crowding game algorithms

As for the URLLC Service Reliability and Resource Utilization efficiency, both algorithms also achieve the same results with a value of 100% (Figs. 4.10 and 4.11).

Figure 4.12 displays the maximum number of iterations required to attain convergence for both the DQN (after fine-tuning the parameters) and Crowding game algorithms. We can conclude that for a given distribution of the users among the service types, the number of iterations required to achieve that convergence does not exceed 500 for the DQN algorithm which is much greater than the number of iterations needed for the crowding game algorithm to converge (only 2 iterations). With a confidence interval of 95%, the training time needed with 40 users and for all combinations of users between URLLC and eMBB types of users is around 6 minutes instead of several hours thanks to this astute parameters adjustment and algorithm adaptation as well as the drastic reduction of the number of actions (from exponential to linear in the number of users) which reduces notably the algorithm complexity.

4.7 Algorithm Implementation in O-RAN Architecture

4.7.1 Distributed Dynamic RAN Slicing Algorithm in the O-RAN

The Best Response algorithm is to be executed at the level of the near-real-time RIC since convergence is attained swiftly.

In our case, the time spent for slice selection is equivalent to one time slot. After the slice selection, the calculated KPI in terms of throughput or delay is sent to the near-RT RIC which is the entity that will calculate the cost functions for each user and store the appropriate strategy in each round. During each round, we have a certain number of users coined N_{users} where each user needs TS time slots to select all strategies. Consequently, the time needed to reach the Best Response Algorithm convergence is $N_{users} \times TS \times R_{max}$ where R_{max} is the maximum number of rounds for convergence. Since R_{max} is as low as 2 rounds and with N_{users} and TS having assigned values in normal conditions, the Best Response Dynamics algorithm converges within a time range of 10 ms to 1 s and therefore can be implemented at the level of the near-RT RIC. This is not the case of RL based algorithms that usually take several minutes to converge. In that case, these types of algorithms are best implemented at the level of the Non-RT RIC which will find the

best policy needed by the near-RT RIC to execute the appropriate action based on certain calculations and decisions transmitted over the A1 interface connecting the Non-RT RIC to the near-RT RIC.

4.7.2 Centralized Dynamic RAN Slicing Algorithm in the O-RAN

The DQN algorithm requires a training phase where learning of the Q-values is done to take appropriate actions. This training may require several hours to find the best policy. In our case, the training requires around 6 minutes as was previously mentioned. Consequently, the training phase which is done offline will take place at the level of the Non-RT RIC which acts beyond 1 s. Once the training phase is finished and the appropriate actions are learned based on the KPIs of users, the appropriate decisions and model to be executed are transmitted to the near-RT RIC over the A1 interface. Therefore, it is the near-RT RIC that adjusts the resource sharing between the slices. During the training phase, the agent in the Non-RT RIC will explore the environment and take random actions to assess the consequences and find the Q-values. Upon the termination of the training phase, the near-RT RIC executes the decisions of the slice selection for each user based on the network inputs (i.e. number of users) which is fast enough and within the time range of the near-RT RIC (between 10 ms and 1 s).

4.8 Comparison between the distributed and centralized Dynamic RAN Slicing algorithms

Both approaches achieve the same results since we obtained the same KPIs after convergence which proves the efficiency and adaptability of both algorithms to satisfy and prioritize the users' needs. This is due to the fact that both algorithms converge to the same strategy. In fact, the PNE in the game theory based approach is the minimum of the game potential function. The latter scales with the reward function adopted in the DQN approach. That is why both approaches reach the same strategy set at convergence. Nevertheless, the crowding game approach is much faster in terms of convergence. Therefore, the implementation of this algorithm only involves the near-RT RIC of the O-RAN architecture. However, a crowding game algorithm requires to meet certain criteria and properties to reach the PNE. In fact, existence of PNE is no longer guaranteed if users need to choose between more than two strategies (URLLC slice and eMBB slice), contrarily to the centralized scheme that can scale with any number of slices. However, increasing the number of available slices directly impacts the convergence of the underlying DQN algorithm. Additionally, even though the solution for the game based approach can be centralized in a certain entity, its solution is not global. The approach is rather autonomous and selfish with regards to each user or player of the game. This is not the case for the DQN based algorithm. In fact, the reward function can be defined with more liberty without meeting stringent requirements. Therefore, the approach is more global and takes into account the benefits and KPIs of all users. While it is true that convergence is much slower with the DQN algorithm, it only concerns the training phase which can be done offline in the Non-RT RIC. Once the training phase is over, the execution of decisions by the near-RT RIC can be fast enough similarly to the crowding game algorithm. It is also worth to note that both algorithms are executed swiftly compared to other works in the state of art using ML methods [66][51][52]. Also, an additional benefit for the DQN is its adaptability to changes in the hypothesis and inputs which will require additional training but fast decision making time once the training is done. Finally, the entities of the O-RAN architecture, the flexibility of the solution and the convergence time needed must be considered when implementing any of these algorithms. Table 4.4 summarizes the comparison.

Table 4.4: Comparison of both centralized and distributed dynamic slicing approaches

	Centralized	**Distributed**
URLLC Reliability	100%	100%
Resource Utilization	100%	100%
eMBB Throughput	Same results	Same results
Convergence	Swift after offline training	Attained swiftly
Approach	Global and scalable	Selfish
O-RAN components	Non-RT and near-RT RIC	near-RT RIC

4.9 Concluding Remarks

In this chapter, a dynamic slicing algorithm for eMBB and URLLC in a single VO context was proposed via a distributed crowding game solution and a centralized DQN solution where:

- Both approaches achieve the same performance in terms of eMBB throughput and URLLC reliability and resource utilization efficiency thanks to the defined cost and reward functions.
- Results show the efficiency of our dynamic RAN slicing algorithm and its adaptability against the variation of load conditions that avert the need to increase the available bandwidth.
- The proposed solution achieves better eMBB throughput compared to the SOTA work in [64] thanks to the dynamic readjustment of slice resources while maintaining a high reliability and high resource utilization efficiency compared to the legacy scheme.
- The alignment of this solution with the O-RAN architecture is also discussed.
- The distributed approach may reach faster convergence than the centralized one. Nonetheless, the distributed solution lacks scalability.

However, this contribution does not consider the numerology, users' radio conditions and arrival process and the mMTC slice. Therefore, these aspects are considered in the next chapter with a three-level algorithm solution.

Chapter 5

A Three-Level Slicing Algorithm in a Multi-Slice Multi-Numerology Context

In this chapter, we propose a solution that extends the previous work to include the numerology, the mMTC slice, both preemptive and orthogonal scheduling for eMBB and URLLC coexistence as well as users' radio conditions and arrival process. The numerology is a paramount factor that should be considered in the radio resource allocation problem since different services and slices may require different numerologies. In this work, three numerologies and four BWPs are considered where we have a BWP for each slice (eMBB, URLLC and mMTC) and one that is shared between eMBB and URLLC services under preemptive scheduling. The proposed solution is a three-level algorithm that selects the BWP serving URLLC users (choice between preemptive and orthogonal scheduling), attributes resources to each slice and BWP and dimensions a Guard Band (GB) between BWPs using different numerologies. Therefore, various tools are used to tackle each problem from game theory and heuristics to DQN. Also, users' KPI such as throughput, delay and Signal-to-Interference-plus-Noise Ratio (SINR) as well as the Inter-Numerology Interference (INI) are taken into account in order to take the appropriate decisions at each level. The advantages brought by this solution compared to the previous contribution and another SOTA work are also highlighted along with the alignment of this solution with the O-RAN architecture.

5.1 Introduction

The previous chapter introduced a novel dynamic slicing algorithm specifically for eMBB and URLLC. Despite its efficiency and simplicity, this solution disregards some important aspects such as the numerology, the mMTC class of service and the users' radio conditions. In fact, heterogeneous services may require different numerologies. For example, the URLLC service requires a higher numerology to attain lower latency while the eMBB service requires a lower one since it offers a higher payload. However, the use of multiple numerologies on the same band causes INI which is an additional challenge. In such a multi-slice multi-numerology context, the radio resource allocation problem is very challenging since multiple parameters come into play such as thwarting the INI, reducing the URLLC latency, increasing the eMBB Throughput, and ensuring high Signal-to-Interference-plus-Noise Ratio (SINR). To that aim, we propose a three-level scheme that takes into account multiple performance metrics complimentary to the SLA fulfillment where:

- The first level selects the numerology-specific BWP to serve URLLC users using game theory.
- The second level adjusts the dedicated band for each slice using heuristics.
- The third level performs the dimensioning of the guard band separating the BWPs using different numerologies to curb the impact of INI using DQN.

This three-level algorithm deals with all possible challenges induced from a multi-numerology setting while considering both preemptive and orthogonal scheduling for eMBB and URLLC coexistence. This is different from certain SOTA works which consider a single challenge while ignoring others and other works focusing on a single scheduling option for eMBB and URLLC coexistence. Simulations results prove the efficiency of our solution compared to our previous contribution and another SOTA work [73] that disregards the addition of a GB between BWPs using different numerologies. The organization of this chapter is as follows:

Section 5.2 presents the system model of the targeted problem. Sections 5.3, 5.4, and 5.5 describe each level of our three-level scheme as well as the problem to be solved at each stage while Section 5.6 summarizes the overall process. Section 5.7 provides simulation results and performance evaluation of our proposed solution. Section 5.8 discusses the implementation feasibility and mapping of the solution in an O-RAN architecture. The conclusion of this chapter is drawn in Section 5.9.

5.2 System Model

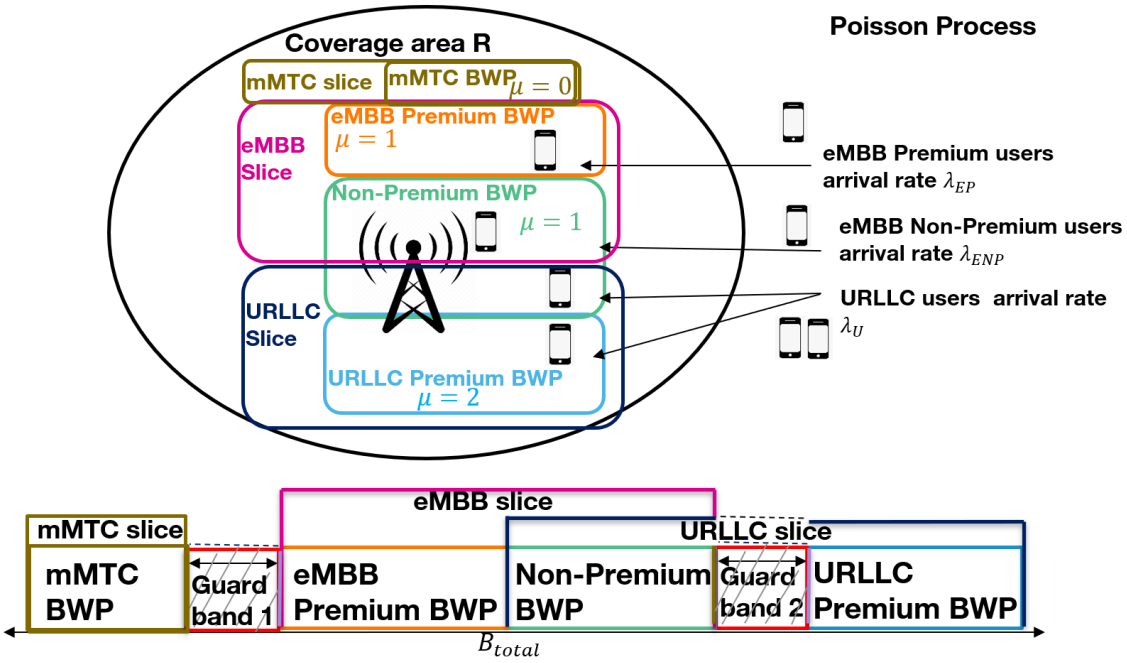

Figure 5.1: The System Model for Multi-Numerology Multi-Slice Context

As represented in Fig. 5.1, we consider a single gNB with $B_{total} = 90$ MHz bandwidth divided between four BWPs. The gNB covers an area with radius R. This gNB operates on the $f_{operator} = 3.5$ GHz frequency (FR1) in Time-Division Duplex (TDD) mode. In the case of low traffic load, the whole operator bandwidth may not be entirely allocated and the surplus remains unused for energy efficiency and for BWPs separation to curb the INI. Additionally, only the downlink is taken into account in this work as the INI effect is magnified in this case. Moreover, to avoid inter-cell interference (as the main focus is inter-numerology interference), we consider that the neighboring gNBs are using orthogonal bands.

Note that since a high number of symbols are used, Table 5.1 displays the most important ones with their description.

5.2.1 The Slices

The three considered slices for each service are the following:

- The eMBB slice $eMBB$ where all eMBB users are attached.
- The URLLC slice $URLLC$ where all URLLC users are attached.
- The mMTC slice $mMTC$ where all mMTC users are attached.

5.2.2 Choice of numerology and Bandwidth Parts

Three different numerologies and four BWPs are considered as follows:

- The mMTC BWP (denoted MP) is the one dedicated for the mMTC slice and allocated to mMTC users which can be IoT devices. This BWP is associated with $\mu = 0$ (SCS=15 kHz) and a fair resource scheme scheduler is used for its users.
- The eMBB Premium BWP (denoted EP) is the one dedicated for the eMBB slice and allocated to eMBB users paying the operator a higher monetary cost than other users for a higher throughput guarantee in return. This BWP is associated with $\mu = 1$ (SCS=30 kHz) and a fair resource scheme scheduler is used for its users.
- The Non-Premium BWP (denoted NP) is the one shared between eMBB and URLLC slices and allocated to both eMBB and URLLC users paying the operator a lower monetary cost than other premium users. Consequently, the operator provides lower throughput for these eMBB users and higher latency for these URLLC users. This BWP is also linked to $\mu = 1$ (SCS=30 kHz), and preemptive scheduling is applied where URLLC packets are scheduled on top of on-going eMBB transmissions. The latter fairly share the remaining PRBs that are not endowed to URLLC users.
- The URLLC Premium BWP (denoted UP) is the one dedicated for the URLLC slice and allocated to URLLC users paying a higher monetary cost for a lower latency guarantee in return. This BWP is linked to $\mu = 2$ (SCS=60 kHz). In this BWP, the PRBs are attributed based on each user's demand using a weighted fair queuing scheme.

Each BWP can have a maximum and a minimum band defined depending on the operator's traffic expectations. Additionally, the attributed band to each BWP along with the used numerology determine the number of PRBs available at the level of each BWP.

Additionally, when the whole operator band is used, a guard band between the BWPs using different numerologies is configured. Therefore, since the eMBB Premium and Non-Premium BWPs are using the same numerology, no guard band is required between them as the INI effect is absent and the addition of one leads to radio resource wastage. As for the choice of numerology, $\mu = 0$ should be selected for mMTC according to Table 4 from the work in [16]. Regarding eMBB and URLLC, a lower numerology should be selected for eMBB while a higher numerology should be selected for URLLC as explained previously. Since we are using the sub-6 GHz frequency range, we are limited to numerologies 0, 1 and 2 as advocated by 3GPP specifications [12]. The highest one ($\mu = 2$) is selected for URLLC Premium BWP to provide lower latency. As for the Non-Premium BWP, we chose $\mu = 1$ since the INI effect will be reduced when the SCS gap is smaller meaning that the use of $\mu = 1$ with $\mu = 2$ causes less INI than the use of $\mu = 0$ with $\mu = 2$ for the adjacents BWPs NP and UP. Also, $\mu = 1$ provides lower latency than $\mu = 0$ for URLLC users associated with the Non-Premium BWP. As for the eMBB Premium BWP, a wide band may be attributed

to this BWP since it requires a high throughput and the used bandwidth may be higher than 50 MHz. However, according to 3GPP specifications, the use of $\mu = 0$ with a total bandwidth higher than 50 MHz is not possible [12]. For this reason and in order to allow all eMBB users to use the same numerology regardless the BWP, we resort to $\mu = 1$ for the eMBB Premium BWP as well.

5.2.3 Users and Traffic Distribution

We consider a number of users $NbUsers$ randomly distributed in the gNB coverage area within the radius R with each user associated to one type of service (one slice) exclusively. For eMBB and URLLC users, the users' arrival to the network follows a Poisson process, and these users are divided between three sets:

- The eMBB Premium users attached to the eMBB slice and linked to the eMBB Premium BWP arriving to the network following a Poisson process with a mean of λ_{EP} users/sec.
- The eMBB Non-Premium users attached to the eMBB slice and linked to the Non-Premium BWP arriving to the network following a Poisson process with a mean of λ_{ENP} users/sec.
- The URLLC users attached to the URLLC slice and that will be associated to either the URLLC premium BWP or Non-Premium BWP depending on the BWP assignment algorithm in the first level. These users arrive to the network following a Poisson process with a mean of λ_U users/sec.

The eMBB users have a given amount of data V_{eMBB} to download, drawn randomly. Once the data is fully downloaded, they leave the network. The URLLC users remain active in the network for a fixed period of time where a number of packets are generated continuously following a Poisson process with a mean of λ_{PktU} packets/s with a fixed size. As for mMTC users, we consider that we have a fixed number of IoT devices $IoTNodes$ distributed in the coverage area and hence they do not follow an arrival process. These users are actively receiving a fixed number of packets per second Pkt_{IoT} with a fixed size of a few bytes.

5.2.4 Computing the network parameters and KPIs

We use the analytical formula for the INI resulting from the simultaneous use of multiple numerologies as proposed in [73] based on [71]. In fact, the INI affecting BWP k using a narrow numerology and caused by BWP k' using a wider numerology is expressed as follows:

$$I(k,k') \approx \frac{P_{k'}}{N_{k'}} \sum_{i=1}^{N_k} \sum_{j=1}^{N_{k'}} \frac{g_{k'}}{N_k N_{k'}} \left[\left| \frac{\sin\left[\frac{\pi}{N_k} w(i,j)\, \delta N_{k'}^{(T)}\right]}{\sin\left[\frac{\pi}{N_k} w(i,j)\right]} \right|^2 + \delta \left| \frac{\sin\left[\frac{\pi}{N_k} w(i,j)\, N_{k'}^{(T)}\right]}{\sin\left[\frac{\pi}{N_k} w(i,j)\right]} \right|^2 \right] \tag{5.1}$$

The INI inflicted on BWP k' by BWP k is expressed as follows:

$$I(k',k) \approx \frac{P_k}{N_k} \sum_{i=1}^{N_k} \sum_{j=1}^{N_{k'}} \frac{g_k}{N_k N_{k'}} \left| \frac{\sin\left[\frac{\pi}{N_k} w(i,j)\, N_{k'}\right]}{\sin\left[\frac{\pi}{N_k} w(i,j)\right]} \right|^2 \tag{5.2}$$

where:

- N_k denotes the total number of subcarriers of BWP k
- $N_k^{(T)}$ denotes the total number of subcarriers of BWP k including those employed for cyclic prefix
- P_k is the transmitted power of BWP k

- g_k is the channel gain over BWP k
- $w(i,j)$ corresponds to the spectral distance between subcarriers i and j of different numerologies
- δ is the number of OFDM symbols of the higher numerology that are transmitted within the time transmission window of one OFDM symbol of the lower numerology

After retrieving the INI, the SINR in dB of user u with its resources allocated from BWP k is calculated as follows:

$$SINR\_dB_u = Pt + Gt + Gr - PL - M\_shadow - I\_dB_u(k, k') \tag{5.3}$$

where:

- Pt is the transmit power of the gNB in dB
- Gt denotes the antenna gain at transmission in dBi
- Gr denotes the antenna gain at reception in dBi
- PL is the channel Path Loss in dB
- M_shadow corresponds to the shadowing effect in dB with a standard deviation of $Shad_{SD}$
- $I\_dB_u(k, k')$ denotes the INI in dB impacting user u having resources from BWP k affected by BWP k'

Once the SINR is computed, the modulation order MO_u and coding rate CR_u of user u are retrieved from a Channel Quality Indicator (CQI) table used in the literature [80]. As for the KPIs, we chose the throughput for eMBB users, the latency for URLLC users and the SINR for mMTC users. The throughput of eMBB user u is computed as follows:

$$Thr_u = \frac{AllocatedPRB_u \times Bits\_Per\_PRB}{TTI_{duration}} \tag{5.4}$$

where $AllocatedPRB_u$ is the number of PRBs allocated to the user u during a TTI, $Bits\_Per\_PRB$ is the number of bits per PRB and $TTI_{duration}$ is the duration of the TTI corresponding to 0.5 ms for numerology 1. In fact, the number of bits in a PRB is determined below based on the channel conditions of the user:

$$Bits\_Per\_PRB = 12 \times 14 \times \log_2(MO_u) \times CR_u \tag{5.5}$$

where 12 and 14 represent the number of subcarriers and OFDM symbols respectively in a PRB since the latter is considered to be composed of 12 subcarriers in the frequency domain and 14 OFDM symbols in the time domain. MO_u and CR_u are the modulation order and coding rate selected for user u based on its SINR. Moreover, $AllocatedPRB_u$ is determined by the fair resource scheme scheduler which is:

$$AllocatedPRB_u = \lceil \frac{Tot\_PRB_{BWP}}{NbUsers_{BWP}} \rceil \tag{5.6}$$

where $\lceil . \rceil$ is the ceiling function, Tot_PRB_{BWP} is the total number of PRBs available at the BWP scanned by the user and $NbUsers_{BWP}$ is the number of users linked to this BWP.

Note that Tot_PRB_{BWP} is determined by Table 5.3.2-1 from [12] depending on the attributed band and numerology.

To determine the latency of URLLC users which are served based on a weighted fair queuing algorithm based on their demand, the number of PRBs required by each URLLC user should be determined first. In fact, the number of PRBs required by a user of any type u is determined using the following expression:

$$RequiredPRB_u = \lceil \frac{Pkt_u \times PktSize}{Bits\_Per\_PRB} \rceil \tag{5.7}$$

where $\lceil . \rceil$ is the ceiling function, Pkt_u is the number of packets to be received by user u and $PktSize$ is the packet size in bits. $Bits\_Per\_PRB$ is none other than the number of bits in a PRB determined previously by Equation (5.5) that takes into account the channel and radio conditions of user u. Consequently, the number of PRBs required by user u is its number of packets to be received multiplied by the packet size in bits and divided by the number of bits in a PRB. Then, the total number of PRBs required by the URLLC users linked to a specific BWP is computed as follows:

$$Tot\_ReqURLLC_{BWP} = \sum_{u \in BWP} \sum_{u \in URLLC} RequiredPRB_u \tag{5.8}$$

In the next step, we compare $Tot\_ReqURLLC_{BWP}$ to the total number of PRBs available at the BWP (Tot_PRB_{BWP}) to verify availability:

- If $Tot\_ReqURLLC_{BWP} \leq Tot\_PRB_{BWP}$, this means that the BWP is sufficient to satisfy all URLLC users demands and a weighted fair queuing scheduler is applied based on each user's demand with the weight $w_u = \frac{RequiredPRB_u}{Tot\_ReqURLLC_{BWP}}$ and the number of allocated PRBs to each URLLC user is $AllocatedPRB_u = \lceil w_u \times Tot\_PRB_{BWP} \rceil$ with $\lceil . \rceil$ the ceiling function.
- Otherwise, when the BWP is unsufficient to fulfill all its served users' requirements, a weighted fair queuing scheduler is still applied where the available resources are divided between the users based on their original demand and the number of allocated PRBs to each user is $AllocatedPRB_u = \lceil w_u \times Tot\_PRB_{BWP} \rceil$ with $\lceil . \rceil$ the ceiling function.

Subsequently, the latency of URLLC user u is expressed as follows:

$$L_u = d_t + d_{al} + d_{ue} + d_{bs} \tag{5.9}$$

where:

- d_t is the transmission delay in ms
- $d_{al} = 1$ TTI is the packet alignment time in ms according to [81]
- d_{ue} is the UE processing time equal to 4.5 OFDM symbols according to [81]
- d_{bs} is the BS processing time equal to 2.75 OFDM symbols according to [81]

Hence, in this equation, since the URLLC users are served promptly based on their demands, only the transmission delay is considered and the queuing delay is not taken into account. Note that d_{ue}, d_{bs} and d_{al} depend on the numerology used since they depend on the TTI and OFDM symbol duration. As for the transmission delay, it is determined as follows:

$$d_t = \begin{cases} 0 & \text{if } Tot\_ReqURLLC_{BWP} \leq Tot\_PRB_{BWP} \\ \frac{PktLength}{Thr_u} & \text{Otherwise} \end{cases} \tag{5.10}$$

We consider that the transmission delay is null if there are enough PRBs available in the BWP ($Tot\_ReqURLLC_{BWP} \leq Tot\_PRB_{BWP}$) since users are served promptly. Otherwise, the transmission

time is the ratio of packets length in bits $PktLength = Pkt_u \times PktSize$ over the URLLC user throughput Thr_u (determined similarly to eMBB users by using equation (5.4)).

Note that for the Non-Premium BWP, the number of PRBs available for the eMBB users is given by:

$$Tot\_PRBeMBB_{NP} = Tot\_PRB_{NP} - Tot\_ReqURLLC_{NP} \tag{5.11}$$

which is the difference between the total number of PRBs available at the Non-Premium BWP Tot_PRB_{NP} and the total number of PRBs required by the URLLC users linked to the Non-Premium BWP $Tot\_ReqURLLC_{NP}$ which are served immediately on top of eMBB Non-Premium users' transmissions. Those PRBs $Tot\_PRBeMBB_{NP}$ are shared equitably among the eMBB users using a fair resource scheme.

Regarding mMTC users, this type of users is contented with a low throughput and can tolerate a higher delay than URLLC. Hence, they are less demanding than the other two classes of services. Therefore, the main concern for these users is to allot them an appropriate bandwidth for their assigned BWP. To that aim, their BWP size is selected based on the bandwidth that offers a number of PRBs higher than what is requested by mMTC users. Therefore, with the assumption that all mMTC users receive the same number of packets and have the same packet size, only the number of mMTC users and the required PRBs per mMTC user are required to determine the appropriate band. For the required number of PRBs per mMTC user, it is determined thanks to equation (5.7) under the worst radio conditions where the user is considered to be located at the edge of the cell.

In addition, the chosen KPI for mMTC users is the SINR which is calculated thanks to equation (5.3) due to the fact that the higher their SINR, the less power they consume which is an important aspect for these users as energy efficiency is paramount for the mMTC class. In fact, when the SINR is low, power consumption should be increased to improve the SINR.

These network parameters and KPIs, which are summarized in Table 5.1, are essential for the execution of our algorithm operating on three levels: the first level assigns the BWP for each URLLC user, the second level adjusts the BWP size, and the third level configures an appropriate guard band to reduce the INI between BWPs using different numerologies.

Table 5.1: Symbol Description for Multi-Slice Multi-Numerology Problem Context

Parameter	**Description**
MP, EP, NP, UP	mMTC, eMBB Premium, Non-Premium, URLLC Premium BWPs
$AllocatedPRB_u$	Allocated PRBs for user u
$Bits\_Per\_PRB$	Number of bits per PRB
$TTI_{duration}$	Duration of a TTI
MO_u	Modulation Order of user u
CR_u	Coding Rate of user u
L_u	Latency of user u and URLLC KPI
Thr_u	Throughput of user u and eMBB KPI
$SINR_u$	SINR of user u and mMTC KPI
Tot_PRB_{BWP}	Total Number of PRBs available at the BWP
$NbUsers_{BWP}$	Number of Users linked to BWP
$RequiredPRB_u$	Required number of PRBs for user u
Pkt_u	Number of Packets to be received by user u
$PktSize$	Packet size

5.3 The First Level: URLLC BWP Selection

The first level of the algorithm consists of the BWP selection for URLLC users between the Non-Premium BWP and URLLC premium BWP. For this level, we resort to non-cooperative game theory since the problem can be modeled as a competition between self-interested users for limited resources. Therefore, this problem is tackled as a non-cooperative game $\mathcal{G}$ where the players are the URLLC users competing over common PRBs resources available in the mentioned BWPs. The game framework is presented as follows:

- The set $\mathcal{U}$ is the set of players (URLLC users).
- The set $\mathcal{S} = \{np, up\}$ is the set of strategies where np and up designate the Non-Premium BWP and URLLC Premium BWP respectively. The vector y_u is the strategy vector of URLLC user u whose components are the binary variables $y_{u,bwp}$ equal to 1 when URLLC user u chooses the BWP bwp. Hence, $\mathbf{y} = (y_u)_{u \in \mathcal{U}} \in \mathcal{S}$ is the strategy profile, and $\mathcal{S} = S_1 \times S_2 ... \times S_U$ is the space of all profiles.
- The set of cost functions $\{C_1, C_2, ..., C_U\}$ quantify the players' profitability over the possible outcomes of the game.

5.3.1 The Cost function

In this game $\mathcal{G}$, each player (URLLC user) aims at minimizing its cost function by selecting the appropriate strategy (BWP) as portrayed in Fig. 5.2.

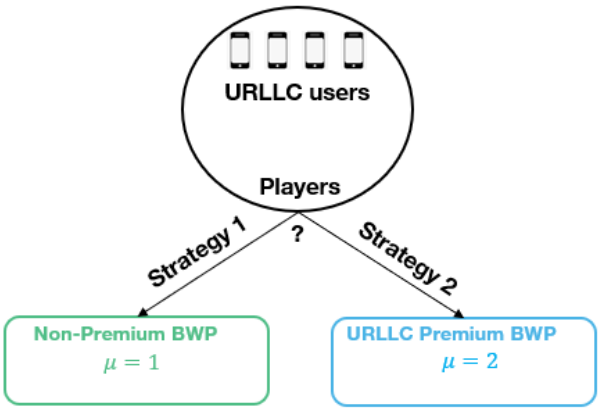

Figure 5.2: URLLC BWP Selection Game representation

The cost function is carefully defined to take into account all network aspects including the URLLC users' latency, energy efficiency and incurred monetary cost. Hence, the following cost function is considered when an URLLC user u selects BWP bwp:

$$C_u^{bwp} = a \cdot \frac{L_u^{bwp}}{Lc_u} + b \cdot K^{bwp} + c \cdot \alpha_{bwp} \tag{5.12}$$

where a, b and c are normalizing factors and:

- L_u^{bwp} is the latency of user u when selecting the numerology-specific BWP bwp using Equation (5.9) depending on the numerology and transmission delay

- Lc_u is the maximum latency tolerated by user u. For this target KPI, we draw a random value for each user between 0.8 and 1 ms as the URLLC latency should not exceed 1 ms with a reliability of $1 - 10^5$ [6]

- K^{bwp} is the incurred monetary cost to be paid by the user when selecting BWP bwp which is higher for the URLLC Premium BWP compared to the Non-Premium BWP

- α_{bwp} is a parameter representing the user energy consumption. It depends on the scanned BWP bwp. Hence, if the user selects the smaller BWP, $\alpha_{bwp} = 0$ since the energy consumption would be lower reducing the cost function. Otherwise, if the user selects the larger BWP, the energy consumption is higher and $\alpha_{bwp} = 0.2$

Note that the latency provided by the URLLC Premium BWP is lower owing to the higher numerology used. Moreover, the transmission delay goes to zero if the BWP has enough PRBs. Consequently, users are more likely to choose this BWP to avoid deteriorating eMBB Non-Premium users' performance. However, by astutely fine-tuning the incurred monetary cost (which will be set higher for the Premium BWP), we can load balance users among BWPs to avoid overcrowding the URLLC Premium BWP and disrupting Non-Premium eMBB users. In non-cooperative games, Pure Nash Equilibria are sought after and we will discuss how to attain them in the next subsection.

5.3.2 Reaching the Pure Nash Equilibrium

In this non-cooperative game, we seek the NE in a similar manner to the crowding game of the previous chapter. We show that $\mathcal{G}$ has the FIP property which guarantees the existence of PNE [35] for our BWP selection game.

Proposition 8. *$\mathcal{G}$ has the FIP property.*

Proof. The game $\mathcal{G}$ is an unweighted crowding game. In fact, although the cost function is player specific, it is non-decreasing in the number of players that selected the same strategy (BWP). The latter property is because the latency L_u^{bwp} is non-decreasing in the number of players that selected the same BWP. According to [37], player specific unweighted games with only two strategies have the FIP property which is the case for our game with two strategies np and up. □

Games with FIP are guaranteed to converge to PNE through simple Best Response dynamics [38] presented in Algorithm 5. In this algorithm, each player in turn, will choose the strategy minimizing its cost

Input: BWP cost
Output: BWP selection based on lowest cost
1 **repeat**
2 Calculation of BWP cost C_u^{np} and C_u^{up} by each user;
3 BWP with lowest cost is selected by the user;
4 **until** *BWP selection is the same as previous iteration*;
Algorithm 5: Level 1: URLLC BWP Selection Best Response Dynamics Algorithm

function in response to other players' strategies till convergence when the chosen strategy of each player is the same as in the previous round. Therefore, the complexity of this algorithm is $O(NbUsersU \times NbBWP \times NbIterations)$ where $NbUsersU$ is the number of URLLC users, $NbBWP$ is the number of BWPs that can

be selected for these users, and $NbIterations$ is the number of iterations till convergence is reached. Its duration is later discussed in Section 5.8.

In the next section, the second level of the algorithm is discussed.

5.4 The Second Level: Dynamic Slicing

The aim of the second level of our proposed algorithm is to determine the adequate amount of bandwidth for each BWP based on the users' KPIs and network conditions to eventually determine the slice bands. To that end, we rely on smart heuristics to strike a good balance between high performance efficiency and low computational cost. In fact, this simple algorithm uses the users' KPIs in order to immediately adjust the band.

5.4.1 Heuristic algorithm inputs and outputs

The second level algorithm requires specific inputs in order to dimension the BWP size. In fact, for the eMBB and URLLC services, computing a certain ratio for each BWP $ratio_{BWP}$ based on the users' KPIs as input, the algorithm should compute the amount of bandwidth for each BWP B_{BWP}. Thus, it requires computing the throughput of eMBB users and the latency of URLLC users. Once these KPIs are obtained, the algorithm calculates the number of unsatisfied users: unsatisfied eMBB Premium users are those whose throughput is below $\beta_{EP} = 10$ Mb/s, unsatisfied eMBB Non-Premium users are those whose throughput is below $\beta_{ENP} = 5$ Mb/s, and unsatisfied URLLC users are those whose delay is beyond $\beta_U = 1$ ms. These threshold values are used as an example for simulations but can be set freely by the operator. Afterwards, the ratios for each BWP ($ratio_{BWP}$) are computed based on the ratio of unsatisfied users of each BWP UR_{BWP} along with the ratio of allocated PRBs to URLLC users particularly in the Non-Premium BWP $PRBR\_URLLC_{NP}$. Finally, these parameters are used to decide if the BWP band should be increased or not and set it accordingly. The band is increased by 5 MHz in our case but this value can be freely determined by the operator.

Hence for eMBB and URLLC services, the algorithm input which is the ratio for each BWP ($ratio_{BWP}$) is defined below:

- For the eMBB Premium (EP) BWP, it is the ratio of unsatisfied eMBB Premium users denoted by UR_{EP} ($ratio_{EP} = UR_{EP}$) which is the number of eMBB Premium users with a throughput lower than a threshold set to $\beta_{EP} = 10$ Mb/s divided by the number of users linked to this BWP.

- For the Non-Premium (NP) BWP, it is the ratio of unsatisfied Non-Premium users denoted by UR_{NP} ($ratio_{NP} = UR_{NP}$) which is the number of eMBB Non-Premium users with a throughput lower than a threshold set to $\beta_{ENP} = 5$ Mb/s and the number of URLLC Non-Premium users having a delay surpassing the limit of $\beta_U = 1$ ms divided by the total number of users linked to this BWP.

- For the URLLC Premium (UP) BWP, the ratio is composed of the below two parameters ($ratio_{UP} = (UR_{UP}, PRBR\_URLLC_{NP})$):

  - The ratio of unsatisfied URLLC Premium users denoted by UR_{UP} which is the number of URLLC Premium users enduring a delay higher than a threshold set to $\beta_U = 1$ ms divided by the total number of users linked to this BWP.

- The ratio of allocated PRBs to the URLLC service in the Non-Premium BWP denoted by $PRBR\_URLLC_{NP}$ which is the number of allocated PRBs to the URLLC service in the Non-Premium BWP divided by the total number of PRBs available at this BWP. The higher this ratio is, the more severe the degradation of eMBB Non-Premium throughput.

As for the mMTC service, since all users have the same requirements (number of packets to be received and packet size), only the number of PRBs required per user and the number of active users are sufficient to determine the required band of the mMTC BWP.

The outputs of the algorithm are the computed BWP bands and size denoted by B_{MP} for the mMTC BWP, B_{NP} for the Non-Premium BWP, B_{EP} for the eMBB Premium BWP and B_{UP} for the URLLC Premium BWP.

5.4.2 Algorithm workflow and process

First, we start by determining the mMTC BWP. For this type of service, we need the number of PRBs required by all users which is determined by the following equation:

$$Tot\_ReqmMTC = IoTNodes \times RequiredPRBmMTC_u \tag{5.13}$$

Where $Tot\_ReqmMTC$ is the total number of PRBs required by the service, $IoTNodes$ is the total number of mMTC users connected to the MP BWP and $RequiredPRBmMTC_u$ is the number of required PRBs of a mMTC user u with the worst radio conditions located at the edge of the cell. After determining the total number of PRBs required for mMTC, the smallest band from Table 5.3.2-1 in [12] that offers a number of PRBs higher than the one requested is selected for the mMTC BWP. Hence, the mMTC BWP band B_{MP} is determined in a simple way since this class of service is not demanding in terms of throughput nor latency.

Afterwards, the bands for the BWPs dedicated for eMBB, and for URLLC and the one shared between them should be determined. Therefore, for eMBB and URLLC services, the whole process is described in Algorithm 6. As can be seen in the latter, we start by attributing the minimal bands to each BWP as defined by the operator's strategy which is set to null to circumvent allocating a band to a BWP with no active traffic. The next step is to calculate the ratios for each BWP $ratio_{BWP}$ (UR_{EP}, UR_{NP}, ($PRBR\_URLLC_{NP}$ and UR_{UP})) and check if any ratio violates the corresponding limit value l_{ratio}. If that happens for a given BWP, a BWP-specific flag is raised and increasing the BWP band is considered if the maximum band per BWP (set to 90 MHz in simulations) is not reached and if the total operator band is not used. Otherwise, the flag is lowered. For example, if $UR_{EP} > 0$ (with $l_{UR_{EP}} = 0$) meaning that at least one eMBB Premium user is unsatisfied, an eMBB Premium flag is raised to increase this BWP band. If the maximum band per BWP is not reached (90 MHz), the algorithm moves on to the next step. Otherwise, the flag is lowered. The same process is done for the other two BWPs. A Non-Premium BWP flag is raised if $UR_{NP} > 0$ (with $l_{UR_{NP}} = 0$). As for the URLLC Premium BWP, since two parameters are considered for $ratio_{UP}$, the URLLC Premium BWP flag is raised if $UR_{UP} > 0$ (with $l_{UR_{UP}} = 0$) or $PRBR\_URLLC_{NP} > 0.5$ (with $l_{PRBR\_URLLC_{NP}} = 0.5$). The first action is set to increase the URLLC Premium BWP band when at least one URLLC Premium user is unsatisfied. As for the second condition, when the ratio of Non-Premium BWP PRBs allocated to the URLLC service is higher than 0.5, the URLLC Premium BWP band is increased in order to push URLLC users to choose this Premium BWP. In that case, the first-level BWP selection algorithm is run again to avoid deteriorating the performance of eMBB Non-Premium users, that would otherwise suffer from starvation. The next step is to verify if the whole operator band is fully used. If this is the case, all BWP-specific flags are lowered as it is no longer possible to further increase any BWP band. Otherwise, the algorithm increases the BWP band by 5 MHz. Once this is done, the following step is to update the BWP bands and network

Input: $ratio_{BWP}$: UR_{EP}, UR_{NP}, UR_{UP}, $PRBR\_URLLC_{NP}$
Output: B_{BWP}: B_{NP}, B_{EP}, B_{UP}
Attribute minimal bands to each BWP ($B_{BWP} = B_{min} = 0$ MHz);
repeat
  Calculation of UR_{EP}, UR_{NP}, UR_{UP}, $PRBR\_URLLC_{NP}$;
  for *BWP in {EP, NP, UP}* **do**
    if $ratio_{BWP} > l_{ratio}$ **then**
      Raise BWP-specific flag;
      if $B_{BWP} = B_{max} = 90$ *MHz* **then**
        Lower flag;
      else
        if *Operator band fully used* **then**
          Lower all flags;
        else
          Increase BWP band by 5 MHz;
          Update BWP band and size and recalculate network parameters;
        end
      end
    else
      Lower flag;
    end
  end
until *No remaining flag is raised*;

Algorithm 6: Second-level: BWP size adjustment and band attribution heuristic algorithm for eMBB and URLLC services

parameters such as the number of PRBs available at each BWP, the INI and the aforementioned ratios. Afterwards, an additional verification step is performed to check if any flag is still raised. If this is the case, the whole process is repeated where the ratio conditions are checked again. Otherwise, the BWP bands are successfully determined. Regarding the algorithm complexity, it is $O(NbUsers \times NbBWP \times NbIterations)$ with $NbUsers$ the total number of users, $NbBWP$ the number of BWPs, and $NbIterations$ the number of iterations till convergence is reached where no flag is still raised.

As for the BWP order, the algorithm starts with the eMBB Premium BWP, then the Non-Premium BWP to prioritize them and finally considers the URLLC Premium BWP. The reason behind this choice is the fact that the eMBB Premium and Non-Premium BWPs serve eMBB users requiring high throughputs, therefore wider bands. Thus, the algorithm tends first to the needs of the eMBB Premium BWP and the Non-Premium BWP. As for the URLLC Premium BWP, it is kept for last since its users do not require a high amount of resources and, in case of overload, URLLC users can turn to the Non-Premium BWP.

5.5 Third Level: Guard Band Dimensioning

The final stage of the overall algorithm is to select the suitable guard bands that mitigate the INI without reducing the spectral efficiency. To that aim and due to the complexity of finding an appropriate guard band, we have recourse to DQN by taking as input the users' KPIs and radio conditions as well as the INI value. Thanks to DQN, we can determine the adequate guard bands that should be used by defining an

astute reward function which is used by an agent to assess the benefits of the selected action. This stage is only required when the whole operator band is used causing INI between the adjacent BWPs. Otherwise, this level is not executed as BWPs with different numerologies are sufficiently set apart. To note that the algorithm at this third level is run twice as we have 2 guard bands to determine. In the first run, we determine GB1 between the BWPs using $\mu = 0$ and $\mu = 1$. In the second run, GB2 is dimensioned between the BWPs using $\mu = 1$ and $\mu = 2$. Since we are using DQN for this level (which was already introduced in Chapter 1), the tackled problem is represented by Fig. 5.3. Hence, it is important to define the state, environment, actions and rewards of the problem which will be discussed in the next subsections.

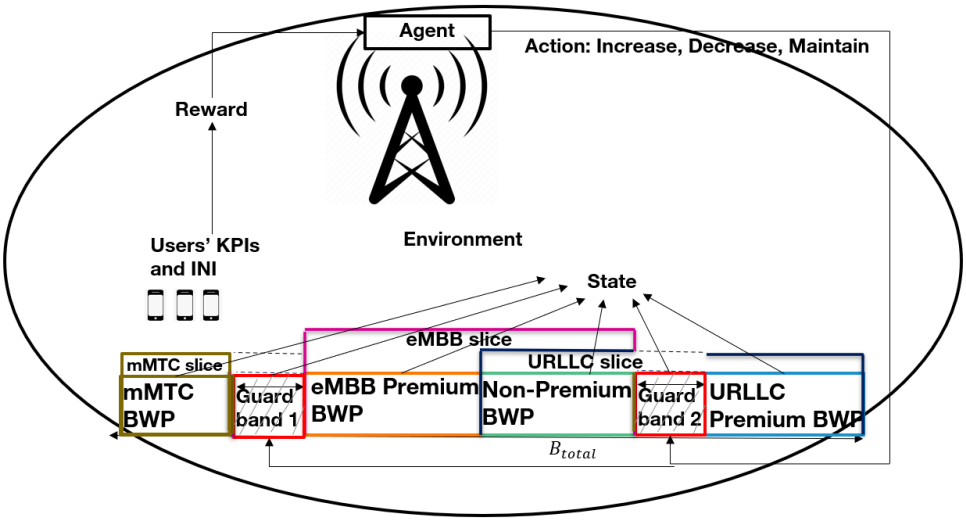

Figure 5.3: Third level DQN Process

5.5.1 The agent, environment and states

In our algorithm, the agent is the intelligent entity of the RAN which is none other than the gNB controllers collecting the adequate metrics that are used to take the appropriate actions. As for the environment, it is the gNB with its configured slices and attached users where the gNB's total band is divided between the BWPs and the guard bands used to reduce the INI between the BWPs using different numerologies. Moreover, the state of the environment is identified as the band attribution to the BWPs using different numerologies as well as the selected GB to separate them. Therefore, to determine the first guard band (GB1), the state of the environment is composed of the band occupied by the BWP linked to $\mu = 0$ (MP), the band occupied by the BWPs linked to $\mu = 1$ (EP and NP) and the assigned guard band (GB1) separating them. As for the second guard band determination (GB2), the state of the environment is composed of the band occupied by the BWPs linked to $\mu = 1$ (EP and NP), the band occupied by the BWP linked to $\mu = 2$ (UP) and the assigned guard band separating them (GB2). To note that the band occupied by each BWP is variable depending on the second level of the algorithm where each band is adjusted. In addition, each time the guard band value and the BWP bands are modified, the INI level and number of PRBs available at the level of BWPs are also changed (since some PRBs will remain unused). This also affects the users' KPI and the state of the environment. Thus, it is important to pinpoint these actions that change the state of the environment.

5.5.2 The actions

In this problem, the aim is to find the appropriate guard band separating BWPs using different numerologies which could take any value. In order to limit the number of possible actions and reduce the algorithm complexity, the system can choose whether to increase, decrease or maintain the selected guard band. Therefore, the set of actions is limited to these three actions. However, the guard band value cannot increase or decrease indefinitely and should be restrained to a certain range of values bounded by a minimum and maximum value (GB_{min} and GB_{max}). In fact, 3GPP standards recommend the use of a minimum guard band depending on the selected numerology and channel bandwidth. From Table 5.3.3-1 in [12], the recommended minimum guard bands can be found. Hence, for GB1, the selected minimum and maximum values for $\mu = 0$ (SCS=15 kHz) are 242.5 and 692.5 kHz respectively. As for GB2, the selected minimum and maximum values for $\mu = 2$ (SCS=60 kHz) are 990 and 1630 kHz respectively. Subsequently, when the selected guard band reaches the value of either 242.5 for GB1 or 990 kHz for GB2 (resp. 692.5 for GB1 or 1630 kHz for GB2), the possible actions are reduced to increase (resp. decrease) the bandwidth allocation or maintain it as is. As for the increase/decrease actions, the step value chosen is 5 kHz. Hence, the possible GB values for each guard band are predefined.

5.5.3 The reward function

Subsequently to the action selection, the guard band value can change and affect the users' KPI and INI level. Hence, to assess the quality of the selected action, a reward function for each guard band is defined. For GB1, the reward function is defined as follows:

$$R_{action} = \sum_{u \in eMBB} \frac{Thr_u}{Thrc_u} + \alpha_{SINR} \times IoTNodes \times SINRmMTC_u - \alpha_{INI} \times I_{dB} - \alpha_{GB} \times GB \tag{5.14}$$

where

- Thr_u is the throughput achieved by eMBB user u.
- $Thrc_u$ is the comfort throughput of eMBB user u randomly defined for each user with a value between 8 and 10 Mb/s for eMBB Premium users and a value between 4 and 5 Mb/s for Non-Premium eMBB users. This parameter plays also the role of a normalizing factor for Thr_u.
- $IoTNodes$ is the number of mMTC users.
- $SINRmMTC_u$ is the SINR in dB for mMTC user u with the worst radio conditions located at the edge of the cell.
- $I_{dB} = I_{dB}(k, k') + I_{dB}(k', k)$ is the total INI level in dB affecting the BWPs using different numerologies.
- GB is the selected GB1 in kHz.
- $\alpha_{SINR} = 0.1$, $\alpha_{INI} = 10^{-2}$ and $\alpha_{GB} = 10^{-4}$ are normalizing factors for the SINR, INI level and guard band value respectively.

For GB2, it is defined as follows:

$$R_{action} = \sum_{u \in eMBB} \frac{Thr_u}{Thrc_u} + \sum_{u \in URLLC} \alpha_{SINR} \times SINR_u - \alpha_{INI} \times I_{dB} - \alpha_{GB} \times GB \tag{5.15}$$

where

- $SINR_u$ is the SINR in dB for URLLC user u.
- GB is the selected GB2 in kHz.

Therefore, both reward functions used to calculate the Q-values take into account the ratio of achieved throughput over comfort throughput for all eMBB users. Since the higher this ratio is, the more advantageous it is for the system, it is counted as a positive reward. Additionally, both functions take into account the INI level and guard band values. The higher these values, the more severe the users' performance degradation is, since we have a higher interference level with higher INI and less spectral efficiency with a higher GB. Hence, these parameters are considered to wreak negative rewards in both functions. Also, both reward functions consider the SINR of the second class of users (mMTC or URLLC). However, for the first reward function for GB1 determination, instead of checking the SINR for each mMTC user, we simply take the SINR of a mMTC user under the worst radio conditions located at the edge of the cell and we multiply it by the number of mMTC users as a substitute to considering all users' SINR individually. This is due to the fact that the mMTC slice has a high number of connected devices and checking the SINR of each device will increase the algorithm complexity. Moreover, the SINR is counted as a positive reward since increasing the SINR is rewarding for the system. As for the second reward function for GB2, the SINR of each URLLC user is taken into account.

Moreover, the devised reward functions require a high computation time, especially for computing the INI values. Nonetheless, at the beginning of this stage, the INI values are calculated offline with all possible combinations of predefined guard band values and stored in a table based on Equations (5.1) and (5.2). In these equations, the GB value is included in the term $w(i,j)$. Therefore, instead of calculating the INI each time the action is changed, it is computed in a single run and stored in a table. Subsequently, the reward functions take the INI value from the table depending on the selected guard band which reduces the algorithm computation time and complexity.

5.5.4 DQN Algorithm Workflow

The DQN algorithm that determines each guard band (GB1 or GB2) is described in Algorithm 7.

Input: Q-values based on the defined reward function
Output: Optimal Guard Band
1 Define DQN inputs (states, discount factor...) and outputs (actions) ;
2 Calculate and store INI values in a table for all possible guard band values ;
3 **repeat**
4 Take a random action with probability ϵ or highest Q-value action with probability $1-\epsilon$ to increase, decrease or maintain guard band within range ;
5 Retrieve INI value from table ;
6 Calculate KPIs: throughput and SINR values of users based on equations (5.4)(5.3);
7 Calculate the reward generated following the action taken;
8 Calculate the Q-values ;
9 Update these values by gradient descent ;
10 **until** *Convergence of Q-values*;

Algorithm 7: Third level: DQN Guard band determination Algorithm

As seen in this algorithm, the DQN agent is created at first with the definition of its number of inputs and outputs used to retrieve the value function based on neural networks. Afterwards, the INI values

are calculated for every possible guard band value based on Equations (5.1) and (5.2) and stored afterwards in a table to reduce complexity. In the next step, the process is repeated where either a random action is taken with probability ϵ or an action with the highest Q-value is executed with probability $1 - \epsilon$. The action is either to increase the guard band by a fixed step value, decrease it or keep it unchanged, while maintaining it in a range of minimum and maximum value. Subsequently to the action taken, the INI value is retrieved from the INI table and used to calculate the throughput and SINR for active users. Afterwards, the reward is calculated and stored along with the newly reached state to update the Q-values based on gradient descent. This process is repeated until convergence is reached where the optimal policy is found and the appropriate decisions can be taken. As for the algorithm complexity, it is reduced to $O(NbUsers \times NbIterations)$ where $NbUsers$ is the total number of users and $NbIterations$ is the total number of iterations till convergence of Q-Values.

5.6 The Three-Level Algorithm Process

After detailing each level of the algorithm, the whole three-level algorithm process is discussed in this section. This algorithm is run periodically by the operator and it combines the three levels discussed earlier in sections 5.3, 5.4 and 5.5. The whole process is depicted in Fig. 5.4.

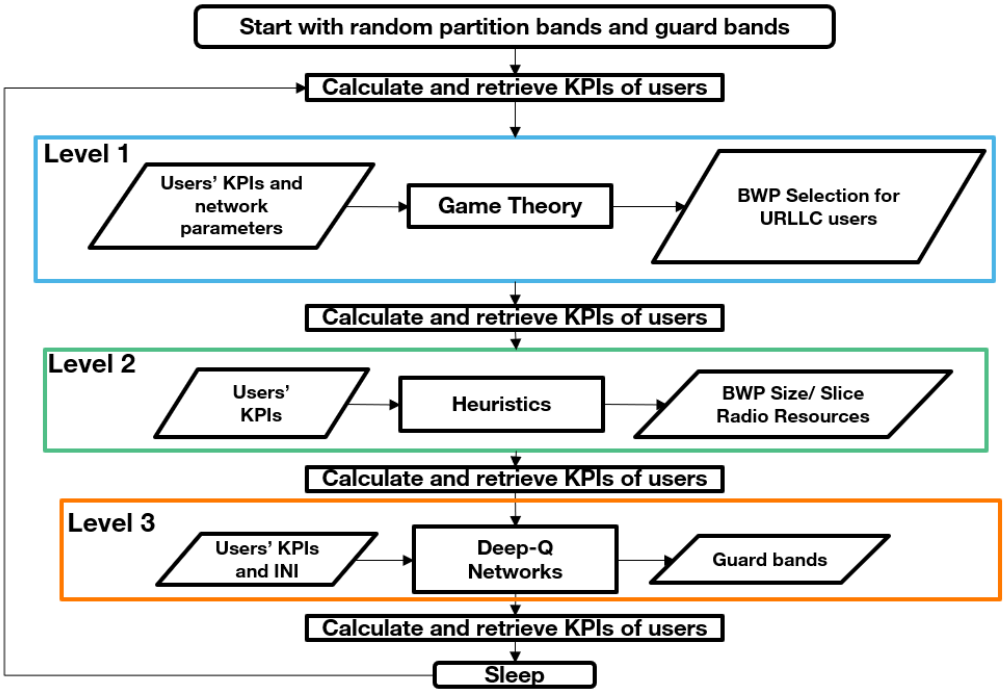

Figure 5.4: Three-Level Process

In fact, the initial phase consists of attributing random bands to each BWP with random guard band values between the defined minimum and maximum ranges. Afterwards, the active users' information will be retrieved (distance from gNB, user type, needed KPI, etc.) along with the updated users' information that have newly arrived to the network following the Poisson process as well as users leaving the network. The eMBB Premium users and eMBB Non-Premium users are immediately attached to the eMBB slice and linked to the Premium and Non-Premium BWPs respectively. As for the URLLC users, the BWP selection for these users between the Non-Premium BWP and URLLC Premium BWP is performed according to the first

level best response algorithm (Algorithm 5) which is executed in the next step where the users' KPIs are also updated. Subsequently, the band adjustment for each BWP is performed according to the second level heuristic algorithm (mMTC band determination and Algorithm 6) where KPIs are also updated. Afterwards, if the total operator band is used, the third level DQN algorithm is executed to re-calibrate appropriately the guard bands. Otherwise, the third level is skipped. After termination, the three-level algorithm is re-executed according to a period T set by the operator mainly depending on the users' traffic arrival rates. This period can be also implemented in an adaptive fashion depending on the measurement transmission period. The three-level algorithm is briefly explained in Algorithm 8.

Input: Active Users' Information (distance from gNB, type...) and KPIs
Output: URLLC user BWP selection, slice and BWP bands, guard band, users' KPIs

```
Start with random BWP bands and guard band ;
repeat
    Retrieve attached users' information and KPIs ;
    Execute first level URLLC BWP selection Best Response Algorithm ;
    Execute second level BWP band adjustment heuristic Algorithm ;
    if Operator band fully used then
        Execute third level DQN guard band determination Algorithm ;
    else
        Skip third level DQN Algorithm ;
    end
    Sleep for period T set by operator ;
until After T;
```

Algorithm 8: The Three-Level Slicing Algorithm

5.7 Performance Evaluation

All simulations including the DQN training were conducted on a machine with a Core i5 CPU at 2.50 GHz, 8GB RAM. To setup the simulation environment, basic functions were coded in Python to retrieve and calculate the KPIs and other necessary parameters using the standard library. As for the DQN environment which was also coded in Python, we used the Pytorch library. To assess the performance of the algorithm, it was run 100 times for every value of the number of users. As for the DQN, the number of iterations set to perform the training was 5000. We display the most remarkable results for two important traffic conditions: low traffic load and high traffic load. In the case of low traffic load, the operator total band is not fully used and the INI effect is negligeable. In the case of high traffic load where congestion is inevitable, the operator band is entirely exerted and the INI effect appears which requires the use of a guard band. The used simulation parameters are shown in Table 5.2.

Table 5.2: Simulation parameters for three-level slicing algorithm

Parameter	Description	Value
$f_{operator}$	Operator Frequency	3.5 GHz TDD
B_{total}	Operator bandwidth	90 MHz
B_{BWP}	BWP bandwidth	0-90 MHz
B_{min}	Minimum BWP bandwidth	0 MHz
B_{max}	Maximum BWP bandwidth	90 MHz
Lc_u	URLLC Comfort Latency	0.8-1 ms
$Thrc_{EP,u}$	eMBB Premium Comfort rate	8-10 Mb/s
$Thrc_{NP,u}$	eMBB Non-Premium Comfort rate	4-5 Mb/s
R	Coverage area	300 m
$IoTNodes$	Number of IoT Nodes (mMTC)	100
Pkt_{IoT}	Number of Packets to be received by IoT Node	1 packet/s
$PktSizeIoT$	IoT Node (mMTC) packet size	80 bits
λ_{EP}	eMBB Premium arrival rate	1 user/s
λ_{ENP}	eMBB Non-Premium arrival rate	2 users/s
λ_U	URLLC arrival rate	1 user/s
λ_{PktU}	URLLC packet rate	1.5 packets/s
$PktSizeU$	URLLC packet size	96 bits
V_{eMBB}	eMBB data volume	60-90 Mbits
K^{NP}	Non-Premium monetary cost	0.1
K^{UP}	URLLC Premium monetary cost	0.68
Pt	Transmission power	50 dBm
Gt	Transmission antenna gain	12 dBi
Gr	Reception antenna gain	3 dBi
PL	Path loss model	Work in [73]
$Shad_{SD}$	Shadowing standard deviation	4 dB
α_{bwp}	Normalized energy efficiency term for BWP selection cost function	0 or 0.2
β_{EP}	Minimum Throughput satisfaction for eMBB Premium users	10 Mb/s
β_{ENP}	Minimum Throughput satisfaction for eMBB Non-Premium users	5 Mb/s
β_U	Maximum Latency satisfaction for URLLC users	1 ms
$l_{UR_{BWP}}$	UR_{BWP} Ratio Threshold limit	0
$l_{PRBR\_URLLC_{NP}}$	$PRBR\_URLLC_{NP}$ Ratio Threshold limit	0.5
GB_{min1}	Minimum Selected Guard Band 1	242.5 kHz
GB_{max1}	Maximum Selected Guard Band 1	692.5 kHz
GB_{min2}	Minimum Selected Guard Band 2	990 kHz
GB_{max2}	Maximum Selected Guard Band 2	1630 kHz
	Low Traffic Mode	10 users without mMTC users
	High Traffic Mode	47 users without mMTC users

As can be seen, the operator has a bandwidth of 90 MHz which corresponds to the normal amount of bandwidth usually owned by an operator in 5G and working on the 3.5 GHz frequency in TDD mode covering a radius of 300 meters. The BWP bandwidth for the eMBB Premium, Non-Premium and URLLC Premium BWPs can take any value between 0 (the minimum BWP band) and 90 MHz (the maximum BWP band) depending on the traffic load and second level algorithm. The number of mMTC users (IoT nodes) is fixed to 100 and each node will receive 1 packet/s with a fixed size of 80 bits. URLLC users arrive in a Poisson process with a rate of 1 user/s while generating packets also following a Poisson process with a mean of 1.5 packets/s with a fixed packet size of 96 bits. The maximum latency of these users is a random value between 0.8 and 1 ms. As for eMBB users arriving following a Poisson process, eMBB Premium users have an arrival rate of 1 user/s while eMBB Non-Premium users have an arrival rate of 2 users/s. These users have a given volume of data to download which is determined randomly between 60 and 90 Mbits. The comfort throughput for these users is also determined randomly between 8 and 10 Mb/s for Premium users and between 4 and 5 Mb/s for Non-Premium users. Regarding the normalized incurred monetary cost used in the first level of the algorithm, the URLLC Premium monetary cost is set to 0.68 which is higher than the Non-Premium monetary cost set to 0.1. The choice behind these values is to load-balance the URLLC traffic between the designated BWPs to avoid overcrowding a given BWP. The transmission power, shadowing standard deviation, transmission and reception antenna gains values are also shown in Table 5.2. As for the Path Loss model, the model used is that of the work in [73] where $PL = 36.7 \log_{10} d + 33.05$. In this equation proposed by [82], the Path Loss is in dB and d is the distance separating the user from the gNB in km.

In Table 5.3, the chosen DQN parameters are displayed. Note that the input size corresponds to the number of parameters considered for the environment state which is composed of the selected GB and the bandwidths of the BWPs using different numerologies. Thus, the input size is 3. As for the output size, it refers to the number of actions possible which is three: increase, decrease or maintain the GB. For the

Table 5.3: DQN parameters for three-level slicing algorithm

DQN Parameter	**Value**
Input size (State parameters)	3
Hidden Layers	1
Hidden Nodes	3
Output size (Number of actions)	3
Discount factor	0.7
Experience replay buffer size	100000
Mini batch size	100
Learning rate	0.001

performance results, the chosen parameters are the eMBB Satisfaction Degree Cumulative Distribution Function (CDF), the URLLC latency Complementary Cumulative Distribution Function (CCDF), SINR CDF for all users which can also serve as a KPI for mMTC, and URLLC user distribution between the Non-Premium and URLLC Premium BWPs. The eMBB satisfaction degree of eMBB user u is computed as follows:

$$Sdeg_u = \begin{cases} 100\% & \text{if } Thr_u \geq Thrc_u \\ \frac{Thr_u}{Thrc_u} \times 100 & \text{Otherwise} \end{cases} \tag{5.16}$$

Therefore, if the eMBB user achieves a throughput higher than its comfort throughput, the satisfaction degree is 100%. Otherwise, it is the percentage of its achieved throughput over its comfort throughput. The simulations are run and compared for three different scenarios:

- Single-numerology (our previous contribution in the previous chapter). In this scenario, no mMTC users are considered since only $\mu = 1$ is used in the system even for the URLLC Premium BWP. This numerology is chosen instead of $\mu = 2$ or $\mu = 0$ since $\mu = 1$ is more adapted to both URLLC and eMBB services and offers a higher number of PRBs for the same bandwidth.
- Multi-numerology which is our proposed three-level algorithm.
- The multi-numerology scenario where no guard band dimensioning (third level of algorithm) is performed (such as the work in [73]) to highlight its importance. Hence, only the first two levels of the algorithm are run.

5.7.1 Low Traffic Load

We begin by gauging performances in the low traffic load. The bandwidth reserved for mMTC BWP after the second level algorithm is 5 MHz which does not change during simulations.

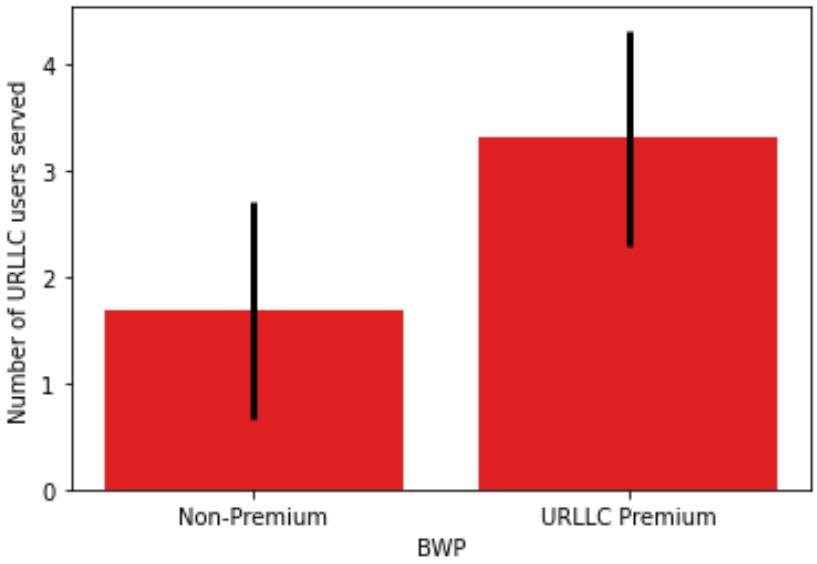

Figure 5.5: URLLC users distribution between the Non-Premium BWP and URLLC Premium BWP using a Multi-Numerology solution with low traffic load

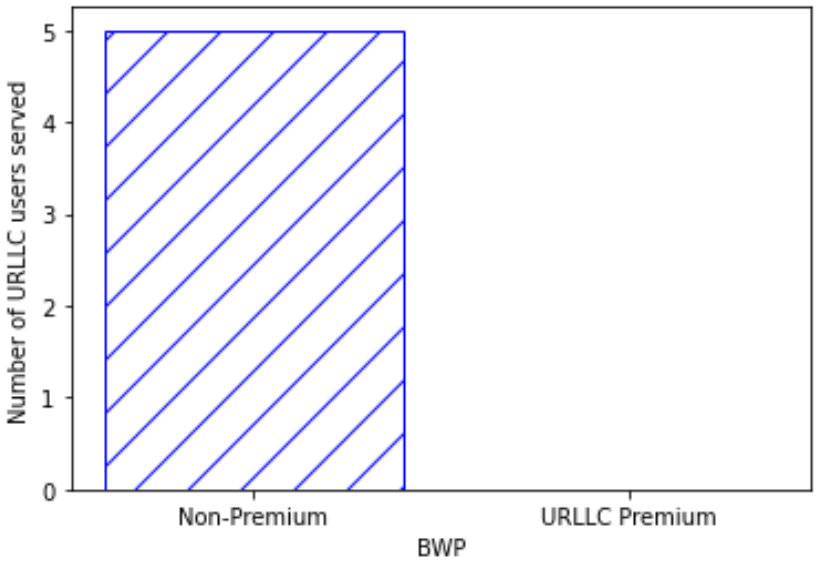

Figure 5.6: URLLC users distribution between the Non-Premium BWP and URLLC Premium BWP using a Single-Numerology solution with low traffic load

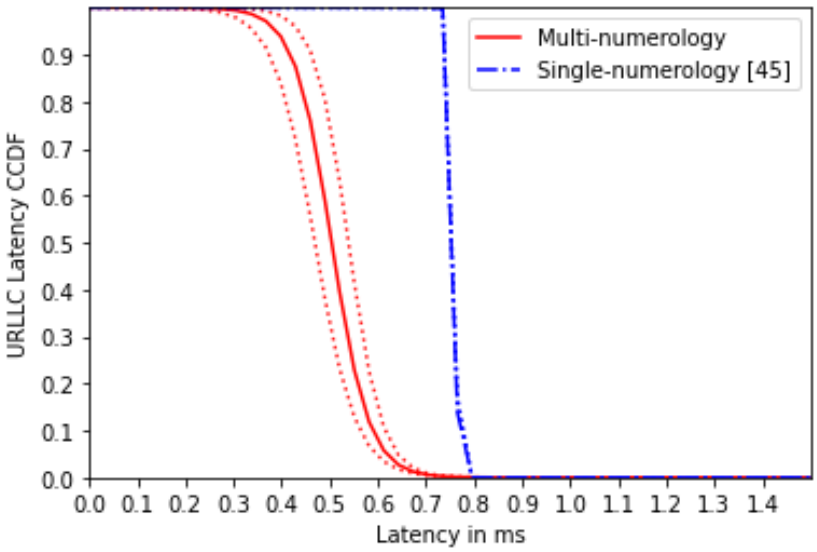

Figure 5.7: URLLC latency CCDF in low traffic load scenario

In Fig. 5.5 and Fig. 5.6, the number of URLLC users distributed between the Non-Premium and Premium BWPs is represented for the multi-numerology and single-numerology scenarios respectively after the first level of the algorithm in the case of low traffic load with 10 users (non-mMTC). The vertical black line represents the confidence interval of the obtained results.

From these figures, it can be concluded that in the multi-numerology scenario, URLLC users are inclined to select the URLLC Premium BWP even though it has a higher monetary cost owing to the lower latency it provides with its wider numerology as well as the energy efficiency criteria. Whereas in the single-numerology scenario, all URLLC users select the Non-Premium BWP due to the lower monetary cost. In fact, with a single numerology, both BWPs offer the same latency.

Figures 5.7 and 5.8 illustrate the URLLC Latency CCDF and eMBB Non-Premium Satisfaction Degree

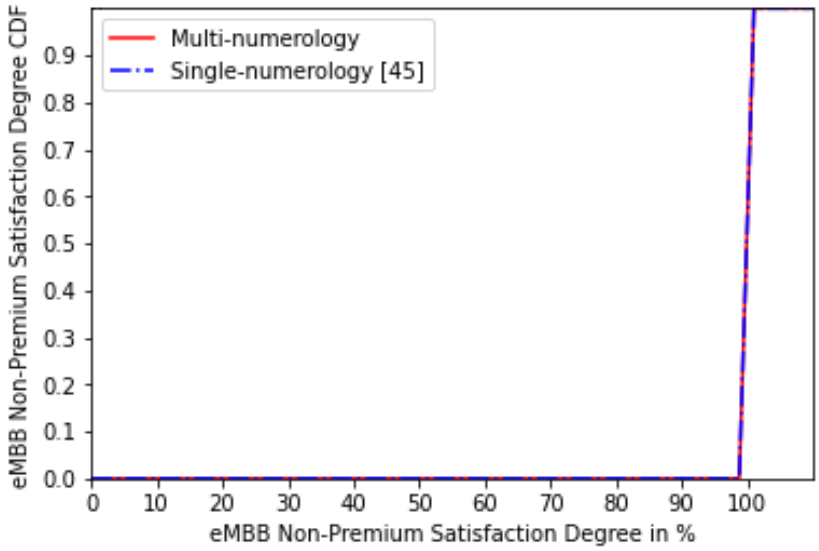

Figure 5.8: eMBB Non-Premium users' satisfaction degree CDF in low traffic load scenario

CDF respectively in the case of low traffic load. The dotted curves represent the confidence interval of the obtained results. In these low traffic load conditions, there are around 10 non-mMTC users in the system divided between the eMBB and URLLC slices. It is evident from Fig. 5.7 that with the multi-numerology solution, URLLC users are bound to have a lower latency with a gain of 37.5% while the single-numerology solution inflicts higher latency on these users. In both cases, the latency does not exceed 1 ms. As for the eMBB Non-Premium Satisfaction Degree, Fig. 5.8 shows that we have the same satisfaction degree of 100% for all users meaning that the comfort throughput is guaranteed for the Non-Premium users. As for the eMBB Premium satisfaction degree and SINR values, they are the same for both the multi-numerology and single-numerology cases with low traffic load, and with a satisfaction degree of 100% for Premium users.

Hence, with the multi-numerology solution, URLLC users tend to have lower latency since most users choose the Premium BWP with numerology 2 while with the single-numerology solution, all URLLC users operate on numerology 1 that leads to a higher latency. Furthermore, with our multi-numerology solution, URLLC users have a lower latency while maintaining a satisfaction degree of 100% for eMBB users. As for mMTC users, a satisfactory bandwidth is granted for them.

5.7.2 High Traffic Load

When the number of non-mMTC users becomes greater than 47 users, this causes congestion in the network. Figures 5.9-5.12 represent the SINR CDF for all users, SINR of a mMTC user under the worst radio conditions, URLLC Latency CCDF, and eMBB Non-Premium Satisfaction Degree CDF respectively in the high traffic scenario.

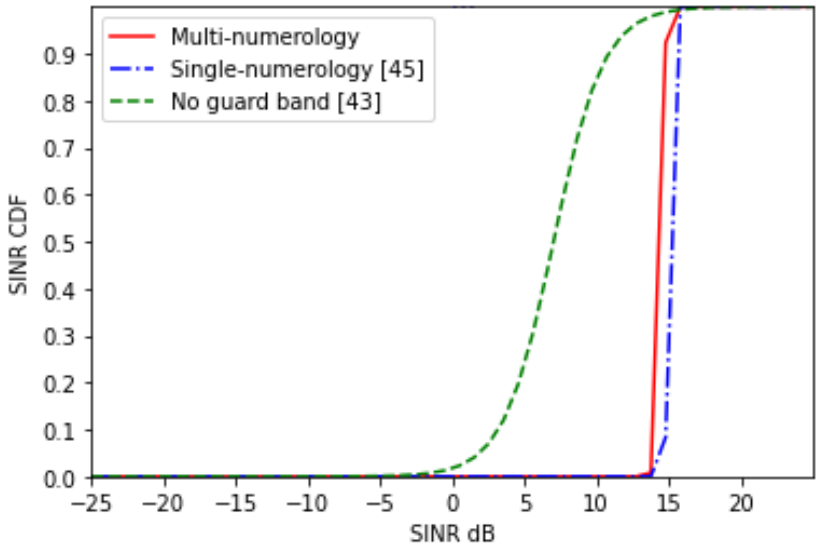

Figure 5.9: SINR CDF for all users in the high traffic load scenario

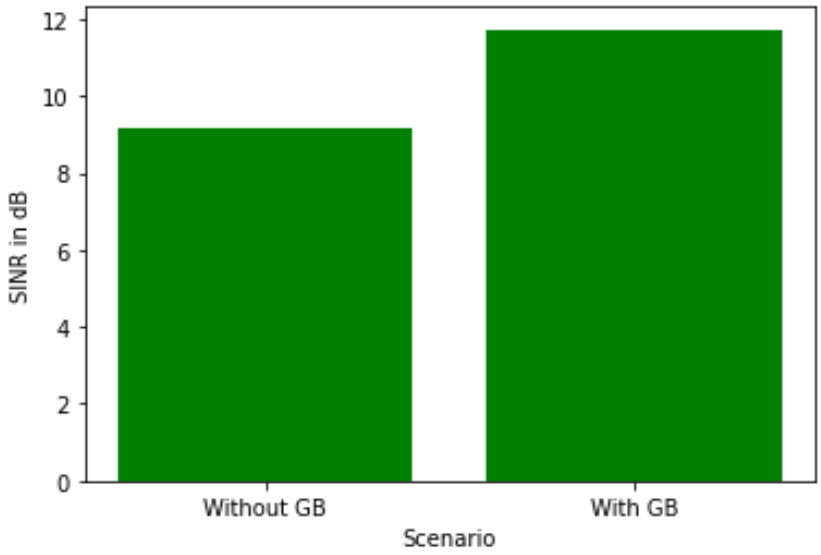

Figure 5.10: SINR of a mMTC user under the worst radio conditions with and without GB dimensioning

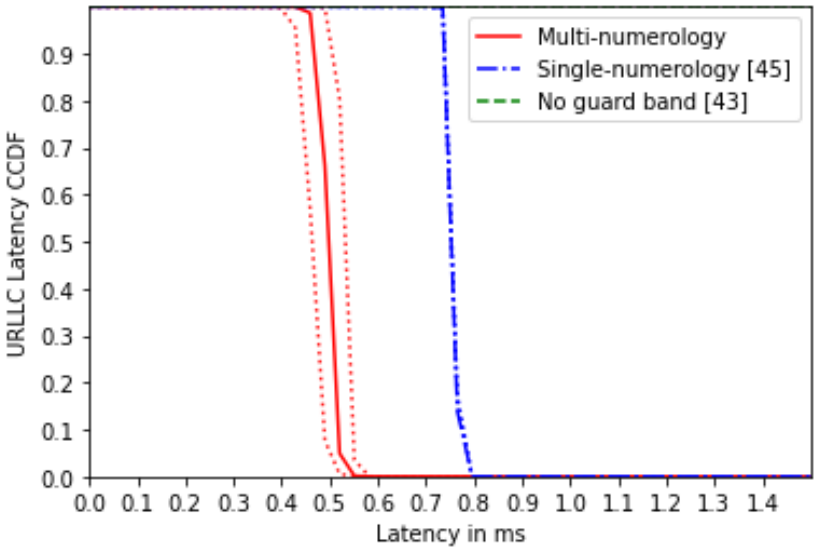

Figure 5.11: URLLC latency CCDF in the high traffic load scenario

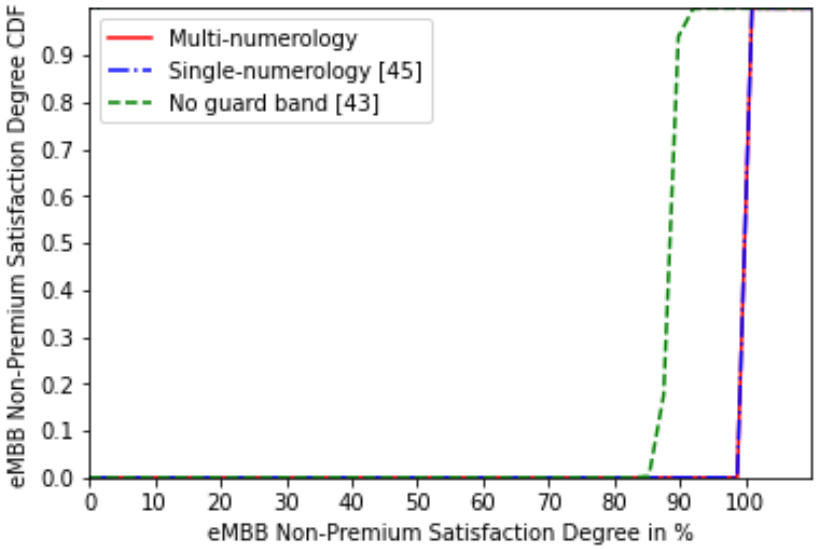

Figure 5.12: eMBB Non-Premium users' Satisfaction Degree CDF in the high traffic load scenario

Figure 5.9 depicts the SINR CDF with high traffic load for all users. Without guard band dimensioning, the INI level is high which deteriorates the users' SINR and leads to the lowest values with this scenario. As for the single and multi-numerology solutions, higher values are observed with a faint enhancement with the single-numerology due to the absence of INI in that scenario while the multi-numerology scheme manages to mitigate its effect owing to the sagacious band guard dimensioning that is set by the third level of the algorithm. Particularly for mMTC users, as displayed in Fig. 5.10 where the SINR of a mMTC user under the worst radio conditions is reported with and without GB, the importance of the third level of the algorithm with guard band dimensioning is highlighted where a better SINR is observed with our multi-numerology solution compared to the scenario with "no guard band".

Regarding the URLLC user distribution between the BWPs, it remains the same with a preference for the Premium BWP with multi-numerology while all users choose the Non-Premium BWP with the single-

numerology scheme.

Figure 5.11 shows that URLLC users' latency with multi-numerology is still lower than the values with single-numerology. In both single-numerology and multi-numerology solutions, the latency does not exceed 1 ms as recommended by the 3GPP standards even with high traffic load which proves the efficiency of our solution. However, without a proper guard band dimensioning, the URLLC latency becomes high, exceeding the 1 ms threshold as all users in the figure have a latency higher than 1.5 ms. This is due to the combination of high URLLC traffic load and high INI which leads to decreased SINR values for URLLC users and consequently to a higher PRB demand. The latter can not be met because of traffic congestion, which results in a higher latency.

Regarding the Non-Premium users in the high traffic load scenario, Fig. 5.12 shows that both single and multi-numerology solutions are able to ensure users' requirements with a satisfaction degree of 100% even with high traffic load. Nonetheless, this is not the case for the "no guard band" solution where the satisfaction degree for Non-Premium users starts to decrease due to SINR degradation with a high INI level. As for the eMBB Premium satisfaction degree, the same performances are observed as for the eMBB Non-Premium class in high traffic load.

Therefore, even in the case of congestion, our multi-numerology solution provides a lower latency for URLLC users. It also keeps eMBB users entirely satisfied and guarantees better SINR values for mMTC users.

5.7.3 Use of Numerology 0 for eMBB Premium and Non-Premium BWPs

For the sake of completeness, we have also performed some additional simulations where the eMBB Premium and Non-Premium BWP use numerology 0 while the URLLC Premium BWP use numerology 2 to highlight our choice of numerology for each BWP and to confirm why numerology 0 is not recommended. The results are displayed in Figs. 5.13, 5.14 and 5.15.

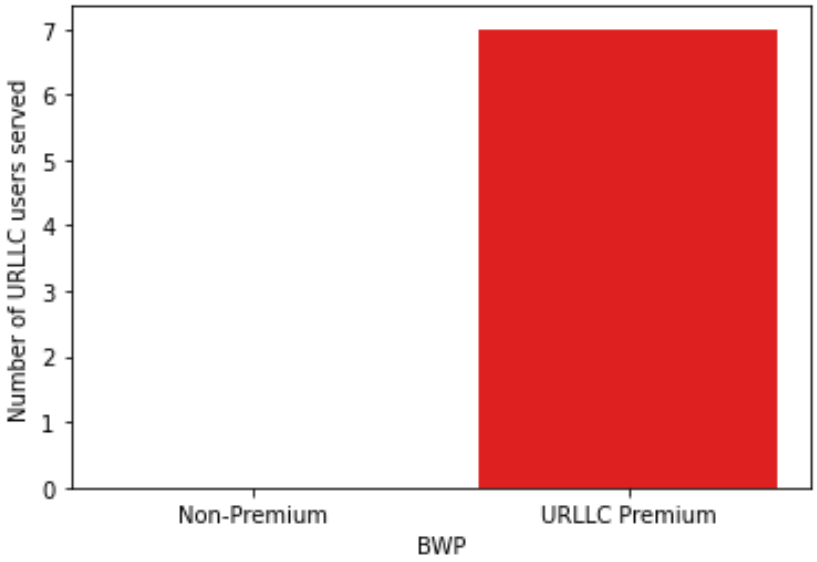

Figure 5.13: URLLC User Distribution Between URLLC Premium and Non-Premium BWPs without monetary cost adjustment

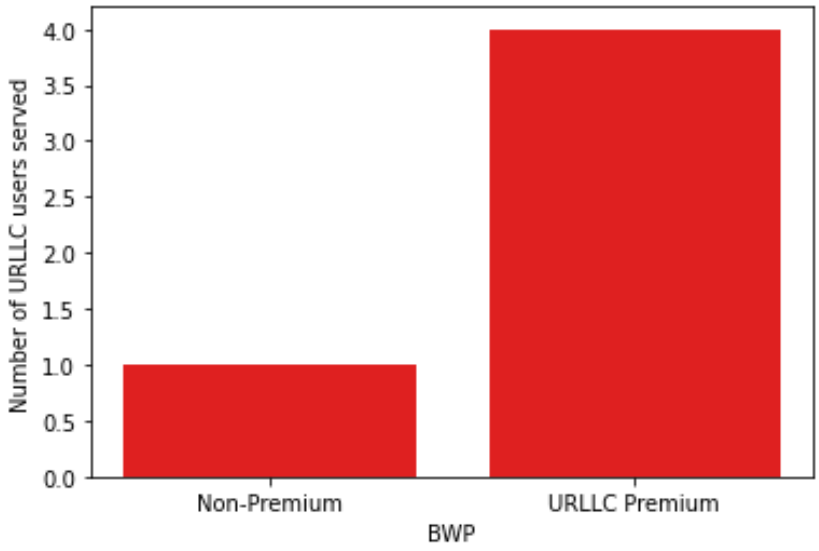

Figure 5.14: URLLC User Distribution Between URLLC Premium and Non-Premium BWPs with monetary cost adjustment

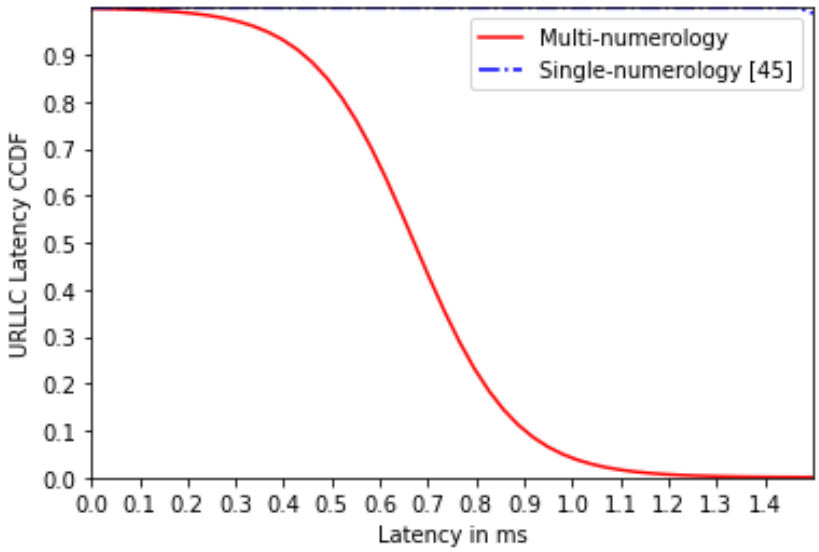

Figure 5.15: URLLC Latency CCDF with monetary cost adjustment

From Fig. 5.13 which represents the URLLC user distribution between the URLLC Premium and Non-Premium BWPs, we can see that all URLLC users will select the Premium BWP since it offers a much reduced latency compared to the Non-Premium BWP using numerology 0. Hence, this will cause a saturation of this BWP as the number of users becomes high unless an adjustment of the BWP monetary cost is done. When we adjust the BWP monetary costs to perform a load-balancing between these BWPs as can be seen in Fig. 5.14, some users may select the Non-Premium BWP. However, the latency of these users will be higher than 1 ms as can be seen in Fig. 5.15 where the URLLC latency will surpass 1 ms for some users. Therefore, the use of numerology 0 is not recommended to improve the performance of URLLC users.

5.7.4 Results highlight

From all these results, the following conclusions can be drawn:

- Under any traffic load condition, our proposed multi-numerology solution outperforms our previous contribution with the single-numerology solution in terms of URLLC latency while meeting eMBB and mMTC users' requirements. This is achieved owing to our three leveled solution as the first level ensures low URLLC latency, the second level allots the appropriate band for each BWP depending on the service's requirements, while the third level mitigates the INI effect that could deteriorate users' performance. This proves the high efficiency of our devised solution (Figs. 5.7, 5.8, 5.10, 5.11, 5.12).
- With the single-numerology scheme, a small SINR improvement is noticed with high traffic load due to the absence of INI in that scenario (Fig.5.9).
- The multi-numerology solution always provides better URLLC latency thanks to the wider numerology used with a significant gain compared to the single-numerology scheme while both maintain a latency lower than 1 ms (Figs. 5.7 and 5.11).
- Compared to the work in [73], our solution provides a lower URLLC latency below 1 ms which is lower than the one considered in the cited work (4 ms) even in high traffic load conditions. Simultaneously, our solution is able to provide high eMBB throughput and satisfaction degrees with values higher than the reference value of the work in [73] which is set to 1.25 Mb/s for eMBB users. Furthermore, we outperform the cited work even in presence of congestion and when the number of users (> 30 non-mMTC users) is much higher than the one used in [73] (12 users) (Figs. 5.7, 5.8, 5.11, 5.12).
- Ignoring the choice of an appropriate guard band ([73]) leads to degraded radio conditions and users' performance including mMTC due to the highly unmitigated INI effect. This results in the deterioration of users' KPIs in the high traffic load scenario. Therefore, the importance of the third level of our algorithm is highlighted when the proposed multi-numerology scheme still achieves high SINR and KPI results when the INI is high (Figs. 5.9 and 5.10).
- The use of numerology 0 for the eMBB Premium and Non-Premium BWPs is not recommended as it inflicts a higher latency for URLLC users with preemptive scheduling (Figs. 5.13, 5.14, 5.15).

5.8 Solution alignment with the O-RAN architecture

In this section, we discuss the alignment of this solution with the O-RAN architecture where we focus on where the algorithms can be implemented in this architecture depending on the corresponding timescale. The integration and testing of this solution in a real O-RAN architecture is outside the scope of this thesis but may become a part of a future work where a collaboration with an integration team will take place.

Therefore, to implement our three-level algorithm in the O-RAN architecture, its duration should be assessed as well as its required time scale loop and period. Consequently, for each level of this algorithm, we discuss its duration as well as the overall time execution. In fact, Algorithm 5 in the first level requires a maximum of 2 iterations to converge while Algorithm 6 in the second level requires a maximum of 10 iterations. With a fast processor such as a Core i5 machine, these algorithms can converge within a time range of 60 and 80 ms. Hence, the first and second levels of the three-level algorithm can be implemented at the level of the near-RT RIC. However, it is not required to run these algorithms within this time range since the URLLC BWP selection process can be run whenever the number of users changes. The latter

changes depending on the Poisson arrival process which varies within a time range above or equal to 1 s. The same applies to the BWP band adjustment as it can be run within a time range above 1 s without affecting users' performance. Consequently, these algorithms are to be implemented at the level of the Non-RT RIC.

As for the guard band dimensioning, Algorithm 7 in the third level requires a training phase taking several iterations to find the optimal policy, which takes around 6 minutes to be executed on a machine with a Core i5 CPU at 2.50 GHz with 8GB RAM. Additionally, the requirement to change the guard band does not have to occur at the time range of the near-RT RIC but at the level of the Non-RT RIC.

Regarding the overall three-level algorithm, for 1 iteration, it requires between 6 and 7 minutes (on a machine with a Core i5 CPU at 2.50 GHz with 8GB RAM) when taking into account the training phase of the DQN algorithm which is above 1 s. Hence, this algorithm cannot be implemented at the level of the near-RT RIC operating within a time range of 10 ms and 1 s. In addition, the need to launch it is within the control loop of the Non-RT RIC (above 1 s) as the traffic variation occurs within a time range above 1 s. Hence, it is best to implement it at the level of the Non-RT RIC.

5.9 Concluding Remarks

A three-level slicing algorithm was proposed in this chapter to efficiently allocate radio resources for the three 5G classes: eMBB, URLLC and mMTC in a multi-numerology context. This solution is 3GPP-compliant and the following key points summarize the chapter:

- The first level of the solution allots the BWP serving the URLLC users between the URLLC Premium BWP with a high numerology, dedicated solely for URLLC users, and a Non-Premium BWP with a low numerology, shared with eMBB users but where preemptive scheduling favors URLLC users. This is done thanks to a non-cooperative game where a well-defined cost function is set to take into account the users' latency, incurred monetary cost and BWP occupation.
- The second level tackles the BWP band adaptation for the four BWPs (mMTC, eMBB Premium, Non-Premium and URLLC Premium) where the band is dynamically adjusted using smart heuristics based on users' KPIs: throughput for eMBB users, SINR for mMTC users and latency for URLLC users.
- The third level resorts to a DQN-based scheme to dimension the guard band among BWPs using different numerologies in order to mitigate the ensuing INI effect while avoiding loss of spectral efficiency.
- Performance analysis demonstrate the efficiency of our proposed three-level multi-numerology multi-slice solution providing better URLLC latency while maintaining high eMBB satisfaction and high SINR for mMTC users compared to the previous single-numerology solution and a work from the SOTA [73] that overlooked the guard band dimensioning to curb the INI effect.
- The alignment of our devised solution with the O-RAN architecture is thoroughly discussed where we pinpoint the level of implementation of the algorithm.

The previous chapters focused on users connected to a single slice. Nonetheless, users with multi-slice connectivity require attention as their consideration in the radio resource allocation problem brings additional challenges from a latency and energy efficiency perspective. Consequently, the next chapters revolve around this type of users.

Chapter 6

Novel BWP Schemes for Multi-Numerology and Multi-Slice Radio Access Networks

For this chapter, focus is shifted to users connected to multiple slices. The radio resource allocation problem for this type of users is quite challenging especially when the connected slices require different numerologies. In that case, to improve radio resource allocation and KPI satisfaction, we tackle the targeted problem from a latency perspective. In fact, adopting the multi-numerology BWP configuration for these users is refrained by BWP switching which inflicts additional latency. The latter is detrimental for services requiring low latency such as URLLC. For this reason, we propose in this chapter three innovative BWP switching mechanisms for multi-slice users where only eMBB and URLLC services are considered. The proposed schemes are based on the Downlink Control Information (DCI)-based BWP switch. In fact, the DCI is a message sent by the gNB to the UE through the Physical Downlink Control Channel (PDCCH) that includes information such as the user's scheduled data and BWP indicator. When the latter is modified, a BWP switch is performed known as the DCI-based BWP switch which is the fastest existing method for a BWP switch. In addition, one of these proposed mechanisms uses the BWP Inactivity Timer that triggers a Default BWP switch as well. We evaluate the performance of the proposed solutions which prove to be efficient in terms of latency and we compare them against each other and against the current baseline approach.

6.1 Introduction

Previous chapters concentrated on users connected to a single slice. Nonetheless, users connected to multiple slices should also be considered especially when the slices require different numerologies. In that case, a multi-numerology BWP configuration should be applied for these users and BWP switching should be performed frequently for these users to retrieve the data of each slice since only one BWP can be active at a time. Frequent BWP switching induces additional latency due to the BWP switching delay and the waiting time to indicate a change of BWP. This can cause QoS degradation for delay-stringent services such as URLLC. Moreover, in the literature, these users are rarely considered and in the few works tackling them, the BWP switching process is overlooked. A patented solution in [83] aims to avoid BWP switching for these users by proposing the use of multiple active bandwidth parts. In the proposed approach, multiple active BWPs may be a solution for UEs linked to multiple slices where each slice requires a different numerology. With their devised solution, a primary and secondary BWPs are activated through a DCI field. In addition, these BWPs may be switched using other fields in the DCI. However, this solution may not be feasible with the current UE limitation where a UE cannot support receiving signals using different numerologies each linked to a different BWP, simultaneously. Also, in current standards, a UE may

be configured to multiple BWPs but only one is active at a time [18]. Therefore, BWP switching is inevitable for these users. Thus, in this work, we focus on the BWP switching aspect by proposing three innovative and UE-compatible BWP switching schemes that help improve performance of multi-slice users configured with multiple BWPs. For each solution, a patent is submitted. To note that only eMBB and URLLC slices are considered. Nevertheless, the proposed solutions can be applied to any number of slices. In fact, these solutions mainly rely on the DCI-based BWP switch which is the fastest method of BWP switching, taking between 1-3 ms [33]. With this BWP switch method, the DCI indicates a change of BWP thanks to the BWP indicator field in the DCI. Particularly, the third solution uses the BWP inactivity timer in addition to the DCI-based method where a default BWP is activated after the expiry of a certain inactivity timer.

Furthermore, the three devised solutions that aim to enhance BWP switching are as follows:

- The first technique consists of modifying the DCI format to support users with multi-slice connectivity to have an improved DCI-based BWP switching.
- The second technique aims at modifying the DCI frequency dynamically to ensure a faster DCI-based BWP switching and reduce overall latency.
- The third technique relies on selecting an appropriate default BWP related to a service with a higher priority while modifying dynamically the BWP inactivity timer to prioritize delay sensitive services (such as URLLC) over others (such as eMBB) to ensure for the former a lower latency.

These techniques are compared against each other and against the baseline approach represented in Fig. 1.10 from Chapter 1 where a DCI-based BWP switch is performed thanks to a single BWP indicator in the DCI and where the DCI frequency is not adjusted. Simulation results prove the efficiency of these schemes especially in terms of URLLC latency. The rest of this chapter is organized as follows:

Section 6.2 details the three devised schemes. Section 6.3 discusses our system model. Section 6.4 provides simulation results of the proposed solutions. Section 6.5 describes concisely the solutions implementation feasibility in the 5G architecture. Finally, Section 6.6 concludes this chapter.

6.2 The Proposed Solutions for BWP Switching

Our three devised techniques are thoroughly explained for users connected to URLLC and eMBB slices simultaneously.

6.2.1 First Solution: DCI Format Modification

Instead of using the same numerology (or BWP) for multiple services or waiting for the next DCI occurring after multiple time slots to perform a BWP Switch, the first solution consists of a DCI adaptation to contain additional fields for UEs having multiple slices. Currently, the DCI contains only one BWP indicator indicating the BWP that should be scanned by the UE. However, we propose to add in the DCI multiple BWPs indicators related to each service or slice that the UE should scan in turn to retrieve its slice-specific data. Furthermore, additional fields should also include the instants or locations in the time domain where the BWP switching should occur between these multiple BWPs.

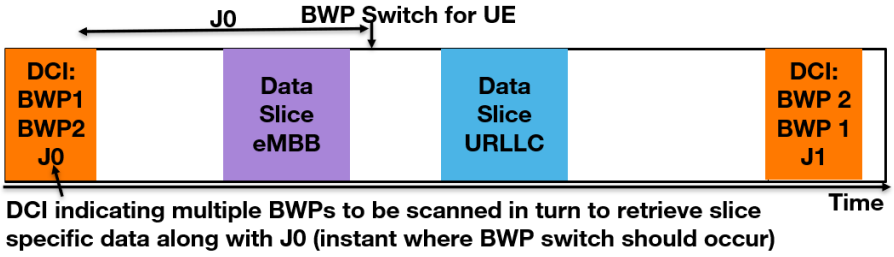

Figure 6.1: DCI Format Modification

Figure 6.1 represents the first solution in the case of two slices: eMBB with BWP 1 and URLLC with BWP 2. Receiving the first DCI that includes the additional fields: BWP 1, BWP 2 and $J0$, the UE scans first BWP 1 and then switches to BWP 2 after a certain time $J0$ as indicated by the DCI. After multiple slots (or ms), it can receive another DCI indicating other BWPs to be scanned in turn along with predefined instants where the BWP switch should occur. With this solution, the waiting time for the UE to be served by the BWP with the optimal numerology is greatly reduced since all the information is included in a single DCI instead of waiting for the next one that occurs after multiple ms as seen in Fig. 1.10 from Chapter 1. Moreover, this format is well adapted for a UE connected to multiple slices and retrieving its slice-specific data from multiple BWPs where BWP switching is frequent. Even though it requires a change in the standards, this solution is feasible since it only requires the modification of the DCI format by adding additional fields.

6.2.2 Second Solution: Dynamic DCI Frequency Adjustment

With this second solution, instead of modifying the DCI format to include multiple BWPs indicators, the timing of the next DCI is adjusted to be as small as possible to quickly perform a BWP Switch by adapting the PDCCH frequency that carries the DCI for UEs having multiple slices.

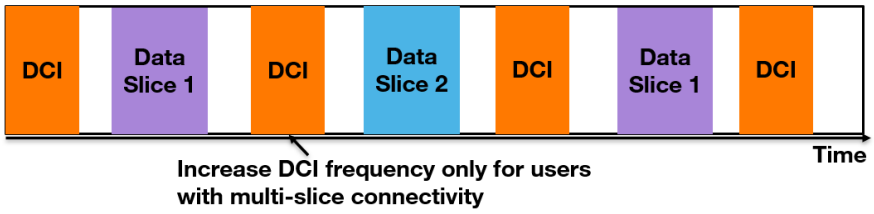

Figure 6.2: DCI Frequency Adjustment

Figure 6.2 portrays the second solution in the case of two slices: eMBB with BWP 1 and URLLC with BWP 2. With the PDCCH channel being more frequent, the UE is able to switch BWPs more frequently to retrieve its incoming data from multiple slice-related BWPs. With this solution, the waiting time for the UE to be served by the BWP with the optimal numerology is reduced since the PDCCH carrying the DCI indicating a BWP change is more frequent which in turn allows more frequent BWP switching when compared to the standard scenario in Fig. 1.10 from Chapter 1. This solution is also feasible since it only requires the modification of the PDCCH frequency which is configurable by the network without modifying the UE capability and DCI format. We resort to a simple yet efficient approach for the dynamic adjustment of the DCI/PDCCH frequency. Accordingly, the PDCCH period is automatically reduced to be as minimal as possible which is 2 time slots using numerology 1 (equivalent to 1 ms) whenever the UE is connected to multiple slices simultaneously. This choice is explained by the fact that the UE needs 1 time slot to receive

the DCI and another to retrieve its data. When the UE is solely connected to a single slice and no BWP switching is required, the PDCCH period is brought back to 3 time slots using numerology 1 (1.5 ms) to reduce power consumption which corresponds to the baseline approach.

6.2.3 Third Solution: Dynamic Selection of Default BWP and BWP Inactivity Timer

The third solution uses both BWP Inactivity Timer Switching and DCI-based BWP Switching while optimizing the default BWP and inactivity timer to prioritize a Premium service such as URLLC over a Non-Premium one such as eMBB.

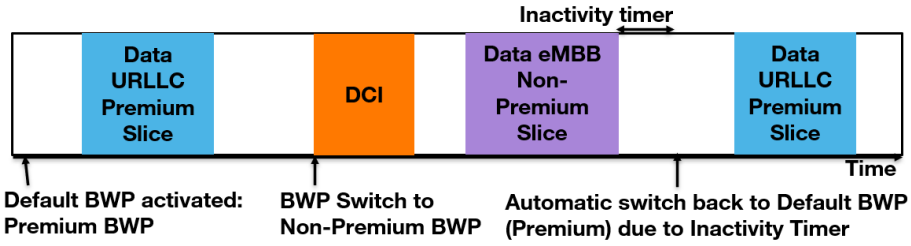

Figure 6.3: Default BWP Selection and BWP Inactivity Timer Adjustment

Figure 6.3 depicts this solution where the URLLC slice associated with BWP 2 (set as default BWP) is prioritized over the eMBB slice associated with BWP 1. As can be seen, the BWP Inactivity Timer Switching is used to select a default BWP which corresponds to the BWP associated with the Premium service (the URLLC service requiring stringent delays) and a DCI-Based BWP switching is used to switch to any other BWP which can be the Premium BWP or BWP associated to a Non-Premium service like eMBB as it is more delay tolerant. After a preset inactivity timer expires, the BWP reverts automatically to the default BWP. The latter is scanned to retrieve data for the Premium service. Thus, by selecting the default BWP as the one used by the Premium URLLC service, URLLC traffic can be scheduled immediately without enduring any BWP switching delay. Only the eMBB service will endure such a delay as it can cope with it. Furthermore, when traffic of the eMBB service arrives, the BS will send a DCI at an appropriate time slot to switch back to the BWP associated to the Non-Premium service for the UE to retrieve its data. Additionally, the inactivity timer is determined astutely in order to reduce the time necessary to switch back to the default BWP. Accordingly, the inactivity timer is reduced to 2 time slots when using numerology 1 (1 ms) whenever the UE is connected to at least two slices. Finally, this third solution is also feasible since it only requires the combined use of existing mechanisms.

6.3 System Model

As seen in Fig. 6.4, we consider a single gNB with $B_{total} = 100$ MHz bandwidth which corresponds to the normal amount of bandwidth usually owned by an operator in 5G. The gNB covers an area with radius R. Two slices are considered: eMBB and URLLC. Each slice will have a dedicated number of radio resources.

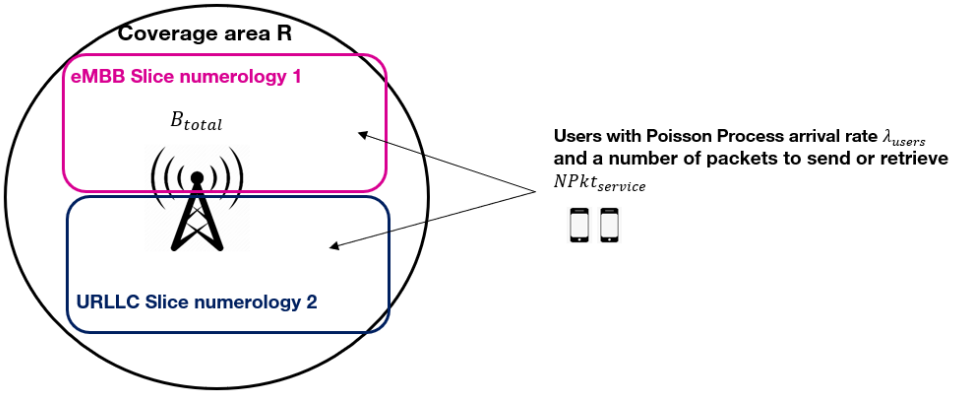

Figure 6.4: System Model for Novel BWP Switching Schemes

Additionally, two bandwidth parts are considered for each slice where each BWP is associated with a numerology. The first BWP, denoted by BWP 1, consists of the band attributed to the eMBB slice and uses numerology 1 (the lower numerology) with a value of $B_{eMBB} = 60$ MHz. The second BWP, denoted by BWP 2, is the band attributed to the URLLC slice using numerology 2 (higher numerology) with a value of $B_{URLLC} = 20$ MHz. The remainder amount of the total bandwidth remains unused.

As for the UEs, we consider an initial number of users $N_{users} = 20$ of type 1 or 2 (Table 1.3) with no mobility randomly distributed in the gNB coverage area within the radius R where each user is connected to both slices. In addition to these users, others arrive to the network following a Poisson process with a mean of λ_{users} users/sec. Users remain active in the network for a fixed period of time where packets are generated continuously for either eMBB, URLLC or both services following a Poisson process with a mean of $NPkt_{service}$ packets/s with a fixed size $PktSize_{service}$.

Regarding the resource allocation, the scheduler serves and addresses the URLLC demand of the UE first to ensure lower latency and then schedules the demands of eMBB. Thus, at each TTI, the following process is applied by the scheduler:

- If not activated, a BWP switch is performed to activate the BWP associated to URLLC and a switching delay is required where no PRB is allocated for the concerned UE till the switch is complete.
- If the BWP switch for a user is being performed, the scheduling of this user is put on hold and the ensuing switching delay is taken into consideration. Otherwise, the scheduler allocates the UE a number of PRBs based on its demand and the PRB availability at the current TTI. When there are no sufficient PRBs, the amount of PRBs to be scheduled is queued for the next TTI with the ensuing queuing delay taken into consideration.
- If all URLLC packets for the concerned user are scheduled and the remaining amount is null, it performs a BWP switch to the BWP associated to eMBB and repeats the previous steps for the eMBB service.

This process is repeated each TTI for a certain period T till the arrival of new packets. This period has a duration of $T_{duration} = 1$ s since new packets arrival for each service is set to 1 s as a simulation parameter. As for the KPIs assessment, throughput is chosen for the eMBB slice and latency for the URLLC slice. The throughput of UE u is computed in a similar manner as the previous chapter as follows:

$$Thr_u = \frac{AllocatedPRB_u \times Bits\_per\_PRB}{T_{duration}} \tag{6.1}$$

where $AllocatedPRB_u$ is the number of allocated PRBs to the UE during a period T considered over a duration $T_{duration}$. Further, $Bits\_per\_PRB$ is the number of bits per PRB that is determined similarly to the previous chapter using Equation (5.5).

As for the number of allocated PRBs to the UE, it depends on the number of PRBs required by the user and the number of PRBs available at the level of the scheduler depending on the band allotted for the selected slice.

The number of PRBs required by UE u for a specific service is determined using the following expression:

$$ReqPRB_{service,u} = \frac{NPkt_{service,u} \times PktSize_{service}}{Bits\_per\_PRB} \tag{6.2}$$

where $NPkt_{service,u}$ is the number of packets transmitted by UE u for the corresponding service and $PktSize_{service}$ is the packet size in bits. As for the URLLC latency of UE u, it is calculated at each period T before the arrival of new packets and it is expressed as follows:

$$L_u = d_q + d_{switch} + d_{al} + d_{ue} + d_{bs} \tag{6.3}$$

where:

- d_q is the queuing delay in ms.
- d_{switch} is the BWP switching delay based on Table 1.3 whenever a BWP switch from a service to another is performed.
- $d_{al} = 1$ TTI is the packet alignment time in ms according to [81]
- d_{ue} is the UE processing time equal to 4.5 OFDM symbols according to [81]
- d_{bs} is the BS processing time equal to 2.75 OFDM symbols according to [81]

The queuing delay d_q is increased by the value of a TTI duration at each TTI where the remaining amount of PRBs to be scheduled for the UE is not null. In addition, the queuing delay is also increased by the value of a TTI if at this TTI, a BWP switch is required to be performed but the scheduler is unable to execute it, due to the absence of a DCI indicating a BWP switch. Note that d_{ue}, d_{bs} and d_{al} depend on the numerology used since they depend on the TTI and OFDM symbol duration.

As for the total number of PRBs available for each slice, it is determined by Table 5.3.2-1 from [12] depending on the attributed slice band and numerology.

These KPIs are used to determine the performance of our devised techniques which will be discussed in the next section.

6.4 Performance Evaluation

We used Python for simulations to assess the performance of our solutions where the same users' KPIs were assessed for every given solution. Also, the unspecified and additional simulation parameters from the system model are shown in Table 6.1.

As for the performance indicators, we represent the URLLC latency CCDF, the eMBB throughput CDF, and the number of DCIs scanned per UE in a frame to have a sort of representation of the power consumption by the UE for each solution and the baseline solution. With the latter, we consider that the DCI is sent every 3 time slots using numerology 1 (every 1.5 ms) to reduce power consumption of the UE and for the latter to retrieve its data after at least 1 time slot from DCI reception. As for the DCI frequency solution,

Table 6.1: Simulation parameters for Novel BWP Switching Schemes

Parameter	Description	Value
R	Coverage area	300 m
λ_{users}	Users arrival rate	2 users/s
$NPkt_{URLLC}$	URLLC packet rate	2 packets/s
$PktSize_{URLLC}$	URLLC packet size	256 bits
$NPkt_{eMBB}$	eMBB packet rate	10 packets/s
$PktSize_{eMBB}$	eMBB packet size	12000 bits

the DCI frequency is set to 2 times slots (1 ms) to reduce it when the UE is connected to multiple slices. Finally, for the BWP inactivity timer solution, the inactivity timer is set to 1 ms and the DCI frequency is set to 3 time slots (1.5 ms) similar to the baseline scheme.

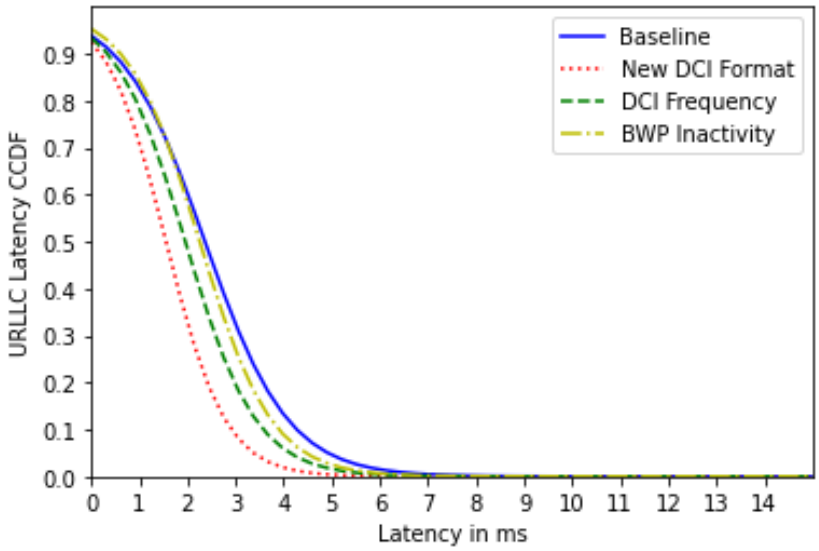

Figure 6.5: URLLC Latency CCDF

Figure 6.5 represents the URLLC latency CCDF for our three solutions and the baseline scheme. As can be seen, all three solutions provide a reduced latency compared to the baseline with the best performance recorded by the first solution. This is because the BWP switch can be performed immediately when necessary for the first solution as indicated by the new DCI format instead of waiting for the next DCI (second solution and baseline) or the inactivity timer (third solution).

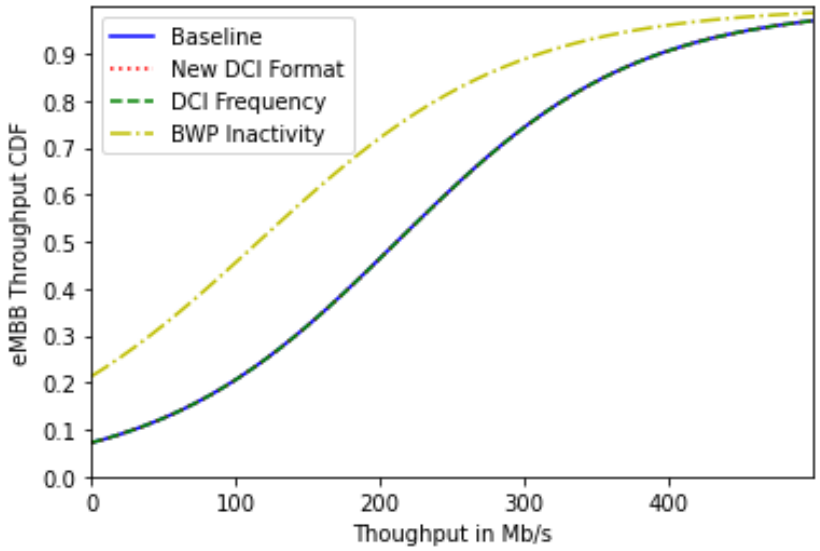

Figure 6.6: eMBB Throughput CDF

Figure 6.6 displays the eMBB throughput CDF for the three solutions and the baseline approach. We note that we have the same eMBB throughput performance for all solutions with the exception of the third solution with the BWP inactivity timer where a degradation is recorded. This can be explained by the fact that this solution prioritizes the URLLC service at the cost of degrading the eMBB service. Hence, this solution is not recommended for stringent eMBB services.

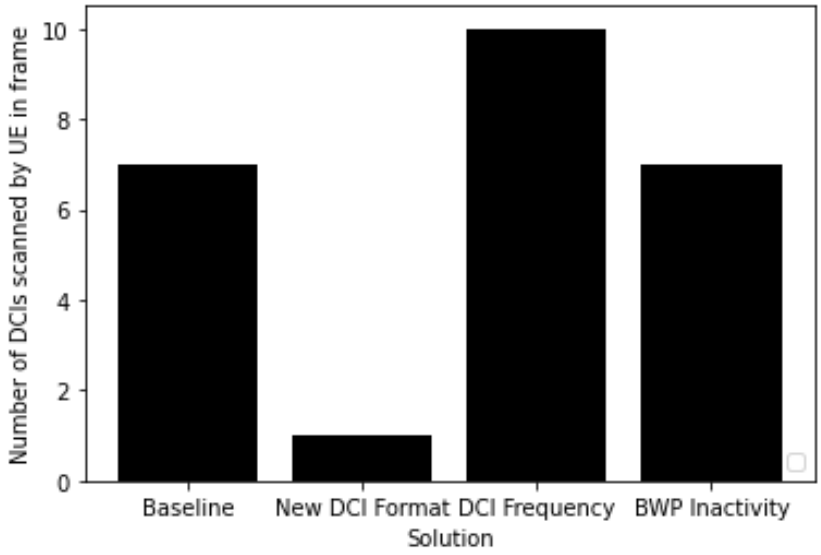

Figure 6.7: Number of DCIs scanned per UE per frame

Figure 6.7 shows the number of DCIs scanned by the UE in a frame for the three solutions and the baseline approach to gauge the power consumption of such schemes. The best performance is attributed to the first solution with the new DCI format modification since the BWP switching information can be sent using a single DCI in a frame at a low frequency. The worst performance is displayed by the second solution with the DCI frequency adjustment since when we increase the PDCCH and DCI frequency, the number of DCIs scanned by the UE will increase.

To summarize, the first solution modifying the DCI format realizes the best performance in terms of latency, throughput and number of DCIs scanned compared to the other approaches. All other solutions show better performances in terms of latency (but with a higher number of DCIs scanned for the second solution because of increased DCI frequency) compared to the baseline scheme.

6.5 Solution Implementation Feasibility

In this section, we briefly discuss the implementation feasibility of the proposed solutions in the 5G architecture.

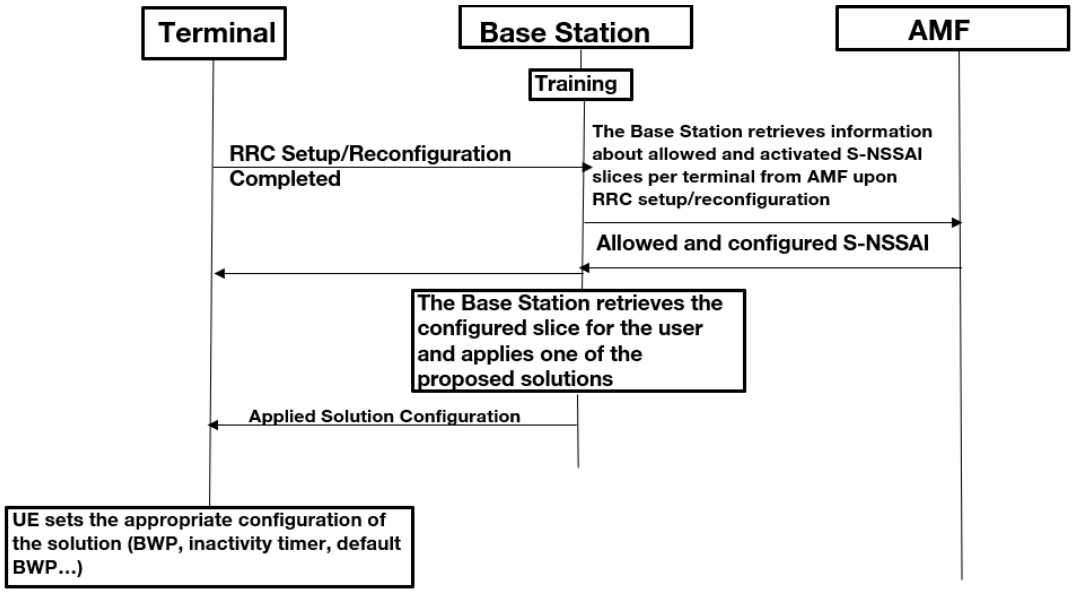

Figure 6.8: Sequence Diagram for Solution Implementation

Figure 6.8 displays the sequence diagram of the involved entities for the solution implementation. First, as we can see, during the establishment of a radio bearer for a terminal via Radio Resource Control (RRC) reconfiguration or setup, the RAN intelligent entity (which is the BS) retrieves information about the allowed S-NSSAI or slices per UE from the Access and Mobility Function (AMF) entity of the core network. Therefore, the BS is aware of the configured slices and services per terminal. Once the BS detects that the terminal is connected to multiple slices, it can apply one of the proposed solution by either constructing the appropriate DCI message or by adjusting the PDCCH frequency or the BWP inactivity timer and default BWP. Afterwards, the BS sends the appropriate configurations to the UE via a RRC or a DCI message. A RRC message is a signalling message sent by the gNB to the UE to configure certain radio parameters which include the PDCCH monitoring frequency, the default BWP and the BWP inactivity timer. Finally, the UE applies these configurations.

6.6 Concluding Remarks

To conclude, three patented solutions that help optimizing the BWP switching process for multi-slice users were proposed in this chapter. The examined scenarios were set particularly for eMBB and URLLC services

and the following key points can be drawn for this contribution:

- The first solution relies on a DCI format modification to include multiple BWP indicators and the instants where the BWP switching should occur. This solution has the best performance in terms of URLLC latency reduction, eMBB throughput satisfaction and power consumption (DCI scanning) reduction.
- The second solution aims to adjust the DCI frequency for multi-slice users by increasing PDCCH frequency. With this solution, the latency is reduced, the eMBB throughput is not impacted but the power consumption due to DCI scanning is increased with increased DCI frequency.
- The third solution dynamically adjusts the BWP inactivity timer while selecting the BWP for the delay sensitive premium service as the default BWP. Simulation results prove the reduction of latency with this solution while maintaining the same usual number of DCIs scanned. Nonetheless, an eMBB throughput degradation is observed due to the prioritization of the URLLC service over the eMBB service.
- The feasibility of these solutions is also discussed.

After dealing with the latency aspect for these multi-slice users, the next chapter focuses particularly on the energy efficiency aspect.

Chapter 7

Energy efficient BWP Configuration for Multi-Slice Users

The study of multi-slice users is carried on in this chapter. However, energy efficiency is the main focus in this contribution for the radio resource allocation problem. In fact, users connected to multiple slices may scan multiple BWPs consecutively with a multi-numerology BWP configuration to retrieve their slice-specific data when these slices use different numerologies. This can be time-consuming and energy intensive. Another option is to use a single numerology BWP configuration for all slices which may not be optimal but helps reducing complexity. Therefore, we propose two energy efficient algorithms that select the appropriate BWP configuration, among the multi-numerology and single numerology, depending on the battery level and QoS satisfaction. The first algorithm is a distributed one based on a congestion game and the second one is a centralized one based on an optimization problem. Both solutions are compared against each other and against the legacy solution applied today in the standards.

7.1 Introduction

This chapter tackles the same problem as the previous chapter which is the radio resource allocation problem for multi-slice users but from an energy efficiency perspective. As specified before, multi-slice users are rarely considered in the literature and those few works who take them into account focus on the PRB scheduling and attribution. Hence, energy efficiency is disregarded. Instead of tackling the same problem as the one studied in the SOTA, we rather focus on the BWP configuration for these users from an energy efficiency perspective. In fact, multi-slice users face two options. The first option consists of a multi-numerology BWP configuration where each slice requires a different numerology (a different BWP). With this option, frequent BWP switching is required to retrieve the data of each slice which can be time and energy consuming. The second option is to use a single numerology and BWP for all slices. This option is currently used for these users in the standards (legacy scheme) since it reduces complex signalling due to BWP switching but at the cost of degrading the slices' QoS. Thus, we devise a sagacious and flexible scheme that selects the most appropriate BWP configuration for each UE among the two previously mentioned solutions: either the Multi-Numerology BWPs per UE slice or a single numerology BWP for all the UE slices, depending on the UE battery level and QoS strictness. This scheme relies on two approaches: a distributed approach using non-cooperative game theory where every UE autonomously selects the BWP configuration (multi-numerology or single numerology) that strikes a good balance between improving its QoS and reducing its battery consumption; and a centralized approach where UEs are assigned optimally to the most adequate BWP configuration. The performances of both approaches are assessed through

extensive simulations where they are compared against each other and against the legacy scheme using a single numerology BWP configuration which they largely surpassed. The organization of the rest of this chapter is as follows:
Section 7.2 discusses our system model. Sections 7.3 and 7.4 tackle the proposed distributed and centralized approaches. Section 7.5 provides simulation results of the proposed solutions. Section 7.6 presents the proposed patents following this contribution. Finally, Section 7.7 summarizes the chapter.

7.2 System Model

We consider a fixed random number of users N_{users} and a single gNB with a total band B_{total} which corresponds to the amount of bandwidth owned by a 5G operator. The gNB covers an area with radius R. These users are randomly distributed in the gNB coverage area within the radius R where each user is connected to two slices: eMBB and URLLC. Each slice will have a dedicated number of radio resources as seen in Fig. 7.1.

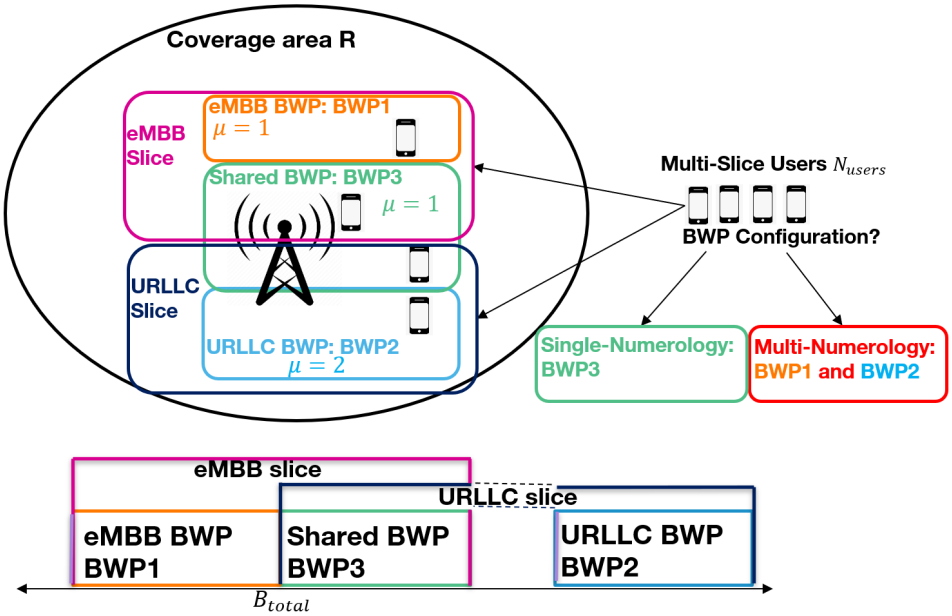

Figure 7.1: System Model for Energy Efficient BWP Configuration Algorithm for Multi-Slice Users

Additionally, three bandwidth parts are considered for each slice. The first BWP, denoted by BWP 1, consists of the band attributed to the eMBB slice and uses numerology 1 (the lower numerology) with a band B_{eMBB}. The second BWP, denoted by BWP 2, is the band attributed to the URLLC slice using numerology 2 (a higher numerology) with a band B_{URLLC}. To note that users selecting the multi-numerology BWP configuration will scan both these BWPs (BWP 1 and BWP 2) consecutively to retrieve the data for each slice. The third BWP, denoted by BWP 3, is the one shared between both slices using numerology 1 with a band B_{mixed} with $B_{eMBB} + B_{URLLC} + B_{mixed} \leq B_{total}$. This particular BWP (BWP 3) is scanned by users affected with a single numerology for both services. Each UE u has a given volume of data $V_{u,s}$ to retrieve for each service s and remains in the network till the total data volume for both services is consumed. A fair queuing scheduling is applied at the level of each BWP where the BWP radio resources are attributed equally among users. For each user, we calculate the throughput to determine at a later stage the user's sojourn time in the network. The throughput of UE u for service s is computed similarly to previous chapters as

follows:

$$Thr_{u,s} = \frac{AllocPRB_{u,s} \times Bits\_per\_PRB_u}{D} \tag{7.1}$$

where $AllocPRB_{u,s}$ is the number of allocated PRBs to UE u for service s from its attached BWP during a TTI with duration D. Furthermore, $Bits\_per\_PRB_u$ is the number of bits per PRB that depends on the modulation and coding rate of the UE based on Equation (5.5) from Chapter 5.

As for the number of allocated PRBs to the UE for service s, it depends on the total number of PRBs $TotPRB_{bwp}$ allotted to its attached BWP bwp which is linked to service s and the total number of connected users to this particular BWP $N_{users,bwp}$ since a fair resource scheduling is applied:

$$AllocPRB_{u,s} = \frac{TotPRB_{bwp}}{N_{users,bwp}} \tag{7.2}$$

As for the total number of PRBs available at each BWP, it is determined by Table 5.3.2-1 from [12] depending on the attributed BWP band and numerology.

Such performance indicators will be used to devise the cost function presented hereafter and used to stir adequately the BWP selection configuration in centralized and distributed approaches.

7.2.1 The Cost function

The cost function for UE u selecting BWP configuration strategy c is given by:

$$C_{u,c} = \sum_{s \in \{eb,uc\}} \alpha_{u,s} \cdot DST_{u,s,c} + \theta_c \cdot SwDl_u + \beta_u \cdot B_c \tag{7.3}$$

where:

- $DST_{u,s,c}$ is the sojourn time of UE u for retrieving the data of a particular service s when selecting strategy c. The service s can be either eMBB denoted by eb or URLLC denoted by uc.
- $SwDl_u$ is the BWP switching delay of UE u (also a part of the user's overall sojourn time).
- B_c is the total band scanned by the user depending on its devised strategy c.
- $\alpha_{u,s}$ and β_u are normalizing factors. The former reflects the class of service s for UE u and the latter represents the battery level of UE u.
- θ_c is an indicator variable that equates to one in presence of BWP switching delay, and to zero otherwise and hence depends on the selected strategy.

In the cost function (7.3), the first term represents the UE's sojourn time in the network, necessary for retrieving the data of all its services. That first term is used as a QoS indicator as the higher the user sojourn time, the lower its QoS. In fact, the user will endure a higher delay and will stay active in the network longer which may increase its energy consumption. Hence, a higher sojourn time increases the cost function. The second term is the BWP switching delay (when applicable) which is also a part of the user's sojourn time in the network. The third term of the cost function represents the scanned BWPs by the UE. The higher this band, the higher the energy consumed by the user for scanning a larger band. In fact, if UE u chooses the multi-numerology strategy MN, it will scan consecutively BWP 1 and BWP 2 to retrieve the data of each service s and the corresponding sojourn time for service s is determined by the following equation:

$$DST_{u,s,MN} = \frac{V_{u,s}}{Thr_{u,s}} \tag{7.4}$$

where:

- $V_{u,s}$ is the volume of data to be retrieved by UE u for service s.
- $Thr_{u,s}$ is the throughput of UE u for service s.

Additionally, with the Multi-Numerology scheme, the BWP switching delay is taken into account ($\theta_{MN} = 1$) and the total scanned band by the user is the sum of BWP 1 and BWP 2 ($B_{MN} = B_{BWP1} + B_{BWP2}$). When UE u selects the Single Numerology configuration SN, it will scan BWP 3 solely to retrieve the data of both services. Therefore, it will have the same achieved throughput for both services since the same number of PRBs is allocated to the user for each service s. Therefore, Thr_u is independent of the type of service in that case and $DST_{u,s,SN} = \frac{V_{u,s}}{Thr_u}$. Also, $\theta_{SN} = 0$ and $B_{SN} = B_{BWP3}$ as only one BWP is scanned which prevents BWP switching. Choosing the multi-numerology configuration will improve user's KPIs and QoS and will increase user's throughput. This in turn will reduce the user's sojourn time (first term) but at the cost of adding a BWP switching delay (second term) and increasing the BWP scanned by the user (third term) and hence the ensuing energy consumption. Contrarily, a single numerology avoids BWP switching (second term) and reduces the energy consumption as the BWP scanned by the user (third term) is narrower but it increases the user's sojourn time (first term). Additionally, the user sojourn time increases when the number of users choosing the same BWP increases as users share the limited amount of resources, which reduces their achieved throughput. Hence, an astute load-balance of users among available configurations (single or multi-numerology) must be attained.

This cost function is used in both the centralized and distributed approaches, which are detailed in subsequent sections.

7.3 Distributed Approach: Congestion game

Users connected to multiple slices strive to choose between the multi-numerology (MN) and single numerology (SN) BWP configurations in order to curb their energy consumption without sacrificing their QoS. We have recourse to non-cooperative game theory since the problem can be modeled as a game where the players are autonomous UEs competing over limited radio resources, which are the PRBs available in the BWPs. The corresponding non-cooperative game $\mathcal{G}$ is presented as follows:

- The set of players is the set $\mathcal{U}$ of UEs connected to multiple slices.
- The set $\mathcal{S} = \{MN, SN\}$ is the set of strategies where MN and SN designate the multi-numerology and single numerology BWP configurations respectively. The vector y_u is the strategy vector of UE u whose components are the binary variables $y_{u,c}$ equal to 1 when UE u chooses the BWP configuration c. Hence, $\mathbf{y} = (y_u)_{u \in \mathcal{U}} \in \mathcal{S}$ is the strategy profile, and $\mathcal{S} = S_1 \times S_2 ... \times S_U$ is the space of all profiles.
- The set of cost functions $\{C_1, C_2, ..., C_U\}$ based on equation (7.3) quantify the players' profitability over the possible outcomes of the game.

Like all previous non-cooperative games, we seek to find the NE (the state where each player has selected an optimal strategy in response to other players' strategies).

Similar to the games from Chapters 4 and 5, the game $\mathcal{G}$ is guaranteed to have a mixed NE since it is a finite game. However, resorting to mixed NEs is burdensome as they represent a probability distribution over available actions. Nevertheless, the defined $\mathcal{G}$ has the FIP property which guarantees the existence of PNE [35].

Proposition 9. *The game $\mathcal{G}$ has the FIP property.*

Proof. We show first that $\mathcal{G}$ is an unweighted congestion game. In fact, although the cost function is player specific, it is non-decreasing in the number of players that selected the same strategy (BWP configuration). This is because the sojourn time $\frac{V_{u,s}}{Thr_{u,s,bwp}}$ is non-decreasing in the number of players that selected the same strategy as the throughput is inversely proportional to the number of users selecting the same BWP configuration. According to [37], player specific unweighted games with only two strategies have the FIP property which is the case for our game with two strategies MN and SN. □

Games with FIP are guaranteed to converge to PNE through simple Best Response dynamics [38] presented in the below Algorithm 9. In this algorithm, each player in turn, will choose the strategy minimizing

Input: BWP configuration cost
Output: BWP configuration selection based on lowest cost
1 **repeat**
2 | Calculation of BWP configuration cost $C_{u,MN}$ and $C_{u,SN}$ by each UE u;
3 | BWP configuration with lowest cost is selected by the user;
4 **until** *BWP configuration selection is the same as previous iteration*;
Algorithm 9: Distributed BWP Configuration Selection Best Response Dynamics Algorithm

its cost function in response to other players' strategies till convergence, when the chosen strategy of each player is the same as in the previous round.

In the next section, the same problem is tackled in a centralized approach.

7.4 Centralized Approach: Optimization Problem

In the centralized approach, a central entity takes the decision of the BWP configuration selection for each user by solving an optimization problem corresponding to minimizing the total cost for all users.

7.4.1 The Objective Function

The optimization problem is the following:

$$\begin{aligned} &\min_{A1,A2} \sum_{u\in\mathcal{U}} C_{u,MN}(A1) + \sum_{u\in\mathcal{U}} C_{u,SN}(A2) \\ &\text{subject to:} \\ &a_{1u}, a_{2u} \in \{0,1\}, \forall u \in \mathcal{U} \text{ and } a_{1u} + a_{2u} = 1, \forall u \in \mathcal{U} \end{aligned} \tag{7.5}$$

where:

- $A1 = (a_{1u})_{\forall u\in\mathcal{U}}$ is the vector of binary decision variable a_{1u} which is equal to 1 when UE u has the MN strategy configured and equal to 0 otherwise.
- $A2 = (a_{2u})_{\forall u\in\mathcal{U}}$ is the vector of binary decision variable a_{2u} which is equal to 1 when UE u has the SN strategy configured and equal to 0 otherwise.
- $C_{u,MN}$ and $C_{u,SN}$ are the cost functions when UE u is configured with the MN and SN strategy respectively and are determined in the below equations (7.6) and (7.7).

$$
\begin{aligned}
C_{u,MN}(A1) = a_{1u} \cdot & \frac{\alpha_{u,eb} \cdot V_{u,eb} \cdot D1 \cdot (\sum_{k \neq u} a_{1k} + 1)}{TotPRB_{BWP1} \cdot Bits\_per\_PRB_u} \\
+ a_{1u} \cdot & \frac{\alpha_{u,uc} \cdot V_{u,uc} \cdot D2 \cdot (\sum_{k \neq u} a_{1k} + 1)}{TotPRB_{BWP2} \cdot Bits\_per\_PRB_u} \\
+ a_{1u} \cdot & (\theta_{MN} \cdot SwDl_u + \beta_u \cdot B_{MN})
\end{aligned} \tag{7.6}
$$

$$
\begin{aligned}
C_{u,SN}(A2) = a_{2u} \cdot & \frac{\alpha_{u,eb} \cdot V_{u,eb} \cdot D3 \cdot (\sum_{k \neq u} a_{2k} + 1)}{TotPRB_{BWP3} \cdot Bits\_per\_PRB_u} \\
+ a_{2u} \cdot & \frac{\alpha_{u,uc} \cdot V_{u,uc} \cdot D3 \cdot (\sum_{k \neq u} a_{2k} + 1)}{TotPRB_{BWP3} \cdot Bits\_per\_PRB_u} \\
+ a_{2u} \cdot & (\beta_u \cdot B_{SN})
\end{aligned} \tag{7.7}
$$

with $D1$, $D2$ and $D3$ are the duration of the TTI when UE u is served by either BWP 1, 2 or 3 respectively.

Equations (7.6) and (7.7) are derived from equations (7.1), (7.2), (7.3) and (7.4) after replacing each term. To note that the number of users attached to each BWP are determined by the sum of the binary decision variables which leads to $N_{users,BWP1} = N_{users,BWP2} = \sum_{k \neq u} a_{1k} + 1$ and $N_{users,BWP3} = \sum_{k \neq u} a_{2k} + 1$. Therefore, the aim of this optimization problem is to minimize the cost function of all users globally by choosing for every user the adequate binary variables a_{1u} and a_{2u}. Note that the constraint $a_{1u} + a_{2u} = 1, \forall u \in \mathcal{U}$ is added to limit the user's selection to only one strategy.

The optimization problem defined in Equation (7.5) is non-convex since it is an integer (binary variables) non-linear problem due to the product of the decision variables with $a_{1u} \cdot (\sum_{k \neq u} a_{1k})$ and $a_{2u} \cdot (\sum_{k \neq u} a_{2k})$. Therefore, exhaustive search may be used to solve this problem. With exhaustive search, all possible combinations for user distributions among the BWPs are assessed to choose the one with the lowest cost function as seen in the below Algorithm 10.

Input: Cost function for all $(a_{1u}, a_{2u})_{\forall u \in \mathcal{U}}$ combinations possible ($2^{N_{users}}$ combinations)
Output: Combination of $(a_{1u}, a_{2u})_{\forall u \in \mathcal{U}}$ with the lowest cost function for all users

1 **repeat**
2 Calculation of BWP configuration cost function for all users $\sum_{u \in \mathcal{U}} C_{u,MN} + C_{u,SN}$;
3 Store the combination of $(a_{1u}, a_{2u})_{\forall u \in \mathcal{U}}$ with the calculated BWP configuration cost function for all users ;
4 **until** *Every combination of* $(a_{1u}, a_{2u})_{\forall u \in \mathcal{U}}$ *is executed*;
5 Select $(a_{1u}, a_{2u})_{\forall u \in \mathcal{U}}$ with the lowest BWP configuration cost function for all users ;

Algorithm 10: BWP Configuration Selection Exhaustive Search Algorithm

Nonetheless, this approach is highly time consuming with a complexity of $2^{N_{users}}$. For this reason, we transform the non-linear integer optimization problem in (7.5) to a linear one by replacing the multiplicative decision variables in what follows.

7.4.2 Integer Linear Programming Formulation

The non-linear terms $a_{1u} \cdot a_{1k}$ and $a_{2u} \cdot a_{2k}$ from (7.5) are replaced by the linear decision variables $\pi_{1u,k}$ and $\pi_{2u,k}$. Additionally, inequality constraints are added to ensure that the new variables are behaving the same way as the replaced non-linear terms. Also, $\pi_{1u,u}$ is none other than a_{1u} since $\pi_{1u,u} = a_{1u} \cdot a_{1u} = a_{1u}$ since a_{1u} is binary. The same applies for $\pi_{2u,u}$. Therefore, our Integer Linear Programming (ILP) problem

is formulated as follows:

$$\min_{\Pi 1, \Pi 2} \sum_{u \in \mathcal{U}} C_{u,MN}(\Pi 1) + \sum_{u \in \mathcal{U}} C_{u,SN}(\Pi 2)$$

subject to:

$$\begin{aligned}
&\pi_{1u,u}, \pi_{2u,u} \in \{0,1\}, \forall u \in \mathcal{U} \text{ , } \pi_{1u,u} + \pi_{2u,u} = 1, \forall u \in \mathcal{U} \\
&\pi_{1u,k} - \pi_{1u,u} \leq 0, \forall u,k \in \mathcal{U} \text{ , } \pi_{2u,k} - \pi_{2u,u} \leq 0, \forall u,k \in \mathcal{U} \\
&\pi_{1u,k} - \pi_{1k,k} \leq 0, \forall u,k \in \mathcal{U} \text{ , } \pi_{2u,k} - \pi_{2k,k} \leq 0, \forall u,k \in \mathcal{U} \\
&\pi_{1u,u} + \pi_{1k,k} - \pi_{1u,k} \leq 1, \forall u,k \in \mathcal{U} \text{ , } \pi_{2u,u} + \pi_{2k,k} - \pi_{2u,k} \leq 1, \forall u,k \in \mathcal{U}
\end{aligned} \tag{7.8}$$

where:

- $\Pi 1 = (\pi_{1u,k})_{\forall u,k \in \mathcal{U}}$ is the vector of binary decision variable $\pi_{1u,k}$ which is equal to 1 when both users u and k have the MN strategy configured and equal to 0 otherwise.
- $\Pi 2 = (\pi_{2u,k})_{\forall u,k \in \mathcal{U}}$ is the vector of binary decision variable $\pi_{2u,k}$ which is equal to 1 when both users u and k have the SN strategy configured and equal to 0 otherwise.
- $\pi_{1u,u}$ and $\pi_{2u,u}$ are the same as a_{1u} and a_{2u} respectively.
- The first two constraints replace the ones defined in the previous problem and the additional ones ensure that the new decision variables behave correctly with $\pi_{1u,k} = a_{1u} \cdot a_{1k}$ and $\pi_{2u,k} = a_{2u} \cdot a_{2k}$.
- $C_{u,MN}$ and $C_{u,SN}$ are the same cost functions when UE u is configured with the MN and SN strategy respectively but taking into account the new decision variables as shown in the below equations (7.9) and (7.10).

$$\begin{aligned}
C_{u,MN}(\Pi 1) = &\frac{\alpha_{u,eb} \cdot V_{u,eb} \cdot D1 \cdot \sum_{k \in \mathcal{U}} \pi_{1u,k}}{TotPRB_{BWP1} \cdot Bits_per_PRB_u} \\
&+ \frac{\alpha_{u,uc} \cdot V_{u,uc} \cdot D2 \cdot \sum_{k \in \mathcal{U}} \pi_{1u,k}}{TotPRB_{BWP2} \cdot Bits_per_PRB_u} \\
&+ \pi_{1u,u} \cdot (\theta_{MN} \cdot SwDl_u + \beta_u \cdot B_{MN})
\end{aligned} \tag{7.9}$$

$$\begin{aligned}
C_{u,SN}(\Pi 2) = &\frac{\alpha_{u,eb} \cdot V_{u,eb} \cdot D3 \cdot \sum_{k \in \mathcal{U}} \pi_{2u,k}}{TotPRB_{BWP3} \cdot Bits_per_PRB_u} \\
&+ \frac{\alpha_{u,uc} \cdot V_{u,uc} \cdot D3 \cdot \sum_{k \in \mathcal{U}} \pi_{2u,k}}{TotPRB_{BWP3} \cdot Bits_per_PRB_u} \\
&+ \pi_{2u,u} \cdot (\beta_u \cdot B_{SN})
\end{aligned} \tag{7.10}$$

Therefore, this ILP problem can be solved with CPLEX solver, achieving the same optimal result as the exhaustive search algorithm but much more swiftly.

7.5 Performance Evaluation

We used Python for simulations to compare both approaches against each other and against the legacy scheme where all users are configured with a single BWP for both services with a band B_{legacy}. CPLEX solver was used to solve the ILP problem in the centralized approach. Simulations were run several times (≈ 100 times) with a different number of users each time. We put focus on the scenario with $N_{users} = 20$. The simulation parameters from the system model are shown in Table 7.1.

Table 7.1: Simulation parameters for Energy Efficient BWP Configuration

Parameter	Description	Value
R	Coverage area	300 m
V_{URLLC}	URLLC volume of data	2-15 Mbits
V_{eMBB}	eMBB volume of data	5-50 Mbits
$SwDl_u$	User's BWP Switching Delay	1 ms [33]
B_{total}	Operator band	100 MHz
B_{eMBB}	eMBB BWP band	40 MHz
B_{URLLC}	URLLC BWP band	20 MHz
B_{mixed}	Mixed BWP band	30 MHz
B_{legacy}	Legacy BWP band	60 MHz
P_{BWP1}	Power consumption for scanning BWP 1 (eMBB)	1000 mW
P_{BWP2}	Power consumption for scanning BWP 2 (URLLC)	500 mW
P_{BWP3}	Power consumption for scanning BWP 3 (mixed)	750 mW
P_{legacy}	Power consumption for scanning legacy BWP	1500 mW
$\alpha_{u,eMBB}$	Normalizing factor for cost function	1
$\alpha_{u,URLLC}$	Normalizing factor for cost function	2
β_u	Normalizing factor for cost function	0.001-0.099

As for the results, we display the Energy Efficiency CDF for all users and the users' overall sojourn time in the network CDF for all users. The energy efficiency of UE u selecting the strategy MN is computed as follows:

$$EE_{u,MN} = \frac{Thr_{u,eb} + Thr_{u,uc}}{P_{BWP1} + P_{BWP2}} \tag{7.11}$$

where:

- $EE_{u,MN}$ is the Energy Efficiency of UE u selecting the MN strategy.
- P_{bwp} is the UE power consumption for scanning BWP bwp.

When UE u selects the SN strategy, its energy efficiency is $EE_{u,SN} = \frac{Thr_u}{P_{BWP3}}$.

As for the overall sojourn time of UE u, it is calculated as follows:

$$ST_{u,MN} = \sum_{s \in \{eb,uc\}} \frac{V_{u,s}}{Thr_{u,s}} + SwDl_u \tag{7.12}$$

$$ST_{u,SN} = \frac{\sum_{s \in \{eb,uc\}} V_{u,s}}{Thr_u} \tag{7.13}$$

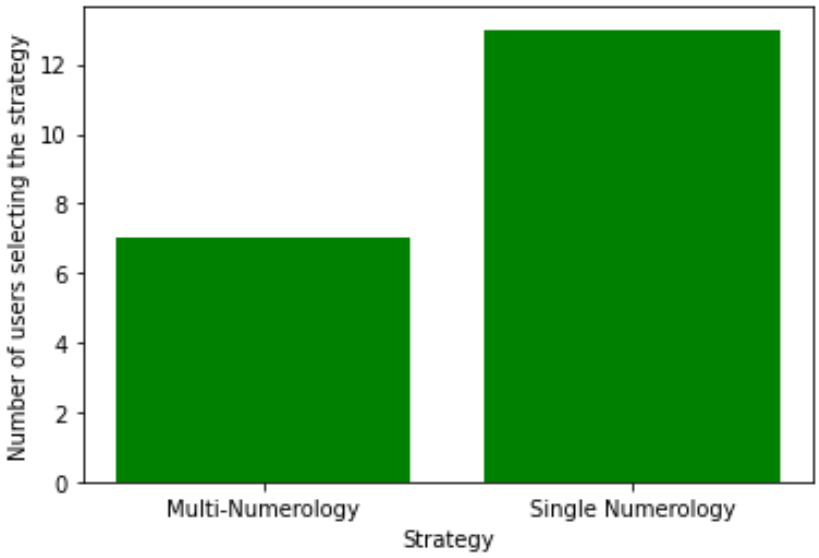

Figure 7.2: User Distribution among strategies with centralized solution algorithm for 20 users

Figure 7.2 displays the number of users associated with each strategy using the centralized solution algorithm for 20 users. Results show that a higher number of users prefer the Single Numerology scheme as it is more adapted to these users from an energy efficiency perspective since users scan a single and narrower BWP without BWP switching. Therefore, a leaning towards this scheme is envisaged in both approaches. Additionally, the Single Numerology strategy is mainly selected for users with a low battery level on average whereas the Multi-Numerology scheme is chosen for users with a high battery level on average. This is due to the fact that users with a low battery level require more energy savings which explains why they favour the single numerology scheme.

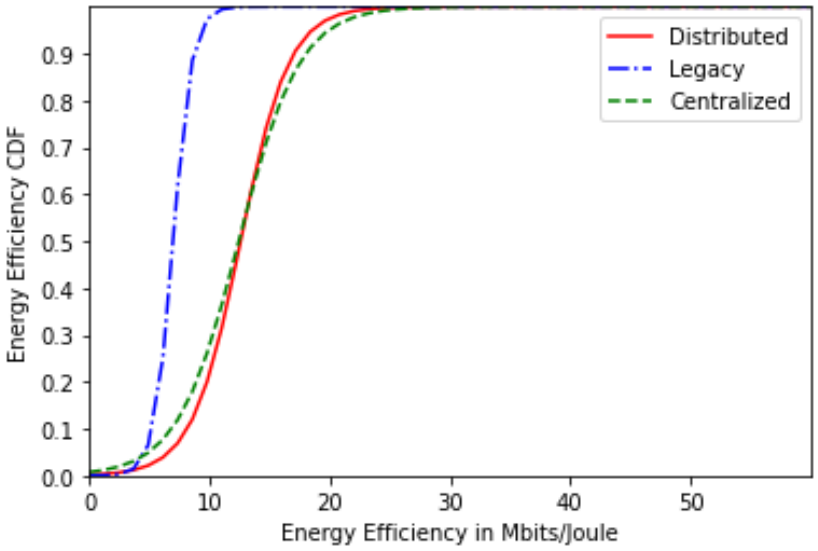

Figure 7.3: Energy Efficiency CDF for 20 users

Figure 7.3 represents the users' Energy Efficiency CDF for the centralized, distributed and legacy schemes for 20 users. It can be concluded that both proposed solutions - centralized and distributed - realize a higher energy efficiency than the legacy scheme thanks to the astute cost function that helped strike a

nice balance between energy efficiency and QoS. Moreover, the centralized scheme performs slightly better than the distributed scheme.

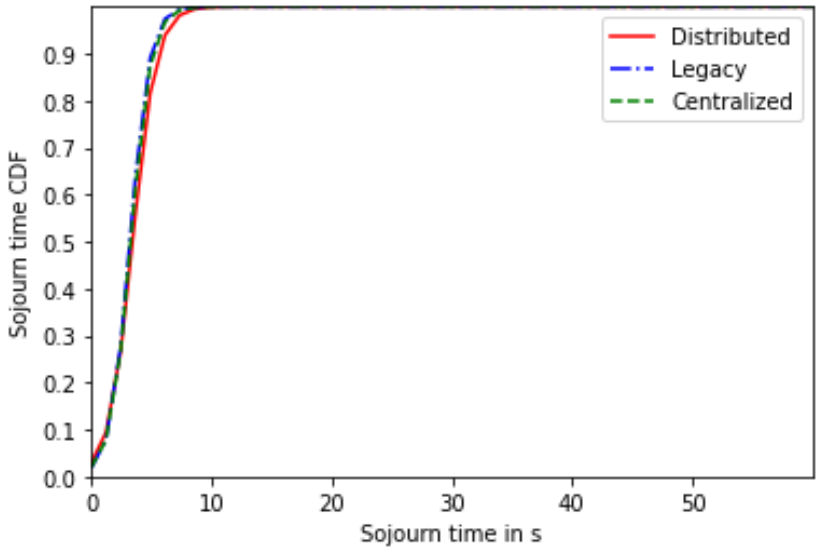

Figure 7.4: Sojourn Time CDF for 20 users

Figure 7.4 shows the users' Sojourn Time CDF for the centralized, distributed and legacy schemes for 20 users. The three schemes realize very close performances which means that the proposed solutions aim to reduce the network's sojourn time to a minimum.

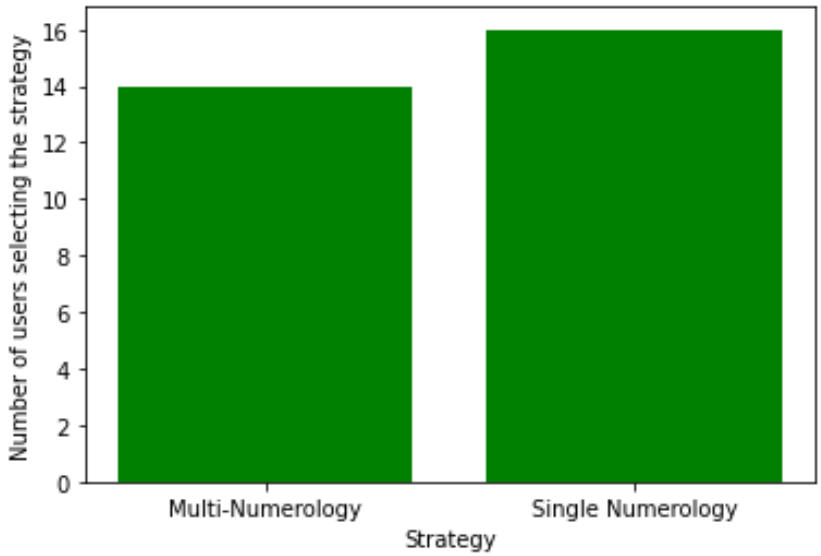

Figure 7.5: User Distribution among strategies with centralized solution algorithm for 30 users

As the number of users increases, the number of users with the MN BWP configuration is also increased to ensure a balance between both options with an inclination towards the SN BWP configuration. This can be seen in Fig. 7.5 that represents the user distribution among strategies for 30 users.

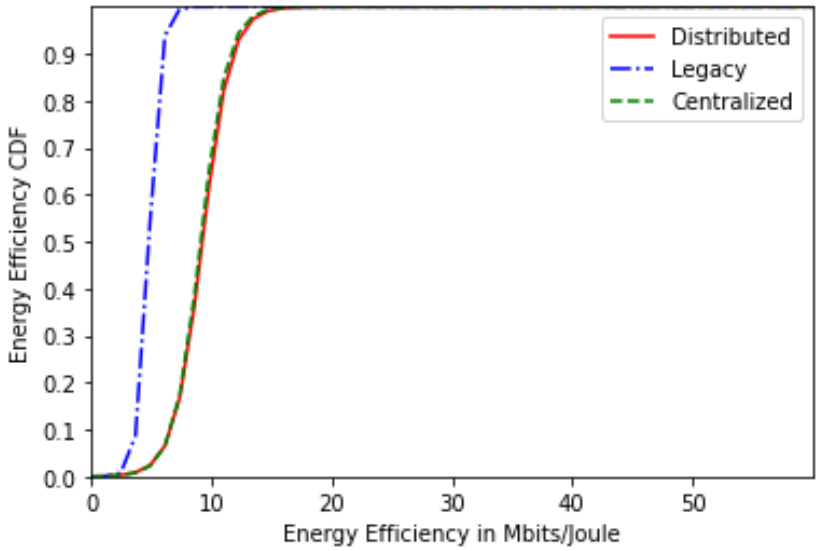

Figure 7.6: Energy Efficiency CDF for 30 users

As for the Energy Efficiency CDF, Fig. 7.6 displays it for 30 users where we can see that both solutions still provide better energy efficiency than the legacy scheme. However, the performance of these solutions becomes closer to the legacy scheme performance as the number of users increases since the network becomes saturated. For the Sojourn Time CDF for 30 users, the same results are observed as the scenario of 20 users.

Thus, we deduce that the proposed solutions (centralized and distributed) achieve better energy efficiency which in turn helps improving the users' battery life span while ensuring the same sojourn time as the legacy scheme.

7.5.1 The Price of Anarchy

To adequately compare the centralized and distributed approaches, we have recourse to the well-known Price of Anarchy (PoA), computed as follows:

$$PoA = \frac{GlobalCost_{optimal}}{GlobalCost_{NE}} \tag{7.14}$$

Therefore, it is the ratio of the sum of all users' costs obtained with the optimal centralized approach and the sum of all users' costs at NE for the distributed approach. The PoA is between 0 and 1 and the higher its value, the closer the performances of the distributed approach to the optimal centralized one.

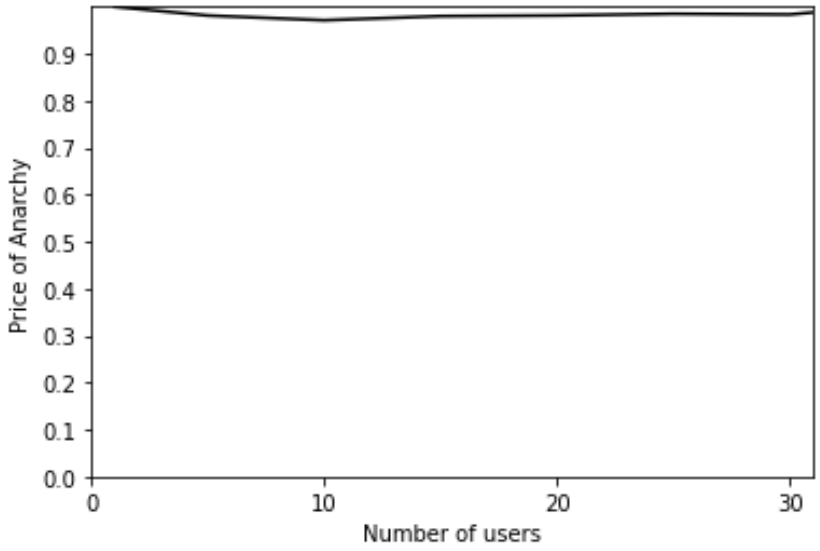

Figure 7.7: Price of Anarchy as a function of the number of users

Figure 7.7 displays the PoA as a function of the number of users. As can be seen, the PoA is ≈ 1 regardless of the number of users. This explains why the distributed approach attains very close performances to the centralized one.

As for the convergence time of each approach, it is represented in Fig. 7.8 for the distributed approach with the Best Response algorithm and the centralized approach with CPLEX solver for the ILP problem.

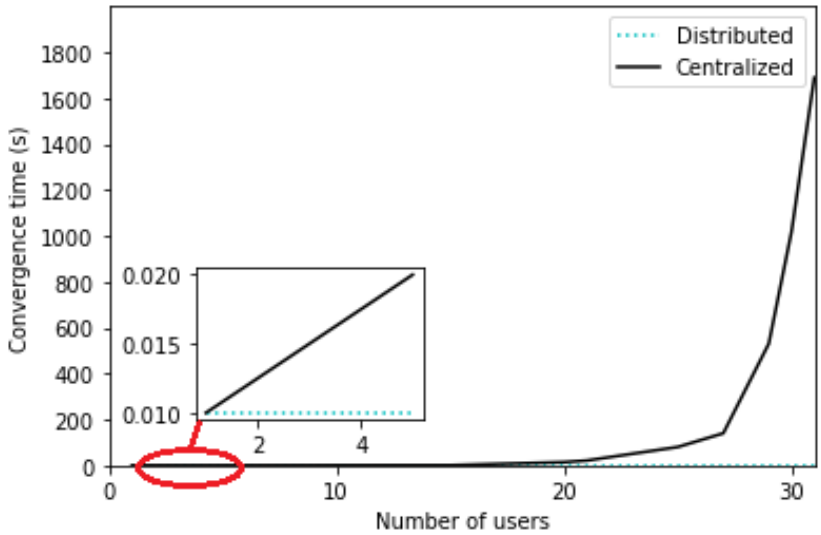

Figure 7.8: Convergence Time as a function of the number of users

In fact, the number of iterations to reach convergence for the best response algorithm is $N_{iterations} = 2$ regardless of the number of users, which is ≈ 0.01 s. The centralized solution with the ILP problem takes a slightly higher computation time of ≈ 10 s when $N_{users} \leq 20$ but starts to increase exponentially when $N_{users} > 20$. It is important to note that for the centralized approach, the ILP problem solver CPLEX remains much faster than the exhaustive search algorithm where the convergence time is ≈ 300 s for $N_{users} = 20$.

We conclude that the distributed approach is able to achieve almost optimal results with a much lesser computational time compared to the optimal centralized approach where the convergence time becomes significantly important with increasing number of users.

The final results also inspired the submission of two patents related to this contribution which will be discussed in the next section.

7.6 Proposed Patents

Following the performance evaluation results, we submit two new patents related to this contribution. The first patent consists of a BWP configuration method for multi-slice users. The BWP configuration whether multi-numerology or single numerology is selected based on the UE battery level, the Discontinuous Reception (DRX) activation and the overheating indicator. The UE battery level is selected as a parameter since we can optimize the slices' QoS when the battery level is high by choosing the multi-numerology BWP configuration. Nonetheless, when the battery becomes low, battery life is prioritized by selecting the single numerology BWP configuration. As for the DRX activation and overheating indicator, these parameters are also indicators of power consumption. In fact, the DRX was introduced in LTE and is a feature available in 5G [84]. Thanks to it, the UE does not have to be awake all the time to monitor the PDCCH which carries the DCI. In fact, the UE enters periodically a sleep mode (called "OFF" duration period) where the PDCCH is not monitored to reduce power consumption. The UE also wakes up to monitor the PDCCH periodically for a certain time called "On" duration period. This reduces power consumption but at the cost of increasing latency. It is the gNB that configures the UE with DRX via a MAC entity through RRC layer. Also, the overheating indicator is a parameter of the UE assistance information [85]. The UE assistance information is a special RRC message sent by the UE to the gNB that includes several information such as the DRX parameters and overheating indicator so that the gNB can take the appropriate measures accordingly. The overheating indicator stipulates that the terminal is overheating due to high power consumption. Therefore, combining these three parameters will help the gNB to select the appropriate BWP configuration for the UE whether single or multi-numerology to prioritize slices' QoS or battery life.

Nonetheless, in current standards, the UE battery level is not a parameter transmitted by the UE. Another patent [86] proposes the addition of this parameter in the UE assistance information. However, this patent does not take into account the battery consumption fields per slice, BWP or application over a certain period of time. In fact, the patent [86] considers only the overall battery consumption. For this reason, we propose a second patent to add these fields in the UE assistance information.

7.7 Concluding Remarks

To summarize, in this contribution, we propose a savvy and flexible scheme to select an appropriate BWP configuration for users connected to multiple slices that help such users reduce their energy consumption without hindering their QoS where:

- The BWP configuration selection between a Multi-Numerology and Single Numerology BWP is assessed for each user depending on multiple factors, including battery level and QoS satisfaction
- Two approaches are adopted:
  - The first approach is a centralized one based on a global optimization problem where a central entity minimizes the total cost of users by selecting for each user the most adequate BWP configuration

  - The second approach is a distributed one based on non-cooperative game theory where each user selects autonomously the BWP configuration that minimizes its own cost
- Extensive simulations prove the efficiency of our devised scheme against the static legacy scheme
- Evaluation of the price of anarchy proves the precedence of the distributed approach over the centralized one as it combines fast convergence and near optimal performances
- Two patents are proposed following this contribution:
  - The first patent proposes a method that selects the appropriate BWP configuration for multi-slice users depending on battery level, DRX activation and overheating indicator
  - The second patent proposes to add the battery consumption fields per slice, BWP or application over a certain period of time in the UE assistance information

This chapter marks the final contribution in the scope of this thesis. The next chapter summarizes all the contributions and proposed solutions tackled in this thesis and provides an overview on the short, medium and long-term perspectives.

Chapter 8

Conclusion

In this chapter, the summary of our contributions is presented, and the short, medium and long term perspectives of the thesis work are provided.

8.1 Summary of Contributions

In this thesis, the radio resource allocation problem in the context of RAN evolution and slicing is addressed through a series of contributions tackling this issue at many levels with many aspects considered. This will open the road for a better multi-slice support. Therefore, many algorithms were proposed and evaluated to prove their efficiency while being compared to salient SOTA works and existing schemes in the standard.

In the first contribution, the problem is addressed from a higher level where multiple VOs compete over an infrastructure provider's radio resources in a multi-slice context. Thus, an algorithm based on DWFQ that determines the portion of radio resources attributed to each VO is devised. The objective of this contribution is to determine the weights of the WFQ scheduler that partitions the infrastructure provider's radio resources between the VOs. This is done via two main approaches: a distributed approach based on a non-cooperative game and a centralized approach based on a Stackelberg game. For the distributed approach, VOs competed over I-P resources in a non-cooperative game setting where the VO utility function strikes a balance between increasing slice throughput and reducing monetary cost. This utility function was defined using two models to attribute the VO's radio resources: a linear model and a proportional fairness model. The best response dynamics was used to attain the unique NE whose existence was proven mathematically and through simulations where the optimal weights were determined given the input monetary cost. Additionally, both utility function models were compared against each other. In the centralized approach, a Stackelberg game is used to represent the problem where the I-P is the leader whose strategy is the resource monetary cost while the VOs are the followers whose strategy is the resource share of the available bandwidth. The Stackelberg Equilibrium was proven mathematically and through extensive simulations. The latter determined the optimal monetary cost and weights and highlighted the significance of the devised algorithms. Simulations also showed how our solution enabled the I-P, through fine tuning of a differentiating factor, to apply service differentiation among VOs. Finally, we discussed the implementation of the proposed solution in an O-RAN-compliant architecture.

The second contribution extends the first one, while focusing on the partitioning of the attributed band to a single VO between its slices. Particularly, two slices are considered: eMBB and URLLC. Therefore, a novel dynamic RAN slicing algorithm is proposed. This solution is based on both traffic engineering and

a dynamic adjustment of slice resources. To this aim, two main approaches are envisaged: a distributed approach based on a crowding game and a centralized approach based on DQN. With the distributed approach, cost functions were defined with a well-thought choice of parameters such as throughput and delay for an adequate slice selection for the user. The latter is performed to satisfy each user's QoS requirements and improve the global resource utilization in the devised problem. For the centralized DQN approach, the state, reward functions and actions are defined in a similar manner as the distributed approach and take into account the same parameters globally for every user. Performance analysis and time convergence of both algorithms alongside the alignment of these solutions with the O-RAN specifications are discussed. Additionally, both approaches are compared against each other and their efficiency is assessed over the legacy scheme where a user is assigned to its natural slice according to its service type. Also, a comparison is done with a SOTA slice selection algorithm [64] where a slice selection scheme is devised for each user depending on its KPIs (such as the throughput, delay and blocking rate). Results show the efficiency of our proposed solution and its adaptability against the variation of load conditions without increasing the needed bandwidth.

The third contribution extends the previous problem by taking into account additional and more complex aspects such as the numerology, the mMTC slice and users' radio conditions. Therefore, the same problem at the level of the VO is tackled in a multi-numerology and multi-slice context. For this reason, a 3GPP-compliant three-level slicing algorithm for the eMBB, URLLC and mMTC services is introduced. In this context, three numerologies, three slices and four BWPs (one for each slice and one that is shared between the eMBB and URLLC slices) are considered. The first level of this algorithm allots the BWP serving the URLLC users between the URLLC dedicated Premium BWP with a high numerology and the Non-Premium BWP that uses a lower numerology and is shared with eMBB users where preemptive scheduling favoring URLLC users is applied. A non-cooperative game is modeled at this level where a BWP is selected for each URLLC user that minimizes a well defined cost function that considers users' latency, BWP occupation and the incurred monetary cost. The second level of the algorithm dynamically adjusts the BWP band for every BWP (mMTC, eMBB Premium, Non-Premium and URLLC Premium) using smart heuristics depending on users' KPIs: throughput for eMBB users, SINR for mMTC users and latency for URLLC users. The third and final level resorts to DQN where the dimensioning of a guard band is performed among BWPs using different numerologies in order to mitigate the INI effect while avoiding radio resource wastage. Performance results prove the efficiency of our proposed three-level solution that ensures lower URLLC latency while maintaining high eMBB satisfaction and high SINR for mMTC users compared to our previous contribution and a SOTA solution [73] that misses the guard band dimensioning. Also, the compliance of our devised solution with the O-RAN architecture is detailed.

The fourth contribution shifts the focus to users connected to multiple slices. These types of users require frequent BWP switching when their connected slices require different numerologies. Therefore, three patented solutions are proposed to enhance the BWP switching for these multi-slice users. The first solution relies on the Downlink Control Information format modification which carries the BWP indicator to include multiple BWPs and the time instants where the BWP switch should be performed to ease the process. The second solution is based on adjusting dynamically the DCI frequency by increasing it to have more frequent BWP Switching when multiple services come into play. The third solution uses both the DCI-based and inactivity timer BWP switching methods and dynamically adjusts the BWP inactivity timer while selecting the BWP for the delay sensitive premium service as the default BWP. Performance evaluation shows that these solutions help reducing latency compared to the baseline approach. Particularly, it is shown that the first solution has the best performance in terms of URLLC latency and number of DCIs

scanned while maintaining eMBB throughput satisfaction. The other two solutions help reducing overall latency without the need to change the DCI format but at the cost of higher energy consumption (second solution) and eMBB throughput degradation (third solution).

The fifth and final contribution also tackles the radio resource allocation problem for multi-slice users but from an energy efficiency perspective. Thus, an energy-efficient scheme is proposed to select an adequate BWP configuration for users connected to multiple slices to help them reduce their energy consumption without hindering their QoS. This selection is based on a cost function that includes multiple factors such as battery level and QoS satisfaction. For this reason, two approaches are adopted. The first one is a centralized approach that aims to solve a global optimization problem so that the central entity minimizes the total cost of users by selecting for each user the most appropriate BWP configuration. The second approach is distributed and uses non-cooperative game theory where each user selects autonomously the BWP configuration that minimizes its own cost. The efficiency of our solution is also assessed through extensive simulations which display the advantages brought by our solution compared to the legacy scheme in terms of energy efficiency. Also, the evaluation of the price of anarchy shows that the distributed approach is more favorable than the centralized one since it reaches faster convergence with near optimal performances. Two patents inspired from this contribution are submitted where the first adequately chooses the BWP configuration for a UE depending on the battery level, DRX activation and overheating indicator and the second proposes to add the battery consumption fields per slice, application or BWP in the UE assistance information.

To highlight further the advantages brought by the contributions, Table 8.1 summarizes these advantages of each contribution in the context of a mobile network operator wishing to implement them.

Contribution	Advantages for the Mobile Network Operator
DWFQ Algorithm for Multi-Slice Multi-VO Approach	• Efficient radio resource algorithm which grants the I-P the ability to control the weight of each VO depending on certain criteria such as monetary cost • Can be implemented in the Non-RT RIC after retrieval of necessary inputs
Dynamic RAN Slicing Algorithm for eMBB and URLLC	• Maintains a URLLC Reliability and Resource Utilization Rate of 100% • Provides better eMBB Throughput • Can be implemented in the Non-RT RIC after retrieval of necessary inputs
Three-Level Slicing Algorithm in a Multi-Slice Multi-Numerology Context	• Ensures lower URLLC Latency and higher SINR for mMTC users • Maintains high eMBB throughput satisfaction • Can be implemented in the Non-RT RIC after retrieval of necessary inputs
Novel BWP Switching Mechanisms for Multi-Slice Users	• Three patents that help reducing latency due to BWP switching for multi-slice users
Energy-Efficient BWP Configuration Algorithm for Multi-Slice Users	• Improves energy efficiency for multi-slice users • Maintains QoS satisfaction • Two patents related to this contribution are submitted

Table 8.1: Advantages of the proposed approaches brought to the Mobile Network Operator

After detailing the advantages of each solution, we further discuss the future perspectives of these contributions in the next section.

8.2 Future Perspectives

We present our vision for the future perspectives of our thesis work in the next subsections 8.2.1, 8.2.2 and 8.2.3, exposing short, medium and long term perspectives respectively.

8.2.1 Short-Term

For short-term perspectives, we aim to include some overlooked aspects in our contributions. These aspects include the multi-cell context and inter-cell interference, uplink slicing and the consideration of additional services for multi-slice users. Additionally, we plan to push in the standardization bodies one of our patented solutions.

Multi-Cell and Inter-Cell Interference

As all our contributions tackle the radio resource allocation problem with a single gNB and cell, we would like to exploit this problem in a multi-cell context. In this context, harmful inter-cell interference incoming from neighboring cells should be considered. For this reason, we propose to examine the inter-cell interference problem by using a multi-agent Deep Reinforcement Learning algorithm similar to the work in [87] where an agent is placed at the level of each gNB to reduce its effect. This can be an extension to our third contribution with the three-level slicing algorithm by including an additional level that treats this problem.

Uplink Slicing

Uplink slicing was overlooked in this thesis since all our contributions focused on the downlink slicing and resource attribution. In fact, the same approaches can be used on the UL. However, the problem of users' multiple access is present on the uplink contrarily to the downlink where only the gNB is the central entity that is involved in the packet transmission. The work in [88] tackles this specific problem where Multi-Agent DRL is used to manage multiple access for the uplink slicing problem specifically for delay-sensitive services such as URLLC. We can propose an incremental solution that builds on the work in [88] in the context of our third contribution.

Consideration of Additional Slices for Multi-Slice Users

In the last contribution, we can add additional slices such as mMTC where multi-slice users can be connected to this slice in addition to other slices such as URLLC and eMBB. To this aim, we can repeat simulations in this context to see if it brings any changes to the algorithm performance evaluation results.

Standardization of Optimized BWP Switching Patent for Multi-Slice Users

The standardization of the patented solutions related to multi-slice users is very advantageous. Particularly for the fourth contribution, we can push the 3GPP standardization of the first patented solution with the Downlink Control Information format modification since it had the best performances in terms of

eMBB throughput, URLLC latency and energy efficiency. Thus, it brings many benefits to multi-slice users if standardized.

8.2.2 Medium-Term

For medium-term perspectives, we aim to test our proposed algorithms in a real O-RAN testbed [4] which brings additional benefits to the mobile network operator.

Full Solution Compliance with O-RAN Architecture

The O-RAN architecture leverages many benefits thanks to its openness and intelligence which reduce the CAPEX and OPEX associated to RAN initial deployment and network operations. In our work, we discussed the alignment of our solutions with the O-RAN architecture. However, the full integration with open interfaces compatibility and solution testing in a real O-RAN testbed were not part of the objectives of our contributions. Therefore, assessing the feasibility of the proposed solutions and checking their full compliance with the O-RAN architecture (thanks to a collaboration with an integration team in Orange's O-RAN Test and Integration Center) can be a promising future work bringing many advantages. However, we are currently limited by the maturity of the open interfaces and their support to our required parameters. Thus, testing our solutions may be done incrementally after resolving current limitations.

8.2.3 Long-Term

For long-term perspectives, the radio resource allocation problem should take into account the emerging features of future mobile networks such as satellite systems, new types of supported services, future generation mobile networks and newly developed AI tools.

Satellite Systems

The radio resource allocation problem in the context of O-RAN can also be tackled in a satellite system. In fact, some works such as [89] are beginning to take interest in this complex problem due to additional challenges such as the satellite orbit mobility and coverage area, the different requirements of users' demands and KPIs, spectrum sharing between operators and interference incoming from terrestrial base station and other satellites. In such a context, it is important to study this problem in the future.

New Types of Services

New categories of services may appear in the future in addition to the traditional eMBB, URLLC and mMTC services. These new services (which may include sensing, imaging and cognition applications) will require the consideration of different constraints and KPIs. This will impact the radio resource management when the operator decides to support these novel services with the rise of the Internet of Everything. The latter aims to connect things, people and data [90] which leads to the emergence of new classes of services. The necessary KPIs for these services may include the priority and severity level for a certain type of service. For example, a service linked to critical applications such as threat detection and health monitoring should be treated differently compared to other less critical services. Therefore, further classification of services can be done for an extended differentiation among them. Thus, the radio resource allocation problem should be adapted continuously to meet these new requirements and challenges.

Future Generation Mobile Networks

Attention is currently being brought to 6G mobile networks (the planned successor of 5G) even though its standardization and release remain years away. In fact, 6G is becoming a trending topic where some researchers are detailing their vision for the next generation of mobile networks [91]. The expectations of 6G are more green solutions, higher data rates and lower latency than the ones provided by 5G. With each new generation of mobile networks, new features and enhancements are added. Hence, the modelling of the radio resource allocation problem will be different from generation to generation depending on the new features. With 6G, new frequencies will be used along with enhanced features from 5G such as beamforming where the transmitted signals are targeted to a specific location to improve SINR and avoid interference. For this reason, it would be compelling to study this problem while taking into account these new various concepts. Additionally, 6G is expected to include new AI techniques.

New Artificial Intelligence Techniques

With the advent of Artificial Intelligence, networks are becoming more intelligent and autonomous facing the new brought challenges. 6G networks are planned to include AI as a feature. Additionally, AI is becoming a hot topic in the research community and new tools and techniques are being developed and examined to be deployed later on in a real network. These enhanced AI tools will help networks to further take appropriate decisions and drastic measures with a faster convergence time. Therefore, many applications will be improved thanks to AI implementation such as traffic prediction, clustering of users and data scheduling. These applications will be considered in the radio resource allocation problem to ensure a satisfactory QoS for each user. Also, this will facilitate the proposal of proactive resource allocation algorithms where radio resources are reserved beforehand for a certain service owing to traffic prediction.

Appendix A

Appendix for Multi-Slice Multi-VO Radio Resource Allocation Problem

A.1 Proof of SE Algorithm Convergence for Multi-Slice Multi-VO Context

A.1.1 Positivity of P(w)

Recall that we have the following iterative function:

$$w_{is}^{(t+1)} = P_{is}^{h}(w_{-is}^{(t)}) = \mathcal{A}_{is}\sqrt{w_{-is}^{(t)}} - w_{-is}^{(t)} \tag{A.1}$$

With $\mathcal{A}_{is} = \frac{1}{\sqrt{\alpha\beta_{is}\kappa_{is}\rho_s}}$.

Since $0 < w_{-is}^{(t)} < 1$, we have that $\sqrt{w_{-is}^{(t)}} > w_{-is}^{(t)}$. Moreover, $\forall \mathcal{A}_{is} > 1$, $\mathcal{A}_{is}\sqrt{w_{-is}^{(t)}} > \sqrt{w_{-is}^{(t)}} > w_{-is}^{(t)}$. Consequently, to prove the positivity of $P(w)$, $\mathcal{A}_{is}$ should verify $\mathcal{A}_{is} > 1$. With realistic adopted parameters $\alpha \sim 10^{-4}$, $0 < \beta_{is} < 1$, $\kappa_{is} \sim 10$, $\rho_s \sim 10$, we have that $\mathcal{A}_{is} = \frac{1}{\sqrt{\alpha\beta_{is}\kappa_{is}\rho_s}} \sim 10 > 1$ which establishes the positivity.

A.1.2 Monotonicity of P(w)

The first derivative $P'(w)$ of $P(w)$ is:

$$P_{is}'^{h}(w_{-is}^{(t)}) = \mathcal{A}_{is}\frac{1}{2\sqrt{w_{-is}^{(t)}}} - 1 \tag{A.2}$$

$P'(w) > 0$ is the condition proving the monotonicity of $P(w)$.
$\mathcal{A}_{is} \sim 10$ and $\frac{1}{\sqrt{w_{-is}^{(t)}}} > 1$ leading to $\mathcal{A}_{is}\frac{1}{\sqrt{w_{-is}^{(t)}}} > 10 > 2$. Hence, $P'(w) > 0$ and the monotonicity is verified.

A.1.3 Scalability of P(w)

To demonstrate the scalability, $P(w)$ should uphold that for $\mu > 1$, $\mu P(w) \geq P(\mu w)$. Since $\mu > 1$ leads to $\mu > \sqrt{\mu}$. Consequently, $\mathcal{A}_{is}\mu\sqrt{w_{-is}^{(t)}} - \mu w_{-is}^{(t)} > \mathcal{A}_{is}\sqrt{\mu w_{-is}^{(t)}} - \mu w_{-is}^{(t)}$.Hence, $\mu P(w) > P(\mu w)$ and the scalability is verified.

A.1.4 Two-Sided Scalability of P(w)

For $\frac{1}{\mu}w \leq w' \leq \mu w$ with $\mu > 1$, $P(w)$ should obey to $\frac{1}{\mu}P(w) < P(w') < \mu P(w)$. From the monotonicity and scalability properties of $P(w)$, for $w' \leq \mu w$, $P(w') < P(\mu w) < \mu P(w)$. Since $\mu > 1$, $\frac{1}{\mu} < 1$ leading to $\frac{1}{\mu} < \sqrt{\frac{1}{\mu}}$. It boils down to $\mathcal{A}_{is}\frac{1}{\mu}\sqrt{w_{-is}^{(t)}} - \frac{1}{\mu}w_{-is}^{(t)} < \mathcal{A}_{is}\sqrt{\frac{w_{-is}^{(t)}}{\mu}} - \frac{1}{\mu}w_{-is}^{(t)}$. Hence, $\frac{1}{\mu}P(w) < P(\frac{1}{\mu}w)$. By the monotonicity of $P(w)$: $\frac{1}{\mu}P(w) < P(\frac{1}{\mu}w) \leq P(w')$ since $\frac{1}{\mu}w \leq w'$ proving the two-sided scalability of $P(w)$.

Publications

Conferences

[92] J. Saad, K. Khawam, M. Yassin, and S. Costanzo, "A Multi-Slice Multi-Operator Dynamic Weighted Fair Queuing RAN Scheduling in a Game Theoretic Framework," in *Proceedings of the 19th ACM International Symposium on Mobility Management and Wireless Access*, 2021, pp. 17–24

[93] J. Saad, K. Khawam, M. Yassin, S. Costanzo, and K. Boulos, "Crowding Game and Deep Q-Networks for Dynamic RAN Slicing in 5G Networks," in *Proceedings of the 20th ACM International Symposium on Mobility Management and Wireless Access*, 2022, pp. 37–46

[94] J. Saad, M. Yassin, S. Costanzo, K. Khawam, "Novel BWP Schemes for Multi-Numerology and Multi-Slice Radio Access Networks," accepted at IEEE WCNC 2024

Journals

[95] J. Saad, K. Khawam, M. Yassin, and S. Costanzo, "A three-level slicing algorithm in a multi-slice multi-numerology context," *Computer Communications*, vol. 212, pp. 324–341, 2023

[96] J. Saad, K. Khawam, M. Yassin and S. Costanzo, "Energy-Efficient BWP Configuration for Multi-Slice Users," *Sensors*, vol. 24, no. 4, p. 1281, 2024

Patents

[97] J. Saad, M. Yassin, S. Costanzo, "Procédé de communication d'informations de contrôle," FR2303470

[98] J.Saad, M.Yassin, S.Costanzo, "Procédés de configuration et de communication, entité d'un réseau de télécommunications et équipement utilisateur," FR2303684

[99] J. Saad, M. Yassin, S. Costanzo, "Procédé de contrôle, entité d'un réseau de télécommunications, procédé de communication et équipement utilisateur," FR2303685

[100] J.Saad, M.Yassin, S.Costanzo, "Procédés de configuration et de communication, entité d'un réseau de télécommunications et équipement utilisateur," FR2315006

[101] J. Saad, M. Yassin, S. Costanzo, "Procédés visant à optimiser l'efficacité énergétique d'un équipement utilisateur, entité d'un réseau de télécommunications et équipement utilisateur," FR2314984

Bibliography

[1] D. Demmer, R. Gerzaguet, J.-B. Doré, and D. L. Ruyet, "Analytical Study of 5G NR eMBB Co-Existence," *2018 25th International Conference on Telecommunications (ICT)*, pp. 186–190, 2018.

[2] T. Mumtaz, S. Muhammad, M. Aslam, and I. Ahmed, "Inter-slice resource management for 5G radio access network using markov decision process," *Telecommunication Systems*, vol. 79, 04 2022.

[3] " System architecture for the 5G System (5GS) ," 3GPP, Tech. Rep. 23.501.

[4] "O-RAN Architecture Description," O-RAN Alliance, Tech. Rep. v02.00, 2020.

[5] I. Parvez, A. Rahmati, I. Guvenc, A. I. Sarwat, and H. Dai, "A survey on low latency towards 5G: RAN, core network and caching solutions," *IEEE Communications Surveys & Tutorials*, vol. 20, no. 4, pp. 3098–3130, 2018.

[6] "Study on Scenarios and Requirements for Next Generation Access Technologies (Release 15)," 3GPP, Tech. Rep. 38.913, Jun 2018.

[7] P. Popovski, Č. Stefanović, J. J. Nielsen, E. De Carvalho, M. Angjelichinoski, K. F. Trillingsgaard, and A.-S. Bana, "Wireless access in ultra-reliable low-latency communication (URLLC)," *IEEE Transactions on Communications*, vol. 67, no. 8, pp. 5783–5801, 2019.

[8] A. Karamyshev, E. Khorov, A. Krasilov, and I. F. Akyildiz, "Fast and accurate analytical tools to estimate network capacity for URLLC in 5G systems," *Computer Networks*, vol. 178, p. 107331, 2020.

[9] S. K. Sharma and X. Wang, "Toward Massive Machine Type Communications in Ultra-Dense Cellular IoT Networks: Current Issues and Machine Learning-Assisted Solutions," *IEEE Communications Surveys and Tutorials*, vol. 22, no. 1, pp. 426–471, 2020.

[10] "5G mMTC: Challenges and Solutions," https://iot.electronicsforu.com/content/tech-trends/5g-mmtc-challenges-and-solutions/, accessed: 2023-08-15.

[11] A. A. Zaidi, R. Baldemair, H. Tullberg, H. Bjorkegren, L. Sundstrom, J. Medbo, C. Kilinc, and I. Da Silva, "Waveform and numerology to support 5G services and requirements," *IEEE Communications Magazine*, vol. 54, no. 11, pp. 90–98, 2016.

[12] "5G; NR; User Equipment (UE) Radio Transmission and Reception; Part 1: Range 1 Standalone (Release 15)," 3GPP, Tech. Rep. 38.101, Jul 2018.

[13] S. R. Pokhrel, J. Ding, J. Park, O.-S. Park, and J. Choi, "Towards Enabling Critical mMTC: A Review of URLLC within mMTC," *IEEE Access*, vol. 8, pp. 131 796–131 813, 2020.

[14] T. Soni, A. R. Ali, K. Ganesan, and M. Schellmann, "Adaptive Numerology—A Solution to Address the Demanding QoS in 5G-V2X," in *2018 IEEE Wireless Communications and Networking Conference (WCNC)*. IEEE, 2018, pp. 1–6.

[15] J. Zhang, X. Xu, K. Zhang, B. Zhang, X. Tao, and P. Zhang, "Machine Learning Based Flexible Transmission Time Interval Scheduling for eMBB and uRLLC Coexistence Scenario," *IEEE Access*, vol. 7, pp. 65 811–65 820, 2019.

[16] S. R. Pokhrel, J. Ding, J. Park, O.-S. Park, and J. Choi, "Towards Enabling Critical mMTC: A Review of URLLC within mMTC," *IEEE Access*, vol. 8, pp. 131 796–131 813, 2020.

[17] E. Dahlman, S. Parkvall, and J. Skold, *5G NR: The Next Generation Wireless Access Technology*. Academic Press, 2020.

[18] X. Lin, D. Yu, and H. Wiemann, "A Primer on Bandwidth Parts in 5G New Radio," *5G and Beyond: Fundamentals and Standards*, pp. 357–370, 2021.

[19] "Bandwidth Part Adaptation: 5G NR User Experience & Power Consumption Enhancements. White Paper, MediaTek." MediaTek, Tech. Rep., 2018.

[20] A. B. Kihero, M. S. J. Solaija, A. Yazar, and H. Arslan, "Inter-Numerology Interference Analysis for 5G and Beyond," in *2018 IEEE Globecom Workshops (GC Wkshps)*. IEEE, 2018, pp. 1–6.

[21] A. B. Kihero, M. S. J. Solaija, and H. Arslan, "Inter-Numerology Interference for Beyond 5G," *IEEE Access*, vol. 7, pp. 146 512–146 523, 2019.

[22] B. Peköz, H. Arslan *et al.*, "Fundamentals of Multi-Numerology 5G New Radio," *arXiv preprint arXiv:1805.02842*, 2018.

[23] S. Zhang, "An Overview of Network Slicing for 5G," *IEEE Wireless Communications*, vol. 26, no. 3, pp. 111–117, 2019.

[24] "Study on enhancement of Radio Access Network (RAN) slicing for NR," 3GPP, Tech. Rep. 38.832.

[25] "3rd Generation Partnership Project; Technical Specification Group Services and System Aspects; Management and Orchestration; Provisioning; ," 3GPP, Tech. Rep. 28.531, Dec 2019.

[26] S. E. Elayoubi, S. B. Jemaa, Z. Altman, and A. Galindo-Serrano, "5G RAN Slicing for Verticals: Enablers and Challenges," *Comm. Mag.*, Jan. 2019.

[27] Y.-i. Choi and N. Park, "Slice Architecture for 5G Core Network," in *2017 Ninth International Conference on Ubiquitous and Future Networks (ICUFN)*, 2017, pp. 571–575.

[28] "O-RAN Working Group 1 Use Cases Analysis Report," O-RAN Alliance, Tech. Rep. v05.00.03, 2021.

[29] L. Gavrilovska, V. Rakovic, and D. Denkovski, "From Cloud RAN to Open RAN," *Wireless Personal Communications*, pp. 1–17, 2020.

[30] "Technical Specification Group Services and System Aspects; Release 15 Description," 3GPP, Tech. Rep. 21.915, Mar 2019.

[31] K. Boutiba, M. Bagaa, and A. Ksentini, "Radio Resource Management in Multi-Numerology 5G New Radio Featuring Network Slicing," in *ICC 2022-IEEE International Conference on Communications*. IEEE, 2022, pp. 359–364.

[32] "Technical Specification Group Services and System Aspects; NR; Multiplexing and Channel Coding," 3GPP, Tech. Rep. 38.212, Dec 2022.

[33] "Technical Specification Group Services and System Aspects; NR; Requirements for Support of Radio Resource Management," 3GPP, Tech. Rep. 38.133, Oct 2018.

[34] "Technical Specification Group Services and System Aspects; LTE; Evolved Universal Terrestrial Radio Access (E-UTRA); Medium Access Control (MAC) protocol specification," 3GPP, Tech. Rep. 36.321, Oct 2016.

[35] D. Monderer and L. S. Shapley, "Potential games," *Games and Economic Behavior*, 1996.

[36] R. W. Rosenthal, "A class of games possessing pure-strategy Nash equilibria," 1973.

[37] I. Milchtaich, "Congestion games with player-specific payoff functions," *Games and Economic Behavior*, 1996.

[38] M. Feldman, Y. Snappir, and T. Tamir, "The Efficiency of Best-Response Dynamics," in *Algorithmic Game Theory*, V. Bilò and M. Flammini, Eds. Springer International Publishing, 2017.

[39] H.-T. Chien, Y.-D. Lin, C.-L. Lai, and C.-T. Wang, "End-to-End Slicing as a Service with Computing and Communication Resource Allocation for Multi-Tenant 5G Systems," *IEEE Wireless Communications*, 2019.

[40] R. Ferrus, O. Sallent, J. Pérez-Romero, and R. Agusti, "On 5G radio access network slicing: Radio interface protocol features and configuration," *IEEE Communications Magazine*, vol. 56, no. 5, pp. 184–192, 2018.

[41] R. Su, D. Zhang, R. Venkatesan, Z. Gong, C. Li, F. Ding, F. Jiang, and Z. Zhu, "Resource Allocation for Network Slicing in 5G Telecommunication Networks: A Survey of Principles and Models," *IEEE Network*, vol. 33, no. 6, pp. 172–179, 2019.

[42] P. L. Vo, M. N. H. Nguyen, T. A. Le, and N. H. Tran, "Slicing the Edge: Resource Allocation for RAN Network Slicing," *IEEE Wireless Communications Letters*, vol. 7, no. 6, pp. 970–973, 2018.

[43] G. You and Y. Zhao, "A weighted-fair-queuing (WFQ)-based dynamic request scheduling approach in a multi-core system," *Future Generation Computer Systems*, vol. 28, no. 7, pp. 1110–1120, 2012.

[44] A. Banchs and X. Perez, "Distributed weighted fair queuing in 802.11 wireless LAN," in *2002 IEEE International Conference on Communications. Conference Proceedings. ICC 2002 (Cat. No. 02CH37333)*, vol. 5. IEEE, 2002, pp. 3121–3127.

[45] T. M. Ho, N. H. Tran, S. A. Kazmi, and C. S. Hong, "Dynamic pricing for resource allocation in wireless network virtualization: A stackelberg game approach," in *2017 International Conference on Information Networking (ICOIN)*. IEEE, 2017, pp. 429–434.

[46] T. D. Tran and L. B. Le, "Resource Allocation for Multi-Tenant Network Slicing: A Multi-Leader Multi-Follower Stackelberg Game Approach," *IEEE Transactions on Vehicular Technology*, vol. 69, no. 8, pp. 8886–8899, 2020.

[47] D. A. Ravi, V. K. Shah, C. Li, T. Hou, and J. H. Reed, "RAN Slicing in Multi-MVNO Environment under Dynamic Channel Conditions," *arXiv preprint arXiv:2104.04900*, 2021.

[48] R. Mahindra, M. A. Khojastepour, H. Zhang, and S. Rangarajan, "Radio access network sharing in cellular networks," in *2013 21st IEEE International Conference on Network Protocols (ICNP)*, 2013.

[49] M. Maule, J. Vardakas, and C. Verikoukis, "5G RAN Slicing: Dynamic Single Tenant Radio Resource Orchestration for eMBB Traffic within a Multi-Slice Scenario," *IEEE Communications Magazine*, vol. 59, no. 3, pp. 110–116, 2021.

[50] P. Caballero, A. Banchs, G. de Veciana, X. Costa-Pérez, and A. Azcorra, "Network Slicing for Guaranteed Rate Services: Admission Control and Resource Allocation Games," *IEEE Transactions on Wireless Communications*, 2018.

[51] R. Ferrús, J. Pérez-Romero, O. Sallent, I. Vilà, and R. Agustí, "Machine learning-assisted cross-slice radio resource optimization: Implementation framework and algorithmic solution," 2020.

[52] B. Khodapanah, A. Awada, I. Viering, A. noll Barreto, M. Simsek, and G. Fettweis, "Framework for slice-aware radio resource management utilizing artificial neural networks," *IEEE Access*, vol. 8, pp. 174 972–174 987, 2020.

[53] I. Vilà, J. Pérez-Romero, O. Sallent, and A. Umbert, "A novel approach for dynamic capacity sharing in multi-tenant scenarios," in *2020 IEEE 31st Annual International Symposium on Personal, Indoor and Mobile Radio Communications*. IEEE, 2020, pp. 1–6.

[54] A. Papa, M. Klugel, L. Goratti, T. Rasheed, and W. Kellerer, "Optimizing dynamic RAN slicing in programmable 5G networks," in *ICC 2019-2019 IEEE International Conference on Communications (ICC)*. IEEE, 2019, pp. 1–7.

[55] A. Perveen, R. Abozariba, M. Patwary, and A. Aneiba, "Dynamic traffic forecasting and fuzzy-based optimized admission control in federated 5G-open RAN networks," *Neural Computing and Applications*, pp. 1–19, 2021.

[56] X. Yang, Y. Liu, K. S. Chou, and L. Cuthbert, "A game-theoretic approach to network slicing," in *2017 27th International Telecommunication Networks and Applications Conference (ITNAC)*. IEEE, 2017, pp. 1–4.

[57] S. Bakri, P. A. Frangoudis, and A. Ksentini, "Dynamic slicing of RAN resources for heterogeneous coexisting 5G services," in *2019 IEEE Global Communications Conference (GLOBECOM)*. IEEE, 2019, pp. 1–6.

[58] X. Zhang, X. Guo, and H. Zhang, "RB Allocation Scheme for eMBB and URLLC Coexistence in 5G and Beyond," *Wireless Communications and Mobile Computing*, vol. 2021, 2021.

[59] M. Alsenwi, N. H. Tran, M. Bennis, S. R. Pandey, A. K. Bairagi, and C. S. Hong, "Intelligent Resource Slicing for eMBB and URLLC Coexistence in 5G and Beyond: A Deep Reinforcement Learning Based Approach," *IEEE Transactions on Wireless Communications*, vol. 20, no. 7, pp. 4585–4600, 2021.

[60] M. Morcos, M. Mhedhbi, A. Galindo-Serrano, and S. Eddine Elayoubi, "Optimal resource preemption for aperiodic URLLC traffic in 5G Networks," in *2020 IEEE 31st Annual International Symposium on Personal, Indoor and Mobile Radio Communications*, 2020, pp. 1–6.

[61] L. Feng, Y. Zi, W. Li, F. Zhou, P. Yu, and M. Kadoch, "Dynamic resource allocation with RAN slicing and scheduling for uRLLC and eMBB hybrid services," *IEEE Access*, vol. 8, pp. 34 538–34 551, 2020.

[62] N. NADDEH, S. B. JEMAA, S. E. ELAYOUBI, and T. CHAHED, "Proactive RAN Resource Reservation for URLLC Vehicular Slice," in *2021 IEEE 93rd Vehicular Technology Conference (VTC2021-Spring)*. IEEE, 2021, pp. 1–5.

[63] F. Song, J. Li, C. Ma, Y. Zhang, L. Shi, and D. N. K. Jayakody, "Dynamic virtual resource allocation for 5G and beyond network slicing," *IEEE Open Journal of Vehicular Technology*, vol. 1, pp. 215–226, 2020.

[64] X. Chen, Y. Tang, M. Zhang, and L. Huang, "RAN slice selection mechanism based on satisfaction degree," in *2020 IEEE Wireless Communications and Networking Conference Workshops (WCNCW)*. IEEE, 2020, pp. 1–6.

[65] K. Boulos, K. Khawam, M. Yassin, and S. Costanzo, "A Crowding Game for Dynamic RAN Slicing Algorithm in 5G Networks," in *2021 17th International Conference on Wireless and Mobile Computing, Networking and Communications (WiMob)*. IEEE, 2021, pp. 181–186.

[66] L. Bonati, S. D'Oro, M. Polese, S. Basagni, and T. Melodia, "Intelligence and Learning in O-RAN for Data-driven NextG Cellular Networks," *arXiv preprint arXiv:2012.01263*, 2020.

[67] F. Mungari, "An RL approach for radio resource management in the O-RAN architecture," in *2021 18th Annual IEEE International Conference on Sensing, Communication, and Networking (SECON)*. IEEE, 2021, pp. 1–2.

[68] H. Zhang, H. Zhou, and M. Erol-Kantarci, "Team learning-based resource allocation for open radio access network (O-RAN)," in *ICC 2022-IEEE International Conference on Communications*. IEEE, 2022, pp. 4938–4943.

[69] E. Memisoglu, A. B. Kihero, E. Basar, and H. Arslan, "Guard band reduction for 5G and beyond multiple numerologies," *IEEE Communications Letters*, vol. 24, no. 3, pp. 644–647, 2019.

[70] A. F. Demir and H. Arslan, "Inter-numerology interference management with adaptive guards: A cross-layer approach," *IEEE Access*, vol. 8, pp. 30 378–30 386, 2020.

[71] X. Zhang, L. Zhang, P. Xiao, D. Ma, J. Wei, and Y. Xin, "Mixed Numerologies Interference Analysis and Inter-Numerology Interference Cancellation for Windowed OFDM Systems," *IEEE Transactions on Vehicular Technology*, vol. 67, no. 8, pp. 7047–7061, 2018.

[72] M. Raftopoulou and R. Litjens, "Optimisation of Numerology and Packet Scheduling in 5G Networks: To Slice or not to Slice?" in *2021 IEEE 93rd Vehicular Technology Conference (VTC2021-Spring)*. IEEE, 2021, pp. 1–7.

[73] M. Zambianco and G. Verticale, "Mixed-Numerology Interference-Aware Spectrum Allocation for eMBB and URLLC Network Slices," in *2021 19th Mediterranean Communication and Computer Networking Conference (MedComNet)*. IEEE, 2021, pp. 1–8.

[74] K. Boutiba, M. Bagaa, and A. Ksentini, "Optimal radio resource management in 5G NR featuring network slicing," *Computer Networks*, vol. 234, p. 109937, 2023.

[75] F. Abinader, A. Marcano, K. Schober, R. Nurminen, T. Henttonen, H. Onozawa, and E. Virtej, "Impact of Bandwidth Part (BWP) Switching on 5G NR System Performance," in *2019 IEEE 2nd 5G World Forum (5GWF)*. IEEE, 2019, pp. 161–166.

[76] G. Ponnamreddy, P. Jiniwal *et al.*, "Method to Handle BWP Inactivity Timer to Reduce Latency and to Improve Throughput in 5G Devices," in *2021 IEEE 4th 5G World Forum (5GWF)*. IEEE, 2021, pp. 317–322.

[77] J. B. Rosen, "Existence and uniqueness of equilibrium points for concave n-person games," *Econometrica: Journal of the Econometric Society*, pp. 520–534, 1965.

[78] "NR; User Equipment (UE) radio transmission and reception; part 1: Range 1 Standalone," 3GPP TS 38.101-1, Tech. Rep. v. 15.4.0, Jan. 2019.

[79] T. Bonald and J. W. Roberts, "Congestion at flow level and the impact of user behaviour," *Computer networks*, vol. 42, no. 4, pp. 521–536, 2003.

[80] C. Khirallah, D. Rastovac, D. Vukobratovic, and J. Thompson, "Energy Efficient Multimedia Delivery Services over LTE/LTE-A," *IEICE Transactions on Communications*, vol. E97.B, pp. 1504–1513, 08 2014.

[81] "IMT-2020 Self-Evaluation: UP Latency Analysis for FDD and Dynamic TDD with UE Processing Capability 2 (URLLC)," 3GPP, Tech. Rep., Aug 2018.

[82] M. Series, "Guidelines for Evaluation of Radio Interface Technologies for IMT-2020," *Report ITU*, pp. 2412–0, 2017.

[83] C. C. Communications, "Multiple active bandwidth parts," US10880949.

[84] "5G NR: Connected Mode DRX," http://howltestuffworks.blogspot.com/2021/04/5g-nr-connected-mode-drx.html.

[85] "5G NR: Overheating Index," https://www.sharetechnote.com/html/5G/5G_UE_AssistanceInformation.html.

[86] B. Telecommunications, "User equipment battery consumption," GB2537791A.

[87] T. Hu, Q. Liao, Q. Liu, D. Wellington, and G. Carle, "Inter-cell slicing resource partitioning via coordinated multi-agent deep reinforcement learning," in *ICC 2022-IEEE International Conference on Communications*. IEEE, 2022, pp. 3202–3207.

[88] B.-M. Robaglia, M. Coupechoux, D. Tsilimantos, and A. Destounis, "SeqDQN: Multi-Agent Deep Reinforcement Learning for Uplink URLLC with Strict Deadlines," in *EuCNC & 6G Summit*, 2023.

[89] R. Smith, C. Freeberg, T. Machacek, and V. Ramaswamy, "An O-RAN Approach to Spectrum Sharing Between Commercial 5G and Government Satellite Systems," in *MILCOM 2021 - 2021 IEEE Military Communications Conference (MILCOM)*, 2021, pp. 739–744.

[90] M. H. Miraz, M. Ali, P. S. Excell, and R. Picking, "A review on Internet of Things (IoT), Internet of everything (IoE) and Internet of nano things (IoNT)," *2015 Internet Technologies and Applications (ITA)*, pp. 219–224, 2015.

[91] S. Dang, O. Amin, B. Shihada, and M.-S. Alouini, "What should 6G be?" *Nature Electronics*, vol. 3, no. 1, pp. 20–29, 2020.

[92] J. Saad, K. Khawam, M. Yassin, and S. Costanzo, "A Multi-Slice Multi-Operator Dynamic Weighted Fair Queuing RAN Scheduling in a Game Theoretic Framework," in *Proceedings of the 19th ACM International Symposium on Mobility Management and Wireless Access*, 2021, pp. 17–24.

[93] J. Saad, K. Khawam, M. Yassin, S. Costanzo, and K. Boulos, “Crowding Game and Deep Q-Networks for Dynamic RAN Slicing in 5G Networks,” in *Proceedings of the 20th ACM International Symposium on Mobility Management and Wireless Access*, 2022, pp. 37–46.

[94] J. Saad, M. Yassin, S. Costanzo, K. Khawam, “Novel BWP Schemes for Multi-Numerology and Multi-Slice Radio Access Networks,” accepted at IEEE WCNC 2024.

[95] J. Saad, K. Khawam, M. Yassin, and S. Costanzo, “A three-level slicing algorithm in a multi-slice multi-numerology context,” *Computer Communications*, vol. 212, pp. 324–341, 2023.

[96] J. Saad, K. Khawam, M. Yassin and S. Costanzo, “Energy-Efficient BWP Configuration for Multi-Slice Users,” *Sensors*, vol. 24, no. 4, p. 1281, 2024.

[97] J. Saad, M. Yassin, S. Costanzo, “Procédé de communication d’informations de contrôle,” FR2303470.

[98] J.Saad, M.Yassin, S.Costanzo, “Procédés de configuration et de communication, entité d’un réseau de télécommunications et équipement utilisateur,” FR2303684.

[99] J. Saad, M. Yassin, S. Costanzo, “Procédé de contrôle, entité d’un réseau de télécommunications, procédé de communication et équipement utilisateur,” FR2303685.

[100] J.Saad, M.Yassin, S.Costanzo, “Procédés de configuration et de communication, entité d’un réseau de télécommunications et équipement utilisateur,” FR2315006.

[101] J. Saad, M. Yassin, S. Costanzo, “Procédés visant à optimiser l’efficacité énergétique d’un équipement utilisateur, entité d’un réseau de télécommunications et équipement utilisateur,” FR2314984.